DEVELOPMENT OF A SMART CONTROL AND MONITORING SYSTEM FOR IMPRESSED CURRENT CATHODIC PROTECTION RUNNING ON HYBRID RENEWABLE ENERGY

By

CYNCOL AKANI SIBIYA

Dissertation submitted in fulfilment of the requirements for the degree:

Master of Engineering in Electrical Engineering

In the Department of Electrical, Electronic and Computer Engineering

Faculty of Engineering, Built Environment and Information Technology

Central University of Technology, Free State

Supervisor: Dr P.B. Numbi

Co-Supervisor: Prof K. Kusakana

December 2020

DECLARATION

I, CYNCOL AKANI SIBIYA, Student Number , hereby declare that this research project, which has been submitted to the Central University of Technology, Free State for the degree: Master of Engineering in Electrical Engineering, is my own independent work; complies with the Code of Academic Integrity, as well as other relevant policies, procedures, rules and regulations of the Central University of Technology, Free State and has not been submitted before by any person in fulfilment (or partial fulfilment) of the requirements for the attainment of any qualification.

Student Signature:

Date: 06 December 2020

DEDICATION

I dedicate this dissertation to the memory of my father, David Sibiya. To my Almighty GOD, for the wisdom and strength that he gave me throughout this work. To myself, for maintaining courage, without losing focus and to my mother, Topisa Zondi Sibiya.

ACKNOWLEDGEMENTS

Primarily, I would like to thank the Almighty God for granting me wisdom and providing all these opportunities. Eternal Glory to our Almighty Father, His Son Jesus Christ and the Holy Spirit! Amen!

Furthermore, I would like to express my sincere appreciation to my supervisors, Dr Papy Bubele Numbi and Prof Kanzumba Kusakana, the unfailing and selfless support they provided during the study. For finding new ways to challenge me, guiding me every step of the way, their inspiration and further, for instilling drive and purpose in finalizing this work.

I would like to express my appreciation to Ms Khanyisa Shirinda, Mr Stephan Marais and Mr Percy Andrew Hohne, for their time and patience, assisting me throughout this study. I would like to further, to thank my colleagues Mr Sibonelo Mkhize, Mr Ngwazi, Vuma Mlaba and Mr Stanley Nkonyane, for their assistance during the course of this research.

Gratitude to my late father, David Sibiya, for his unwavering stringent manner in which he raised me, for continuously pushing me to be a better person, a better man. To my mother, for her love and support. To my two sons, Brilliant, Michael, for filling my life with joy.

Finally, I would like to thank the Central University of Technology (CUT), for granting the opportunity, support and financial assistance to undertake this research study.

Thank You.

ABSTRACT

Underground pipelines play a significant role throughout the world as a means of transporting potable and raw water, oil and gases over distances of various lengths; from the source to the ultimate consumers. In South Africa, particularly in KwaZulu-Natal, these pipelines run mostly in remote mountainous areas, to achieve shorter routes.

Due to high connection costs and low electricity consumption rate for Cathodic Protection (CP) systems, a remote electrification through grid extension is needed, which is a challenging solution. Furthermore, it is difficult to recover the initial investment costs, as monthly electricity payments are made for each Transformer Rectifier Unit (TRU), installed along the servitude pipeline.

This Dissertation discusses the use of renewable energy sources, namely, the wind and solar, powering the Impressed Current Cathodic Protection (ICCP) systems, providing protection against corrosion of underground pipelines used for distribution. In this study, an off-grid hybrid wind-solar photovoltaic (PV) system is used, to supply DC current to an ICCP system, with the aim to eliminate the need for grid power in remote CP systems, while further optimizing the running costs. However, due to the unavailability of continuous energy from the sun and the wind, energy storage systems are required to ensure the continuity of power supply, hence improving the reliability of the system.

To demonstrate the technical and economic feasibility of an off-grid hybrid wind-solar PV system, a TRU site located at Ndwedwe Reservoir 2, in Durban, is used as a case study, as this site contains adequate wind and solar irradiance. The purpose of this study is to investigate the technical and cost effectiveness of the proposed off-grid hybrid renewable energy system, by making use of the renewable resources, whilst eliminating the use of grid electricity to supply CP systems.

The sizing of the proposed system is performed using a Hybrid Optimization Model for Electric Renewable (HOMER). The model is then simulated to evaluate the technical performance of the system using MATLAB/Simulink. Furthermore, the baseline system is established, which consists solely of energy supplied by the grid. The proposed system is simulated and compared to the baseline system. The simulations showed that the system

successfully meets the load demand, for various operating conditions, in a South African case.

The prototype of the proposed system is finally carried out to test the smart control and monitoring of the CP system, with the unit being supplied by wind and solar energy. The obtained results reflect that the proposed system is feasible, implementable and viable.

The economic analysis is conducted for a projected period of 25 years, for both the baseline and the proposed system. Results from the analysis indicate that the proposed system would break-even within the first 3 years, with an approximate saving of 87%, translating into savings of R 2 438 259.34, while giving a "true" payback period of 10 years. This clearly demonstrates that the user could save significant energy costs if the system is implemented.

Nonetheless, the study further showed that the use of renewable energy in the CP may be beneficial for pipeline users in South Africa and beyond.

TABLE OF CONTENTS

LIST OF FIGURES

LIST OF TABLES

NOMENCLATURE

A	Total area of a PV panel, Swept area [m²],
AB	Annual benefits
a	Annual increase of 10%
β	Shape/Form Factor, Angle of blade pitch (º)
C_0	Initial investment cost
C_{BAT}	Battery capacity [Ah]
C_{cap}	Initial capital cost for each component [R]
CF_t	Net cash flow of the investment in year [R]
CF_o	Initial cost (first net cash flow) [R]
CF_n	Cash flow at year n
C_{EC}	Annual energy cost for the first year
$C_{initial\text{-}EC}$	Cumulative cost of energy at the end of year one [R]
$C_{initial\text{-}OM}$	Operation and maintenance cost for the first year
C_j	The TOU electricity tariff [R]
C_{OM}	Operation and maintenance cost for the first year
C_p	Power coefficient of a turbine
$Coeff_{VolTemp}$	Voltage temperature coefficient
$Coeff_{CurTemp}$	Current temperature coefficient
C_{TC}	Total annualised costs of a system
C_{rep}	Initial capital cost for each component
$C_{rep\text{-}BAT}$	Replacement cost for batteries
$C_{rep\text{-}MPPT}$	Replacement cost for MPPTs
$C_{rep\text{-}WT}$	Replacement cost of wind turbine

$C_{rep\text{-}PV}$	Replacement cost of solar panels
$C_{rep\text{-}BC}$	Replacement cost of battery charger
$C_{salvage}$	Salvage cost
CRF	Capital recovery factor
D	Turbine diameter [m]
E	Energy [kWh]
E_{emf}	Electromotive force
F_c	Coating breakdown factor
G_I	Global solar irradiance [W/m^2]
H	Turbine height [m]
H	Annual average solar radiation on tilted panels [h]
I_{SC}	Short circuit current
I	Output current
I_{adjmax}	Maximum current at high temperature
I_d	Reverse saturation current of a diode
I_{mp}	Current at maximum power
I_{ph}	Photocurrent
I_{sh}	Shunt current
i	Discount rate
J	Design electric current for bare steel (mA/m^2)
J	Local current density
k	Year at which the cumulative cost should be calculated
K_{ZO}	Coefficient to lay the anode underground
L	Length of the pipeline
LCC_{Grid}	Lifecycle cost of the grid
M	Water mass [kg]

N	Lifespan of the system or a specific component [years]
N_{rep}	Number of component replacement
n	Project period, lifespan of a component
P	Power
PR	Performance ratio (coefficient for losses)
PW_{TB}	Present worth of total benefits
$PW_{TB\text{-}av}$	Annual average of present worth of total benefits
PW_{TC}	Algebraic sum of the discounted project costs
P_{WT}	Power generated by wind turbine
P_{PV}	Power generated by solar panels
P_L	Power required
P_m	Module output power
P_{net}	Net power
P_g	Generated power
P_{rad}	Power of solar irradiance
R	Turbine radius [m]
R_{sh}	Shunt resistor
R_s	Series resistor
P_{Grid}	Power allowed from the grid [w]
r	Average inflation rate, Outer radius of the pipeline, efficiency
S	Seebeck coefficient
$T_{LocalMin}$	Local minimum temperature
T_{CelAdj}	Cell maximum temperature
T_m	Mechanical torque
T_{STC}	Temperature at standard coefficient
t	Time [s]

x	Distance of the anode [m]
v	Capacity of the reservoir [m^3]
V	Local voltage
V_{max}	Maximum operating voltage
V_{mp}	Voltage at maximum power
V_{oc}	Open circuit voltage
v_w	Wind speed
Z_e	Depth of the electrode
σ	Local conductivity
μ	Average/mean wind speed, efficiency
ρ	Air density [Kg/m^3]
∇T	Temperature gradient
Δt	Change in Sampling time [s]
US$	US Dollar [$]
ZAR (R)	South African rand

ABBREVIATIONS

AC	Alternating Current
AB	Annual Benefits
BCR	Benefits-to-Cost Ratio
BEP	Break-Even Point
BESS	Battery Energy Storage System
CCVT	Closed Cycle Vapour Turbogenerators
CF	Cash Flow
CRF	Capital Recovery Factor
COE	Cost of Energy
CP	Cathodic Protection
CPU	Cathodic Protection Unit
CT	Current Transformer
DC	Direct Current
DOD	Depth of Discharge
DoE	Department of Energy
Eskom	South African Electric Utility Company
ESS	Energy Storage System
FIT	Feed-in-Tariff
FV	Fixed Voltage
GHI	Global Horizontal Irradiance
GDP	Gross Domestic Product
HAWT	Horizontal Axis Wind Turbine
HDS	High Demand Season
HOMER	Hybrid Optimization Model for Electric Renewable
IC	Increment Conductance
ICCP	Impressed Current Cathodic Protection
IRR	Initial Rate of Return
KZN	KwaZulu-Natal
LDS	Low Demand Season
LCC	Life Cycle Cost

MATLAB	MATrix LABoratory
MPP	Maximum Power Point
MPPT	Maximum Power Point Tracking
NASA	National Aeronautics and Space Administration
NMD	Notified Maximum Demand
NPC	Net Present Cost
NPV	Net Present Value
NREL	National Renewable Energy Laboratory
O&M	Operation & Maintenance
PBP	Payback Period
PID	Proportional Integral Derivative
PMSG	Permanent Magnet Synchronous Generator
P&O	Perturb and Observe
PV	Photovoltaic
PW	Present Worth
RSA	Republic of South Africa
RE	Renewable Energy
RES	Renewable Energy System
RMS	Root Main Square
SACP	Sacrificial Anode Cathodic Protection
SAURAN	South African University Renewable
SCADA	Supervisory Control And Data Acquisition
SOC	State of Charge
SPP	Simple Payback Period
TEG	Thermoelectric Generator
TOU	Time-of-Use
TRU	Transformer Rectifier Unit
USA	United State of America
VAWT	Vertical Axis Wind Turbine
WT	Wind Turbine

CHAPTER 1: INTRODUCTION

1.1 BACKGROUND

Water in South Africa is scarce and costly, particularly in cities, such as Cape Town, where water reticulation pipelines extend thousands of kilometres, mainly at high pressure buried steel pipelines. These steel pipelines corrode with time and give rise to water leakages, leading to water shortages. Corrosion is frequently set as the deterioration of steel material properties, as a consequence of an interaction with its environment [1]. A lot of significant amount is invested in Cathodic Protection (CP), to add on coating in order to maximize corrosion prevention in underground water pipelines [2]. However, there is doubt that the investment is paying off. CP is the application of an external power source to the underground pipeline, with the intention to shift its potential in order to mitigate corrosion, hence the name of ICCP (Impressed Current Cathodic Protection) [3].

Corrosion takes place as an electrochemical process, where current leaves a metal structure at a certain point (Anode), flows through an electrolyte and enters the structure at a different point (Cathode). This phenomenon is due to potential differences along the pipeline, which according to the principle of thermodynamics, the material constantly seeks the point with the lowest energy state [4, 5].

The process whereby metals convert to lower energy oxides, is called corrosion electrochemical. Without any disregards, the main mitigation of pipelines corrosion, is by coating. However, coating does not maximize prevention of corrosion in pipelines, hence coating alone is not sufficient for prolonging the lifespan of pipelines, or either slowing the rate down of corrosion in underground or buried pipelines, as is seen in Figure 1.1.

Figure 1.1: Corroding pipeline [6]

This raises a dilemma as to what other means of pipeline protection may be applied to prevent preventing pipelines from corrosion. Since corrosion is a result of current flow, which is basically the flow of electrons from anode to cathode as mentioned above, an electrical solution has been proposed, to prevent corrosion by slowing down the rate of corrosion in underground pipelines, using a DC power source.

CP system is utilized in South Africa at a high rate. The newly installed pipelines are installed with an ICCP system. However, it becomes a challenge in most areas of KwaZulu-Natal (KZN), to get a point of supply to power the TRU, due to the areas containing sizable mountains, where the pipeline has to run in between the mountains to achieve the gravity required to push the water. In connection to the above, the CP project becomes costly and takes long periods of time to complete. This further leads to a high maintenance cost, due to the manual data collection to monitor the system.

Occurrence of corrosion involves four components, as shown in Figure 1.2. These are: an electrolyte (water), a cathode (part of metal or pipeline that does not corrode), an anode (part of metal or pipeline where corrosion occurs) and an electrical pathway (the path taken by electrons to move from anode to cathode) [7]. This research will solely focus on the development of intelligent ways of monitoring and controlling the buried pipeline health and utilizing renewable energy as a power source.

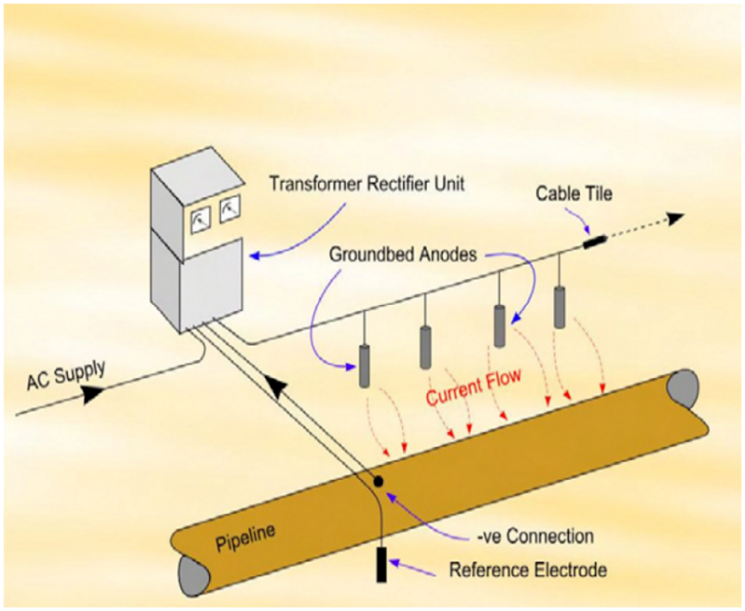

Figure 1.2: Typical ICCP system [8]

1.2 PROBLEM STATEMENT

Cathodic Protection systems are being utilized all over the world, including in South Africa, at a significantly high rate. The newly installed pipelines are installed with an ICCP system. However, it becomes a challenge in most remote and isolated areas, to obtain a point of supply from the electrical grid to power the TRU, due to the areas such as mountains where the pipeline should run in between the mountains, to achieve the gravity required to push the water. Furthermore, even though there is a connection point, the charges from the grid are way higher than the cost of energy consumed, which is an economic drawback. Moreover, the CP project ends up being costly and takes a long period of time to complete. This further leads to a high maintenance cost, due to the manual data collection, to monitor the system.

1.3 AIM AND OBJECTIVES OF THE STUDY

The aim of this work is to develop a smart control and monitoring system of Impressed Current cathodic protection, running on renewable energy, based on DC to DC choppers. The objectives of this research are:

- To design an isolated renewable energy supply system that will be sufficient to power an ICCP system, with remote monitoring and smart control capabilities to enhance reliability.
- To model and simulate performance of the wind and solar-PV Hybrid system with an ICCP system.
- To build a prototype of the CPU supplied by a wind solar-PV hybrid system for experimentation.
- To conduct economic analysis to evaluate the return on the investment and payback period of the developed system.

1.4 RESEARCH METHODOLOGY

To achieve the objectives of the study, the methodology is as follows:

The study is conducted in the selected study region, to investigate application of an off-grid hybrid wind solar PV system, on impressed current cathodic protection. Literature related to the cathodic protection subject, was conducted on factors affecting the proposed

system. This covers all aspects, such as steel pipeline corrosion, types of pipe corrosion, ways of mitigating pipeline corrosion, various types of ICCP power supplied methods related to cathodic protection. A few of the reviews further covered the SA case; context or opportunity for suppling CP with renewable energy.

The TRU load consumption of a pipeline, running from Hazelmere Water Works, to Ndwedwe Town Reservoir, was recorded over a period using the Efergy E2 Data logger. In addition, the tariff structures were retrieved from the electricity supplier brochure of the year 2018/2019, including the bills for TRU selected and a few others used by Umgeni Water. Moreover, the solar radiance and wind speed for the year 2018/2019, were retrieved from the Southern African Universities Radiometric Network (SAURAN) website. The solar radiance was further obtained using Solarius PV software for the selected site.

Optimal sizing of the proposed off-grid hybrid Wind Solar PV System with battery storage, is determined through the use of HOMER (Hybrid Optimization Model for Electrical Renewable Energy) software. The recorded load demand, wind speed extracted from SAURAN, as well as solar radiance extracted from Solarius PV, are used as input parameters, to size the system that will fulfil the load requirement at the study site.

The simulation and modelling are conducted in MATLAB/Simulink. Moreover, it includes the development of an off-grid hybrid wind solar PV model, with a battery storage.

The implemented prototype is constantly at a small scale, to practically evaluate the proposed system, as well as for experimenting the smart control and remote monitoring capabilities. The system is designed using proteus and programmed with Arduino, for simplicity purposes.

An economic analysis was conducted for the resulting size of the off-grid Hybrid renewable system. In the simulation, the baseline (Grid supplied TRU) is compared to the optimized system life cycle cost (LCC), followed by the break-even point and true payback period analysis, conducted for a projected period of 25 years.

1.5 OUTCOMES OF STUDY

With the completion of this research study, a cost-effective CP system in South Africa has been developed. This system is self-monitoring and auto-controlled to maintain the integrity of the pipeline, by preventing over, or under protection, at any given time. Below are the categorised outcomes, driven from the above statement.

- Scientific outcomes:
  - An intelligent ICCP system working on an off-grid hybrid wind and solar system with battery storage.
  - A CP system that returns the investment within 10 years after installation.
  - A Masters dissertation and publications.
- Social and environmental impact:
  - An improved, efficient, cost-effective and environmentally friendly CP technology.
  - Increased awareness level of energy saving, through the use of green energy in South Africa
- Innovations
  - New purely DC cathodic protection units (CPU) developed using choppers and running completely off-grid.

1.6 DELIMITATION OF THE STUDY

The study is carried out with the following limits:

- Modelling of electronic and mechanical control circuits for power, will not be part of this research.
- This study does not suggest any new turbines or designs, as wind turbines and PV panels are currently widely available.

1.7 CONTRIBUTION TO KNOWLEDGE

- Propose potential technologies and developments of renewable energy supply for CP system, with monitoring and control units, within the South African context.
- Developing a unique model to study the use of renewable energy to power CP systems protecting water, oil and gas steel pipelines from corroding.

1.8 RESEARCH OUTPUT

Conference papers:

- Sibiya Cyncol Akani, Kanzumba Kusakana and Bubele Papy Numbi. "Smart system for Impressed Current Cathodic Protection running on hybrid renewable energy". In *2018 Open Innovations Conference (OI)*, pp. 129-133. IEEE, 2018.
- Sibiya Cyncol Akani, Kanzumba Kusakana and Bubele Papy Numbi. "Design of a Cost Optimized Hybrid Renewable Energy system for Impressed Current Cathodic Protection". In *2020 IEEE 29th International Symposium on Industrial Electronics (ISIE)*, pp. 965-970. IEEE, 2020.

Journal papers:

- Sibiya Cyncol Akani, Kanzumba Kusakana and Bubele Papy Numbi. "TRU energy monitoring for potential cost saving in electricity bills for cathodic protection units: South African case."Accepted for publication in *International Journal of Electrical and Electronic Engineering and Telecommunications (IJEETC).*
- Sibiya Cyncol Akani, Kanzumba Kusakana and Bubele Papy Numbi. " Modelling and simulation of a hybrid renewable/battery system powering a Cathodic Protection Unit". Accepted for publication in *International Journal of Electrical and Electronic Engineering and Telecommunications (IJEETC).*
- Sibiya Cyncol Akani, Kanzumba Kusakana and Bubele Papy Numbi. "Development of a smart control and monitoring system for impressed current cathodic protection running on hybrid renewable energy". Accepted in *Energy Reports*.

1.9 OUTLINE OF THE DISSERTATION

Chapter 1 introduces the dissertation, which outlines the context, problem statement, goals, methodology, hypothesis, study delimitation, as well as the outcomes of the research.

Chapter 2 provides an overview of cathodic protection, how ICCP systems are being used and the potential of CP system running on off-grid renewable energy in South Africa. This Chapter further outlines the possible ways of supplying ICCP systems with their advantages and disadvantages, as well the monetary benefits, followed by a thorough survey on the operation principles of wind turbine, solar panels and their components.

Chapter 3 develops the design and optimal sizing of the proposed off-grid hybrid system with battery storage, and performs its techno analysis using HOMER software.

Chapter 4 covers the development of the proposed off-grid hybrid wind solar PV model, as well as the discussion of the simulation results obtained. The performance of the proposed system is analysed for various weather conditions, to reveal its reliability using MATLAB/Simulink.

Chapter 5 presents the prototype and experiments of the proposed ICCP system, outlines the methods and tools used, as well as the obtained results and discussion.

Chapter 6 presents the economic analysis of the proposed system. The financial implications of the system are analysed, based on their life expectancy. The process of analysis is carried out using various methods that include lifecycle cost and payback period analyses.

Chapter 7 presents the conclusion of this dissertation and provides recommendations for future areas of research.

CHAPTER 2: LITERATURE REVIEW

2.1 INTRODUCTION

A brief overview of the status and potential of ICCP schemes in South Africa is given in this Chapter. Water is a basic and important need of life. Furthermore, it is also one of the leading components of economic growth in the agricultural sector. However, since water is collected in dams and later distributed to reservoirs for consumption, steel pipelines are used to distribute water at a high pressure. Metallic structures, such as steel pipes in contact with water, soil, concrete and moist air, are subject to corrosion. CP is one of the few methods that successfully mitigates corrosion, together with Coating, as a primary preventative method.

2.2 REVIEW ON STEEL PIPELINE CORROSION

By definition, corrosion is a process in which metals return to their oxidized form [9]. Pipeline corrosion is the deterioration of pipe material due, to its interaction with the working environment, which leads to damage of the metals [10]. Pipeline corrosion causes pipe leakages, that result in poor to no supply of oil, water, gas or any pipe transported substance and hence, costs billions of Rands to the economy. A report that the U.S. published in 2002, the Federal Highway Administration reported that the direct cost of corrosion in the United States was $276 billion per year or around 3% of the GDP of the country [11]. In other words, pipeline corrosion is a concern for every pipeline dependent industry. It affects all pipelines comprised of metals, copper, aluminum, cast iron, carbon steel, stainless steel and alloy steel pipes, used for buried, underground or submerged pipelines [12].

2.2.1 Pipeline Corrosion

In certain circumstances, such as moist ground with organic material (through a marshy or marine environment), or the presence of polluted water containing dissolved salts or weak acids, the ground itself may have a highly corrosive action on any buried unprotected steel pipe or pipeline. This will initiate the process in which metals returns to their oxidized

forms, causing the pipeline to corrode [13]. The pipeline may as well act as an electrical conductor from some external sources, such as electrified railway line or high voltage transmission lines. In the case where a steel pipeline with small or minor defects in the protective layer or coatings, significant rapid corrosion of the line may be caused, due to the of current flowing away from the pipe through these pinholes. The exposed section of the pipeline becomes anodic, causing the flow of current to the cathode, resulting in the consumption of metal from the anode. The amount of metal that will degrade, or be removed, is directly proportional to the amount of current flow.

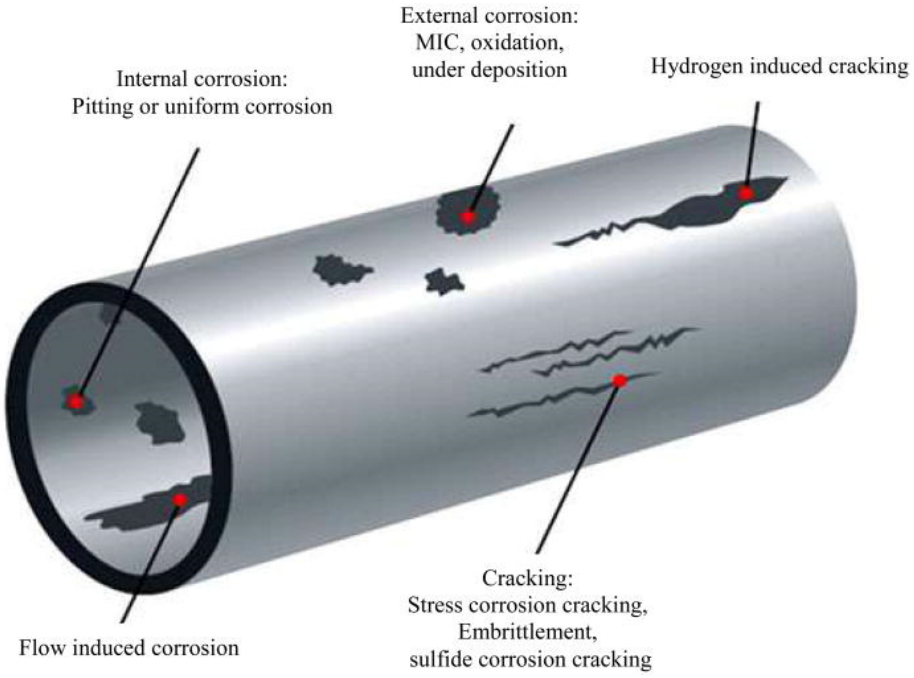

Figure 2.1: Steel pipeline corrosion types [14]

The corrosion of most pipelines occurs due to an electrochemical reaction in the presence of an electrolyte [15] and the resulting types of corrosion are shown in Figure. 2.1. a few of the factors contributing to pipeline corrosion are:

- The oxygen content or reactivity of liquids and gases carried
- The use of dissimilar metals within the piping system
- The temperature, flow rate and pressure of the fluids

2.2.2 Types of Pipeline Corrosion

Corrosion is a significant challenge in pipelines. However, in partaking on how to mitigate this issue, one has to look closely on what makes the pipeline to corrode. Tabulated below are types of pipeline corrosions, their description, causes and possible methods of prevention.

Table 2.1: Corrosion types and methods of prevention [14]

Type of corrosion	Description	Method of prevention
Uniform pipe corrosion	• As the name indicates, uniform pipe corrosion causes uniform loss of the material along the surface of the pipe. • Continuous thinning of a solid structure.	• Cathodic protection • Surface coatings
Stress Corrosion Cracking	• Stress corrosion damage in corrosive environments is the development of pre-existing cracks. • It may lead, particularly at higher temperatures, to the sudden failure of ductile metal pipes under tensile stress. • In the case of alloys, cracks develop quickly, but failure occurs only if the amount of stress reaches a particular threshold level.	• Limiting the loads to ensure that they are below levels of threshold stress.
Stray Current Corrosion	• The movement of stray currents through pipelines, induces stray current corrosion. • This may cause localized pitting on metal surfaces and pinholes at the specific points where the surface is left by stray currents. • Electric railways, electric welding machines, earthed DC source and cathodic protection, are caused by high voltage overhead or buried lines, nearby.	• Controlling electricity leakages • Bypassing stray current to an earth • Additional protective system
Cavitation Corrosion	• In a pipeline, cavitation damage occurs when the operating pressure of the fluid decreases below its vapor pressure, leading to the creation of vapor pockets and vapor bubbles collapsing on the inner surface of the pipeline.	• Avoided at the design level by reducing gradients of fluid pressure and unnecessary pressure drops in the liquid vapor

	• Corrosion by cavitation may further contribute to erosive corrosion.	pressure range, as well as ensuring zero air entry. • Coatings
Selective Leaching	• Selective leaching, or graphitic corrosion, occurs when an alloy is formed by a noble metal and a more reactive material. • Causes a leakage of reactive elements from the surface of the pipeline, causing strength loss and premature failure.	• Cathodic protection
Galvanic Corrosion	• Galvanic corrosion occurs when electrically attached to dissimilar alloys or metals with varying corrosion potential. • Solely the metal work as an anode may deteriorate, in comparison to the other.	• Combination of metals that are closer in the galvanic series • Applying insulation (Coatings)
Crevice Corrosion	• Crevice corrosion is caused by an accelerated reaction due to unequal oxygen availability at joints and other crevices of a pipeline. • The oxygen starving surfaces become the anode in an electrochemical reaction.	• Replacing riveted joints with welded joints
Intergranular Deterioration	• Intergranular deterioration refers to the selective deterioration at the grain boundaries of a surface (due to elevated temperature), when the grain boundary exceeds high corrosion-prone activity. • Heat treatment and heat welding may cause this conversion, resulting in corrosion.	• Selecting extra-low carbon stainless steel materials.
Erosion corrosion	• Erosion corrosion is caused by the relative movement of fluid and the pipe's inner surface. A rapid increase in erosion rates may result from fluid turbulence. • This may result in a high erosion rate	• The addition of chromium or molybdenum to steel may improve corrosion protection.

2.3 DESCRIPTION OF DIFFERENT METHODS FOR MITIGATING CORROSION

The available options for mitigation corrosion include coating and cathodic protection. The coating is usually used as a basic method of corrosion prevention. However, coating alone does not ensure complete corrosion prevention. Hence, cathodic protection is considered as an additional way of mitigating corrosion.

2.3.1 Coating

The coating is a covering applied on the surface of the pipeline, oftentimes referred to as a substrate and is used to prevent the pipe surface to come into contact with the environment. In Ref. [16], it is explained that pipes are subjected to harsh environmental conditions that may damage the pipeline coatings. Moreover, manufacturing imperfections, mechanical or thermal stresses, misused handling, trenching backfill rocks, solvents and bacteria in the surrounding soil, may damage coatings and lead to accelerated corrosion. Ref. [17] states that, corrosion accounts for 67.5 % of pipeline breaches, mainly due to the corrosion of external pipeline coatings, according to the Alberta Energy Regulator. As there is no ideal coating, however, cathodic protection is used to minimize the process of corrosion, where defects (holidays) or breaches occur on the surface of the pipe. This contributes to the control of corrosion prevention in advance and the overall integrity protects the pipeline.

2.3.2 Cathodic protection

In South Africa, due to long distances and extensive stray currents, all buried metallic pipelines including water, oil, gas and other hazardous pipelines, should be protected against external corrosion by the application of an external coating and cathodic protection [18]. By definition, Cathodic protection is a technique used to control the corrosion of a metal surface, by making it the cathode of an electrochemical cell. The principle of CP aims to reverse the electromechanical role of the pipeline, by substituting or deferring the role of the structure to be protected on another structure, that will accept the degradation though oxidation reaction [19, 20]. CP may be implemented in two different ways: which

impressed current cathodic protection (ICCP) and sacrificial anodes cathodic protection (SACP)[21].

A. Impressed current cathodic protection (ICCP)

ICCP is a corrosion prevention process, whereby DC power source or supply is used to overcome corrosion. This is commonly carried out using a TRU as a direct current power supply [5, 7]. The supplied DC power is delivered to the anode groundbed that showers the pipeline with electrons. When designing an ICCP system, availability of desired electrical energy and rectifier type turn to be the key factors[18]. Figure. 2.2 below, shows an ICCP system followed by the formulas used to qualify the current and power requirements when designing an ICCP system. Eq. (2.1) [18], is used to determine the current requirements.

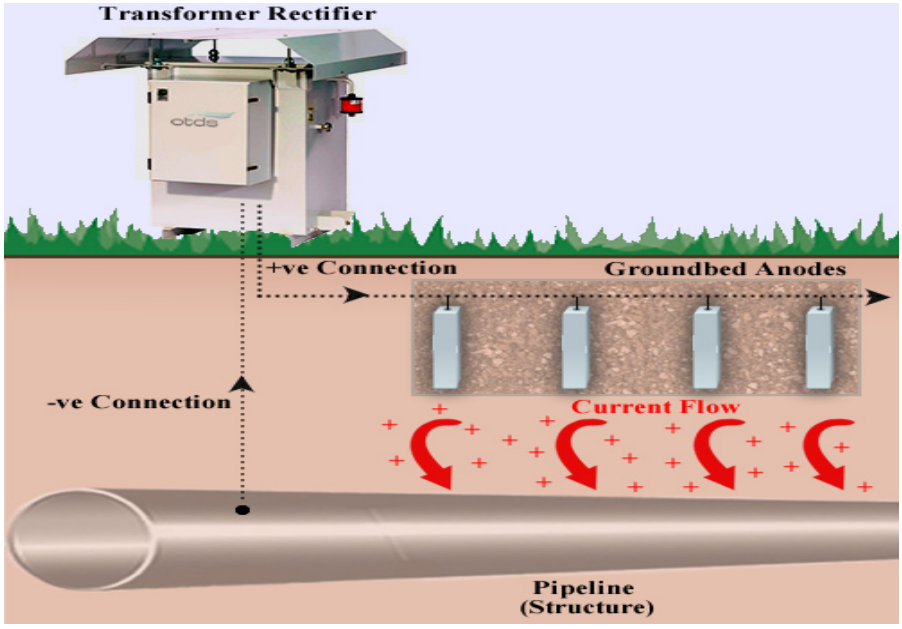

Figure 2.2: ICCP system[22]

$$I_{tot} = J \times F_c \times 2\pi rL\ , \tag{2.1}$$

Where: F_c is the coating breakdown factor; r is the outer radius of the pipeline (m); L is the length of the pipeline; J is the design electric current for bare steel (mA/m^2).

To determinr the power requirement Eq. (2.2) adopted from [23] is used;

$$P(i,x) = f(i_e) + K_{zo} \times Z_e, \tag{2.2}$$

Where: P= Power (W);

x= Distance of the anode (m);

i= Current density (A/m²);

Z_e= Depth of the electrode ;

$f(i_e)$= Polarization curves of cathode and anode ;

K_{zo}= Coefficient to lay the anode underground.

B. Sacrificial anode cathodic protection (SACP)

SACP is a form or way of practicing CP, without the use of external power. This form of CP is used to temporarily protect newly installed pipelines, or existing pipelines. It is used for the long term, where maintenance of an ICCP system in a certain area is impractical. Moreover, SACP is further used where remote ICCP systems cannot be implemented, in extremely cold areas, such that the soil freezes under thermal insulation on thermally insulated pipelines [18, 24]. A typical SACP system is shown in Figure. 2.3.

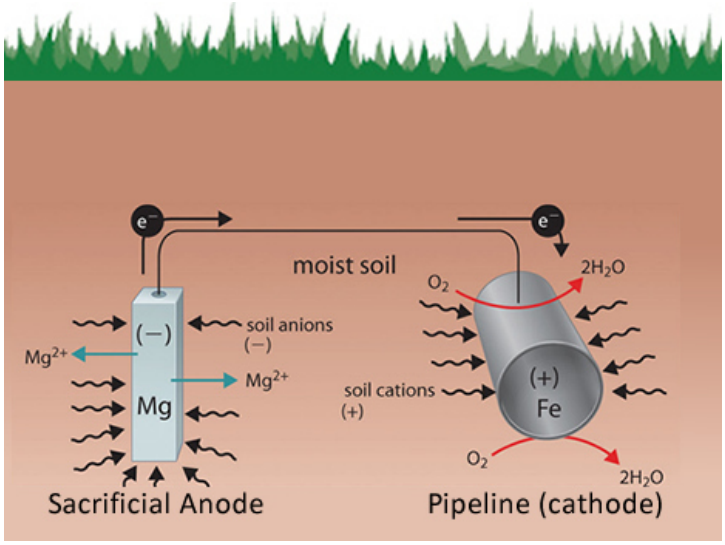

Figure 2.3: SACP system [25]

2.4 REVIEW, DESCRIPTION AND OPERATION OF VARIOUS CP POWER SUPPLIES

AC power Although most ICCP systems utilise AC power for supply, if AC powerlines are not available, many other power sources can be used in conjunction with rectifiers as a source of DC current. For some time, some of these have been in use, others are relatively new and some are in the stage of development. Many of these sources of alternative power

are expensive. The corrosion engineer should therefore make sure that the same degree of safety cannot be obtained by other means, such as galvanic anodes (SACP) [2], at less expense.

2.4.1 AC powered CP systems

AC power is the main and most popular, or most common supply of power to the TRU units [2]. However, there are alternative ways of supplying power to the units. Figure 2.4 below shows a typical application, where a TRU unit, to practice an ICCP system, is supplied with AC power. In this form of application, the supplied power should be converted from AC to DC, using a rectifier [26]. Depending on demand current, this application may be of three-phase or single-phase orientation. To use AC power for CP, power applications should be carried out with the service provider in the area of installation. It may be Eskom or the area Municipality. These applications, however, are costly and time consuming, hence, in most cases, temporary CP is required for the period where AC powerlines are still under construction [27].

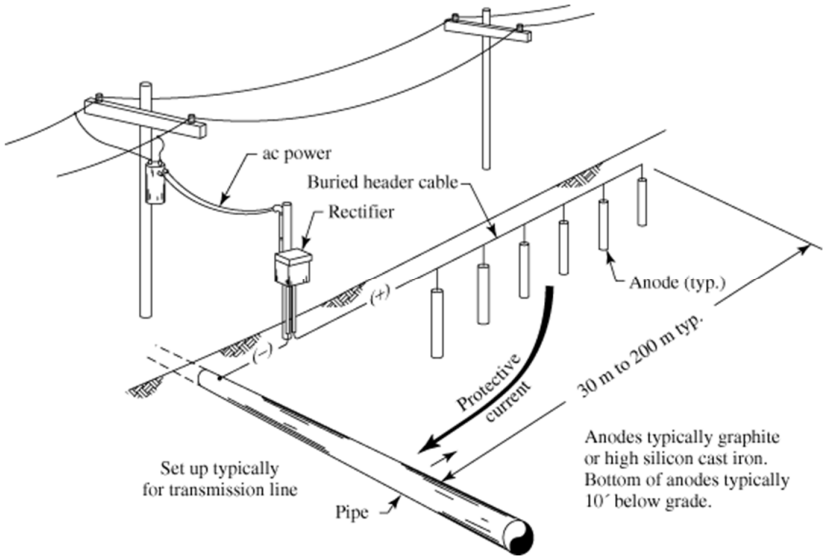

Figure 2.4: ICCP implemented using AC power with TRU[28]

2.4.2 Wind turbines CP installations

Wind-powered generators may be used to supply power to CP systems, where sufficient prevailing winds are available, for an acceptable period. However, this is not the most preferable method to supply power to CP installations, due to the high maintenance requirement, lack of reliability and more cost-effective methods, such as Solar panels and

thermoelectric generators being available. Furthermore, due to the behaviour of wind power, storage batteries will need to be used in conjunction with the system, to help make the wind power steady, continuous and reliable. However, wind energy systems are more in use in remote areas than in other areas, where a variety of other sources are available, due to the convenience of other systems in comparison to wind power [29].

The use of wind energy to power cathodic protection has not been well exploited, particularly in South Africa. However, studies show that wind energy is considered as one of the most cost-effective, compared to other renewable energy sources [30]. Furthermore, the potential wind power available in Africa as a whole, is 109 000 MW, with most of this energy situated in coastal areas, which favours the larger part of places in South African edges [29, 31]. However, from 2017 reports, solely up to 0.81% of the total world capacity is found in Africa [32]. Nevertheless, South Africa has a total amount of approximately 47% wind energy capacity, compared to other African counties, which clearly shows that RSA has a great interest and support of wind energy generation.

In the remote areas where solar radiance may be highly expected throughout the year, a PV system with a battery bank could possibly supply a certain output of power to a CP installation. This power may meet the demand, when evaluated and with the correct sizing of the PV system [33]. Furthermore, this kind of installation could be used to supply continuous flow of current to CP systems. Figure. 2.10 shows an example of how an ICCP installation, using solar energy, is configured.

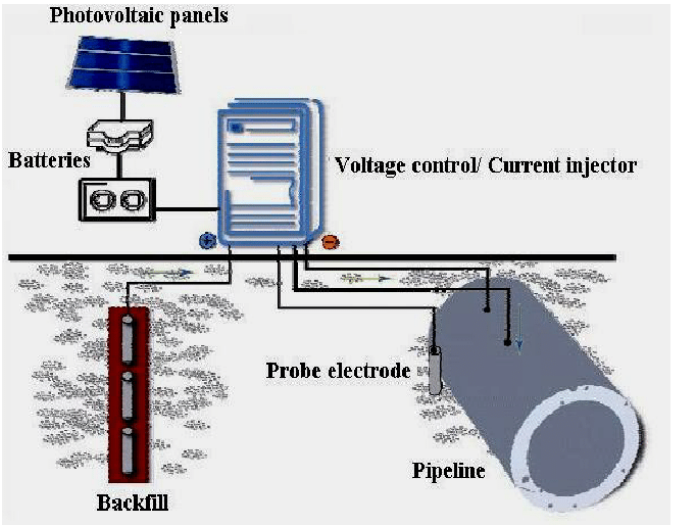

Figure 2.5: Solar based schematic design of ICCP system [34].

2.4.4 Engine Generators

An Engine Generator produces a steady current at a specified voltage, therefore, some steel pipelines contain natural gas and a few petroleum products, that are suitable to fuel the engine generators. If the pipeline contains chemicals of the form mentioned above, with no means to obtain AC power lines, Engine Generators may be utilised to power ICCP systems. In this case, the gas or fuel contained within the pipeline will be used to fuel the generator, making the system reliable, while eliminating the need for fuel transportation to the site. However, water pipelines contain no fuel, solely water, hence fuel should be transported to site at regular intervals, with close monitoring, to ensure the generator does not run out of fuel [35]. In Figure. 2.11 below, is a typical Engine Generator installation on ICCP systems protecting the pipeline against corrosion.

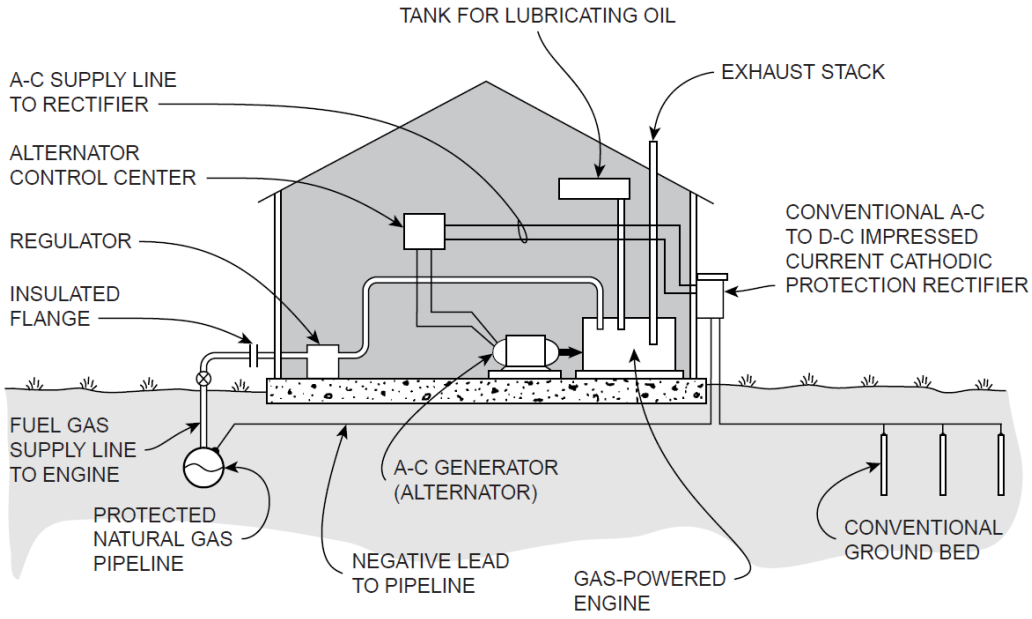

Figure 2.6: Engine generator based CP installation [35]

In this application, periodical transportation of fuel to the site will significantly contribute to the operation costs and may affect the reliability of the system. Engine Generators mainly produces AC power, hence a TRU unit will be required to transform the voltage to a level required and then rectified to DC, to match the form of power required by the application [35].

2.4.5 Gas turbine

A DC generator may be coupled to a gas turbine, which may be used on natural gas pipelines, to generate DC power and supply current to CP systems, installed to protect the pipeline. Pressure measurements will be required to ensure that sufficient pressure is available for power generation. Unlike the diesel generator, gas turbine may solely be applied on gas pipelines and not on water pipelines. However, this application is more efficient with no gas loss during power generation. Hence, gas is diverted to the turbine though a bypass line and returned back to the system, without a loss. Gas turbines may be used on producing gas fields, wellheads and transmission pipelines transporting gas. However, it should be ensured that the gas pressure is adequate for power generation. Given in Figure. 2.12 below, is an illustration of a Gas turbine, powered CP installation.

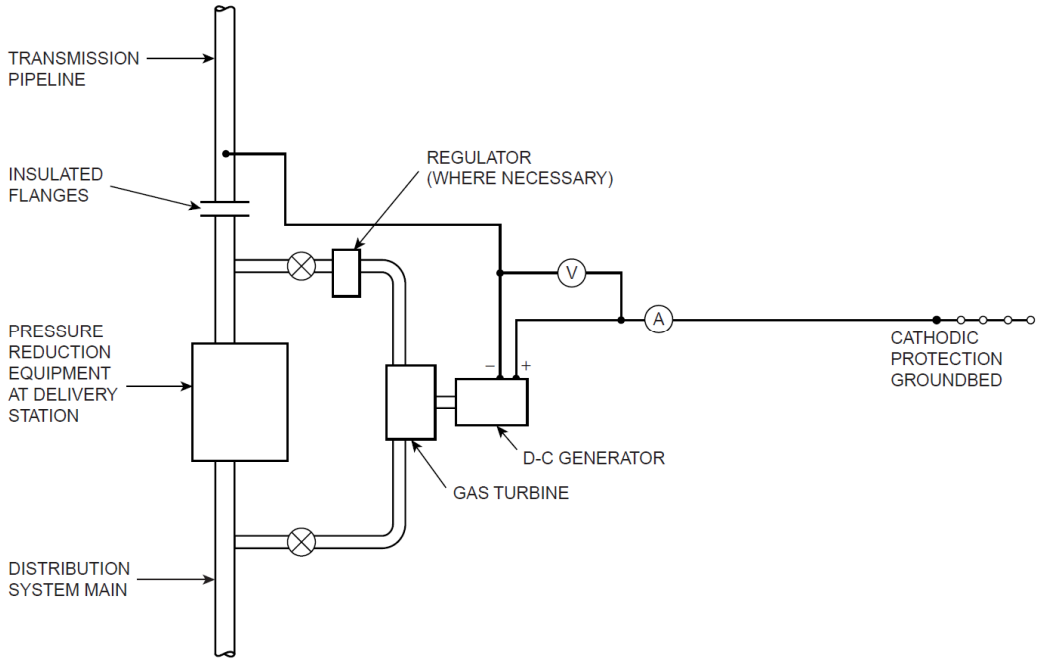

Figure 2.7: Gas turbine CP installation[35]

2.5 OPPORTUNITY IN THE SOUTH AFRICAN CONTEXT

Manual measurements, apart from their high cost and site access, may solely indicate problems after they have occurred, which may result in the pipeline being unprotected until the fault is discovered [36] . In Ref. [37], hybrid renewable energy has been used to supply CP systems in metallic structures. However, TRU's are still used to power the CP systems, which may lead to lower efficiency, due to multiple power conversion steps (stepping down the AC voltage and AC to DC conversion). CP systems require power 24/7, in times when the pipelines remain without power, corrosion occurs. In Ref. [26], studies have been conducted to use solar power to run CP systems for buried pipelines. However, no studies were carried out to ensure continuity of supply throughout the night and when weather conditions do not favour the solar energy.

It is clear from Ref. [37], that very little research has been performed on CP systems supplied by solar power or hybrid power, via a DC to DC controller, such as DC choppers. In Ref. [34], the paper investigates the corrosion of metallic structures and issues designs including the use of solar, wind and solar-wind hybrid systems to feed the CP systems. However, the system still runs using TRU and the energy management of the system is not considered, to ensure the continuity of supply. Furthermore, research conducted in Ref. [38] indicates that AC currents negatively affect. The CP systems and causes the rate of corrosion to rise.

In the past, a few successful studies on remote monitoring have been conducted, using SCADA systems, programmed using LabVIEW. In Ref. [39], studies on simulation and implementation of ICCP control were conducted and yield sufficient results. Ref. [40] studied and developed a PID (Proportional Integral Derivative) corrosion controller, using VI (Lab view). However, introducing smart programmes in the form of system logic, enabling the system to automatically adjust the level of required potential and if the readings continue to remain. Unsteady, the system should communicate to the control centre. Hence, this research will investigate the use of DC to DC choppers against TRU's, for the ICCP protected underground water pipelines.

The use of wind turbines, solar panels and hydropower, requires renewable energy that is available in areas where pipelines in SA run. Hence, this provides an advantage of taking the shortest routes in water reticulations systems designs, as a result of utilizing standalone supply units, therefore, eliminating the need for grid connected systems.

2.6 CONCLUSION

This Chapter provides a global overview of the related Cathodic Security Literature for ICCP systems, as well as the technologies and potential renewable energy sources involved. Many development studies have been carried out based, on the monitoring of the ICCP systems. There is, however, a scarcity of applications and studies demonstrating the technological, economic and environmental benefits of the off-grid hybrid system, for the supply of Cathodic safety ICCP systems. In addition, there is a lack of studies that show this proposed system's optimum sizing technique. This hinders the implementation of technologies for hybrid ICCP units, supplied with intelligent monitoring systems.

South Africa has considerable solar and wind potential, with sufficient wind and solar resources for a small to large-scale system. However, these wind and solar resources are neglected in supplying ICCP systems, since the industry is unaware of its potential benefits in reducing the energy costs for CP to close to nothing. Hence, a resource assessment study of wind and solar availability within South Africa, should be undertaken, with most of the focus based on pipeline routes. This may assist in facilitating the use of renewable energy in ICCP systems.

This Chapter further revealed various types of technologies used to supply power to ICCP systems, with solely a few being utilized in South Africa. It further, defined various types of turbines to be used for the generation of wind power, as well as the factors influencing PV panel output and how to consider them for better solar power generation. It is important to select the correct site application. Therefore in this chapter, the advantages and disadvantages of technologies for supplying power to CP systems are presented.

CHAPTER 3: HYBRID SYSTEM SIZING

3.1 INTRODUCTION

A TRU site with sufficient availability of solar and wind resources was selected in this study. A comparative economic review is required for scaling a stand-alone renewable source. The primary objective of this Chapter is therefore to optimise hybrid energy system, using the Hybrid Optimization Model for Electric Renewable (HOMER) software to achieve a cost-effective hybrid system to power an ICCP system. The use of a hybrid renewable energy system will eliminate payment costs for grid connected ICCP systems and reduce initial costs, where network extensions are required to power such systems.

3.2 DATA COLLECTION

3.2.1 Description of the selected TRU and its geographical location

The CP TRU unit identified for this case study, is found in Durban, KwaZulu-Natal at Umgeni Water Reservoir 2 of Hazelmere on the Ndwedwe bulk water distribution line. This study site was chosen merely due to its security and access availability by Umgeni Water. Figure 3.1 shows the geographical data for the study site. This is a typical South African TRU unit used for CP systems. The load demand profile is the most critical element in the optimization process from the read load profiles and demand perspective [41]. This is crucial in designing an optimal system correctly. The optimal system should meet the power demand at any given time and avoid unnecessary costs, due to the supply system being under- or over-sized. Figure 3.2 shows the TRU unit, where the monitoring device "Efergy E2 Classic" was installed. Paradigm projects have installed the unit and it is the property of Umgeni Water, Cathtect engineering manufactured the unit for corrosion prevention.

The methodology to implement this study, consisted firstly of identifying the study site, which was previously explained. Secondly, the current energy costs for the selected was requested and analysed. Thirdly, the energy monitoring device was installed on the selected TRU, with the software, to analyse the behaviour of the load. Lastly, the obtained data was

used to evaluate the proposed energy-saving techniques and recommend the most effective option.

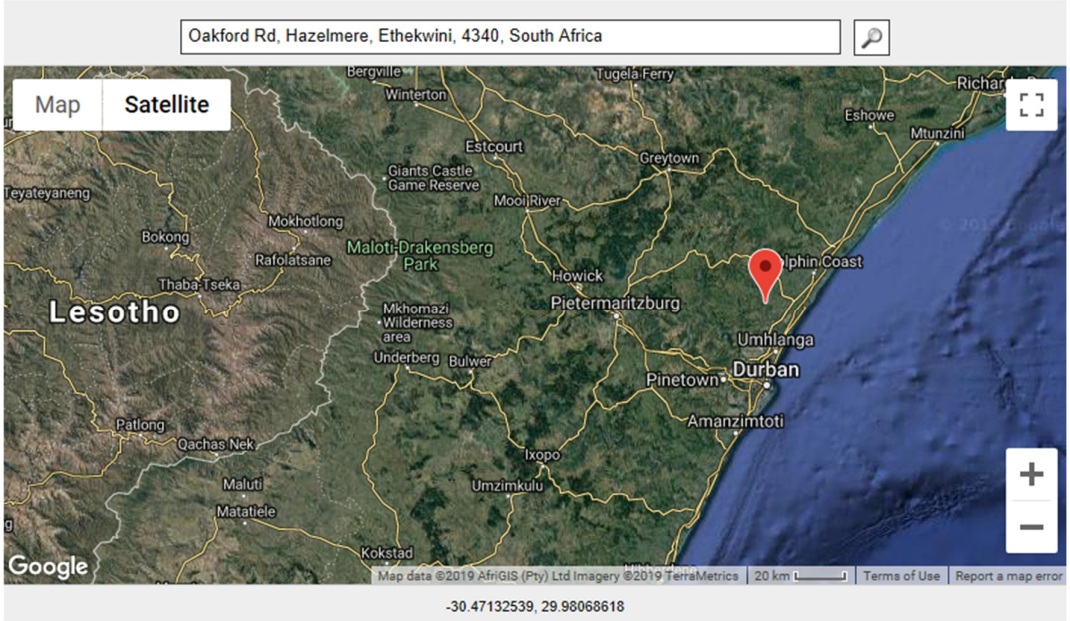

Figure 3.1: Geographical site indication on the MAP


Figure 3.2: Selected TRU for this study.

3.2.2 Energy data collection

The recorded consumptions presented in the following sections below, were achieved by using an energy monitoring device, that measures the energy consumption in real-time. Figure 3.3 shows various components of the Efergy E2 metering, where: (A) is the current transformer, which senses the load current and sends the data through the wireless transmitter; (B). The data is then transmitted to the recording and display unit; (C), which converts this information into Kilowatt-hours (kWh) and keep records.

Figure 3.3: Efergy wireless electricity monitor and data logger

Figure 3.4 shows the annual load data for 2019. The graph shows that the average peak demand during the recorded year (2019) was 1.56 kWh/day, with an average peak consumption of 240W. The load consumption was constant during both the winter and summer months.

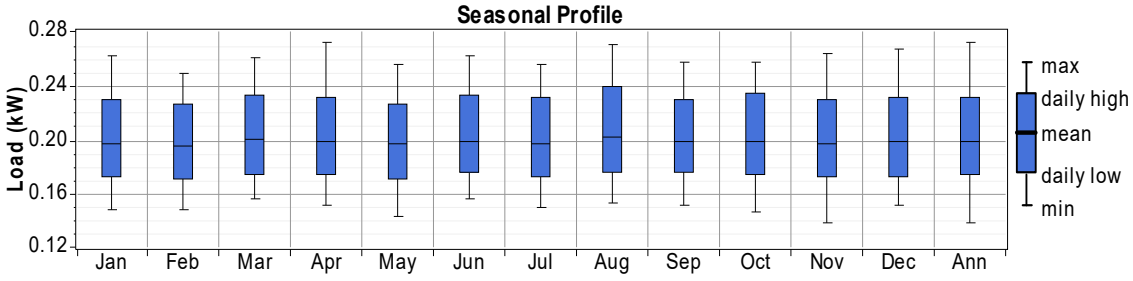

Figure 3.4: Acquired annual TRU load demand using Efergy monitoring device

Figure 3.5 shows how the Efergy monitoring set was installed in a TRU unit. In this Figure, (A) indicates the Current transformer (CT), installed after the main circuit breaker, feeding the entire unit. (B) is the transmits, which is connected to the CT, such that it reads the information sent by the CT and transmitter it to the monitoring display unit (C). (D) is the TRU control unit.

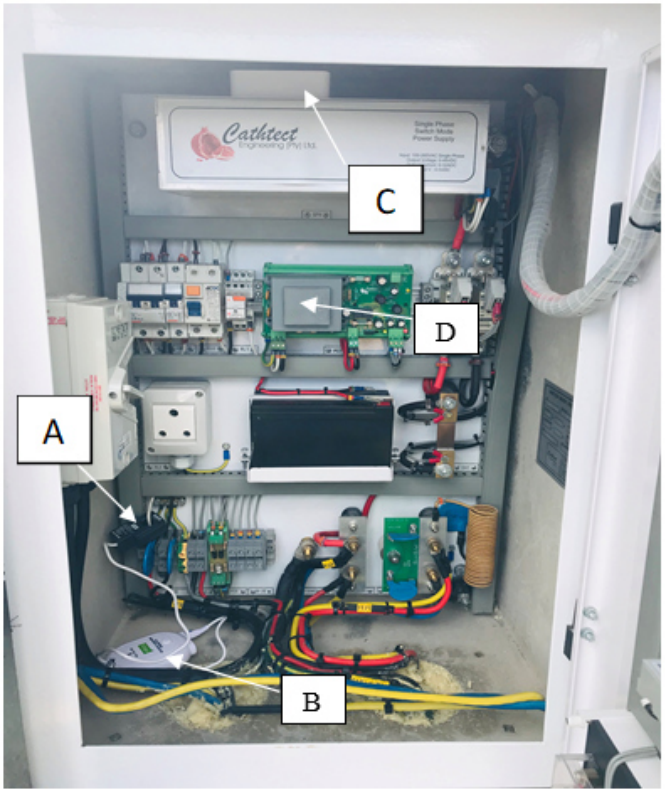

Figure 3.5: Efergy installed in the selected TRU.

3.2.3 Energy consumption analysis and discussions

ICCP systems supply DC current to the pipeline to prevent corrosion, and these systems run 24 hours a day [41]. However, an ICCP is implemented by use of TRU units, which convert AC to DC power and supply this to the pipeline through the anodes [26]. Below is the record of TRU consumption over a period of time.

A. Hourly energy analysis

When referring to Figure 3.6, it may be seen that the TRU Unit consumes an equal amount of energy at all times. Figure 3.6 shows the load profile on Wednesday 02/10/2019. The corresponding energy consumption was found to be 4.74kWh. The peak energy demand on this day was 230W, which occurred at 05:16. The pattern of hourly load consumption is in a table shape, confirming a continuous uniform consumption. The total energy cost on this day was evaluated to be R5.39, with fixed daily charges of R56.92, which is 11 times the energy charges.

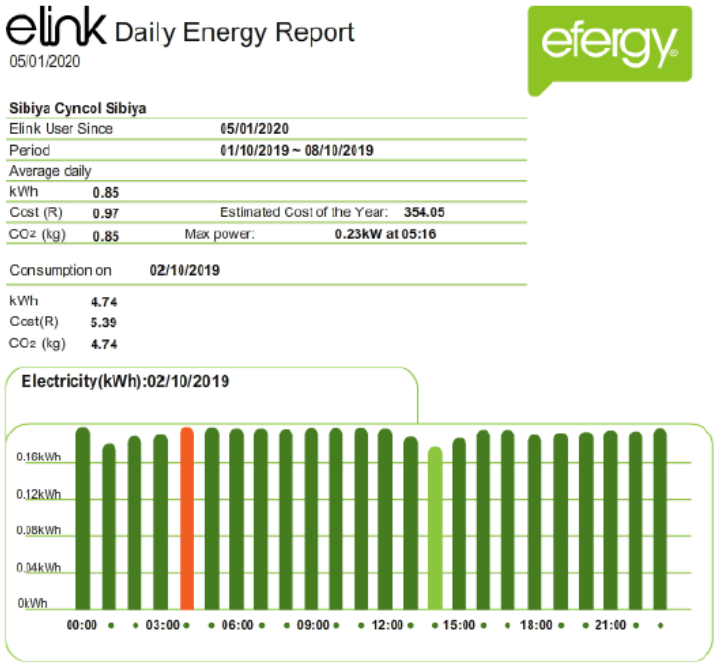

Figure 3.6: Hourly load profile of a TRU for 02/10/2019.

Figure 3.7 shows the hourly load consumption recorded on the 03/10/2019. It may be seen that the peak load demand on this is 230W, which is the same as that of the previous day. The energy consumption was found to be 4.69kWh, which is only 0.05kWh units less, compared to the energy consumption on the previous day. The energy cost for the day is R5.33, with the hourly consumption amounting close to the same value.

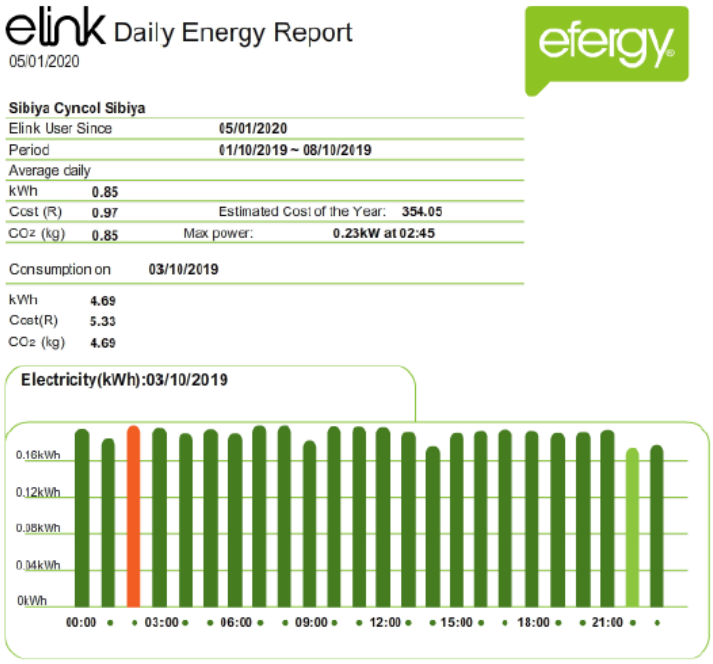

Figure 3.7: Hourly load profile of a TRU for 03/10/2019.

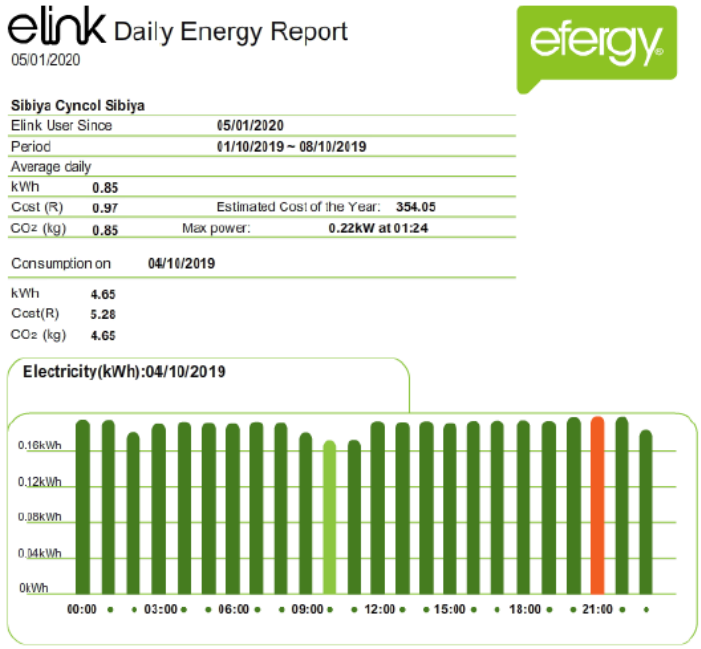

Figure 3.8: Hourly load profile of a TRU for 04/10/2019.

With reference to Figure 3.8, the total energy consumed for the day of 04/10/2019 is 4.75 kWh, which is 0.09kWh less than that on the 02/10/2019 and 0.4kWh less than that on the 03/10/2019, with an energy cost of R5.19. The peak load demand recorded is 220W, which is merely 10 W less than the previously recorded peak load demand values and this

was recorded after 10 pm. Figure 3.9, shows the hourly load profile recorded on the 06/10/2019. It may therefore be seen that the peak load demand is 230W and this was recorded around 4 am. The total energy consumed on the day was 4.74 kWh, amounting to R5.39, which is roughly the same as the cost of energy consumed for the previous days. Hence, from the above-recorded energy consumptions, it may be seen that the TRU unit consumes energy in a fairly uniform manner.

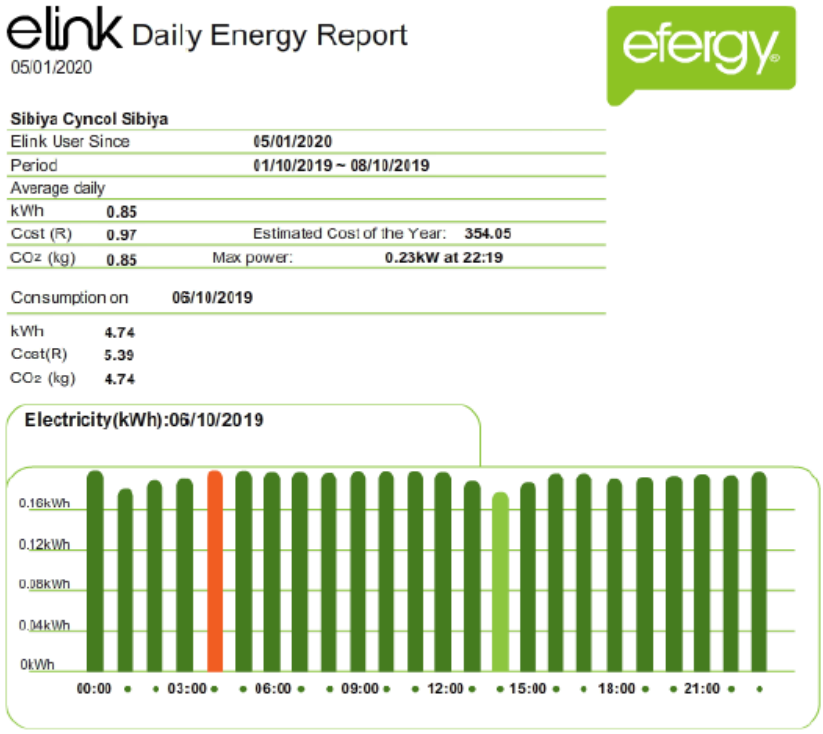

Figure 3.9: Hourly load profile of a TRU for 06/10/2019.

B. Daily energy analysis

The obtained daily energy consumption data is presented in this section. The behaviour of the load is analysed and discussed as per the load profile obtained.

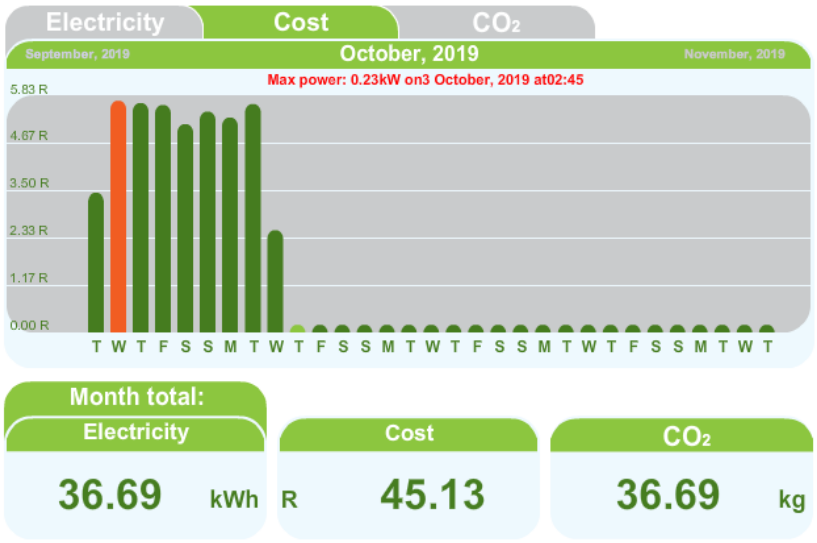

Figure 3.10: Daily load profile of a TRU recorded for a week.

Figure 3.10 shows a 7-day load profile for a selected site TRU unit and it may be seen that the peak demand was 230W on a Tuesday. This is used as the load demand for this study. Furthermore, the daily average consumption presents constant throughout the day, as supported by Figures 3.11 and 3.12. The unit consumed 36.69kWh in 7 days. At the tariff rate of R1.23/kWh, the total energy cost is therefore evaluated to R45.13, leading to 36.69 Kg of Carbon emission.

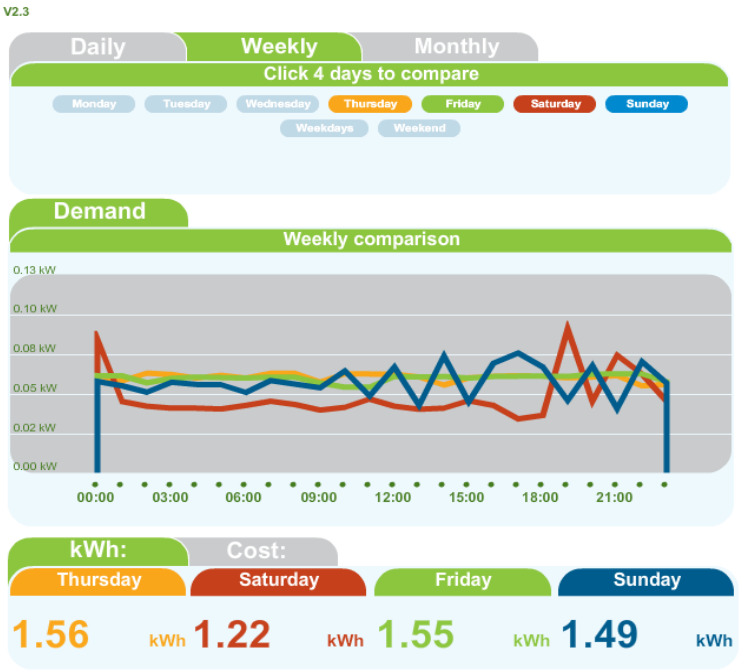

Figure 3.11: Load profile of a TRU for weekday's comparison.

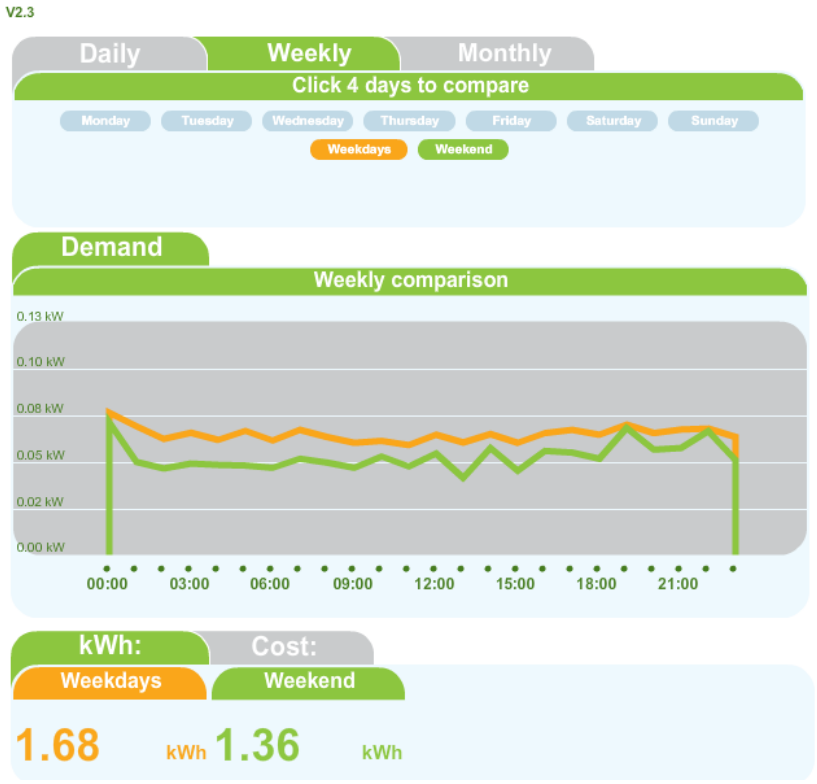

Figure 3.12: Load profile of a TRU for weekdays and weekend comparison.

The analysis of Figure 3.12 shows that the weekdays' consumption average is slightly higher than that of the weekend consumption average. Furthermore, the unit seems to have a peak reading at 00h00. The trends for Week and Weekend averages are similar, which confirms the behaviour of the load as a fairly constant load.

3.3 SOLAR AND WIND RESOURCES ASSESSMENT

The proposed design for this application is the combination of wind power and solar panels. The dimensioning of a hybrid system requires a specific technique, built on the basis of renewable resources at the installation site. Sizing a hybrid system requires a specific technique, developed based on the renewable resources available at the site of installation. To obtain average solar irradiation, various methods may be used. These are: the use of satellite data, direct measurement using Pyranometers or silicon sensors, etc.

3.3.1 Solar resource

For the selected area, solar resource profile data was obtained from a satellite using Solarius PV v.BIM 2 and the Southern African Universities Radiometric Network (SAURAN) database, for verification purposes. Figure 3.13 shows the solar radiation used in this study, with Table 3.1 below showing the monthly average solar radiation levels for the selected site. Table 3.1 shows that the maximum amount of radiation occurs during the months of January and December.

Table 3.1: Annual resource data at the selected site

Month	Clearness Index	Daily Radiation (kWh/m²/d)
January	0.573	5.770
February	0.532	5.530
March	0.476	5.000
April	0.408	4.160
May	0.356	3.440
June	0.339	3.150
July	0.349	3.290
August	0.390	3.870
September	0.418	4.320
October	0.468	4.850
November	0.519	5.240
December	0.579	5.740

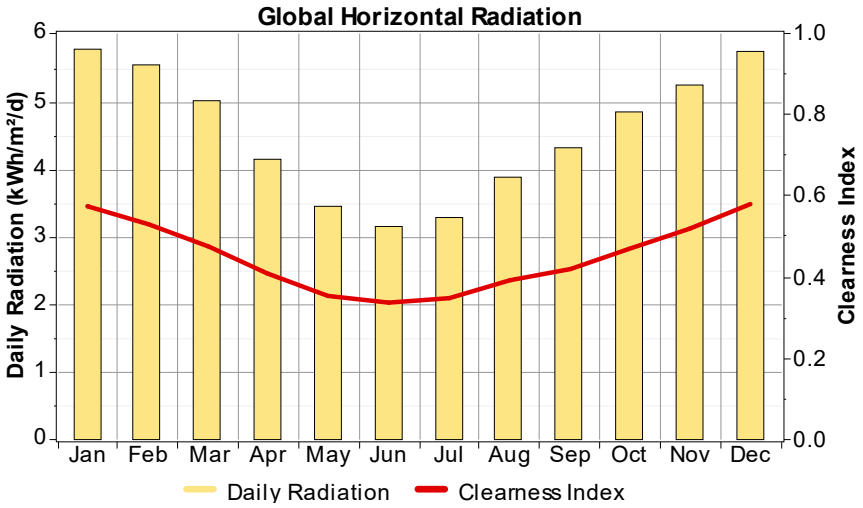

Figure 3.13: Solar radiation data for 2019

3.3.2 Wind resource

Table 3.2 shows wind speed data for the selected area, which has the average monthly wind speed ranging from 4.48 m/s to 5.4 m/s. The average wind speed was further obtained from SAURAN website for the nearest station, which is the University of KwaZulu-Natal Howard College. However, the monthly wind average from RSA weather services was used, together with NASA's global satellite data, for verification. The annual wind speed is 4.47 m/s.

Table 3.2: Average annual wind speed at the site chosen

Month	Wind Speed (m/s)
January	5.140
February	4.917
March	4.690
April	4.515
May	4.470
June	4.480
July	4.900
August	5.1
September	5.36
October	5.8
November	5.4
December	5.23

3.4 ECONOMIC METHODS AND COMPARATIVE COST ANALYSIS

In any engineering design, economic feasibility is particularly crucial, as this is usually the key for decision making. To perform comparative cost analysis, various methods of financial evaluations may be used. These are commonly internal rate of return (IRR), payback period and net present value (NPV) and they assist, or allow, an appropriate selection decision for the project [42]. HOMER requires both technical and economic data on system components. This data is run through HOMER software, which compares all possible configurations of the hybrid system and lists these configurations, based on the least net present costs (NPC) [41].

3.5 POTENTIAL ENERGY COST-SAVING TECHNIQUE EVALUATION, RESULTS AND DISCUSSIONS.

This section evaluates the potential energy saving measures to determine the one which will result in optimal savings. The results from each are discussed, following the evaluation of the technique in the same section.

3.5.1 Time of Use (TOU) tariff

This section analyses the possibility of changing the energy tariff for cost reduction. This exercise is mainly based on the recently approved customer choice, to subscribe to either flat rate or TOU tariff [42]. The advantage of this tariff, is that customers are charged based on the time at which they use the energy. These rates differ, depending on the season and time of day. However, the rates during off-peak are lower than those of standard rates. The TOU tariff periods are shown in Figure 3.14.

According to Eskom Tariffs and charges 2019/2020, if it is possible to change the tariff from Landrate 1 to Ruraflex non-local authority rates, it is possible to reduce energy costs. Ruraflex is TOU electricity tariff for rural customers, with dual and three-phase, provided that Notified Maximum Demand (NMD) is from 25 KVA, with a supply voltage <22KV [43]. Changing the tariff should offer lower energy charges, most especially during Low Demand Season (LDS), with the highest electricity rate being R1.3 during peak hours. On the High Demand Season (HDS), the electricity rate will be R3.97 during peak hours. Moreover, it has a lower charge for Network capacity charge, which is R11.7 less than that of Landrate Tariff. A service charge rate is R6.42 less than that of landrate tariff per day. However, Network demand charge and ancillary service charge are the same for both tariffs. Hence, charging the tariff will bring savings in electricity bills.

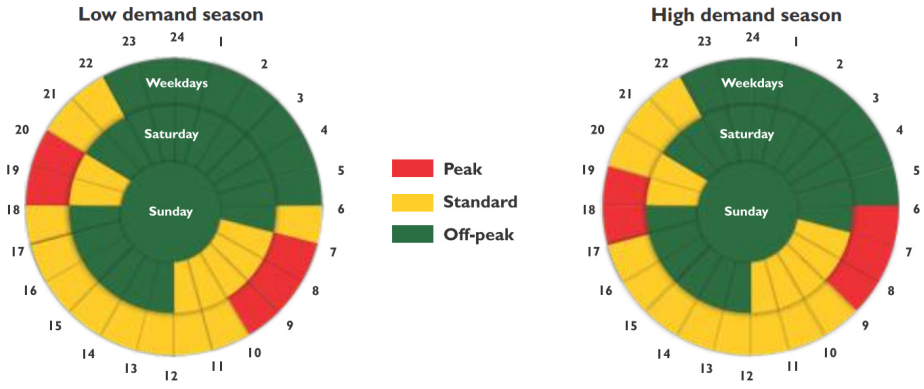

Figure 3.14: Periods of time-of-use tariff [43]

With reference to Figure 3.14, it is clear that for the application where a TRU has constant consumption, the change from low demand season to a high demand season will not make much difference, since for both, there are 5 hours of peak hours, 11 hours of standard consumption hours and 8 hours a day.

3.5.2 Battery Energy storage systems

With TOU tariff, energy becomes affordable during off-peak. However, consumers might not require energy during these hours. Nevertheless, this allows consumers to use Battery Energy Storage Systems (BESS) to reduce their electricity bills. Ref. [44] shows that it is possible to reduce the cost of energy consumed by the load, by up to 52%. This may be accomplished by storing the energy into batteries, through charging during the off-peak periods and solely use it during peak periods, where the electricity prices are high [45]. This section will focus on evaluating whether or not the BESS strategy benefit of electricity cost reduction is sufficient to compensate for storage costs.

The more widespread and most commonly used electrochemical technology, is the lead-acid batteries [46]. However, these have a short lifespan, low energy density and slow cycling rates. Nevertheless, they are the most popular and the least expensive. More details of BESS may be found in [47]. For this study, a GEL battery is evaluated to supply a 230W peak load during peak hours. This is due to the energy costs being the highest during this period, namely R3.97/kWh, during HDS and R1.30/kWh during LDS. This indicates that in terms of rates, it will be of more benefit during the HDS, simply because the current tariff (Landrate) energy charge is R1.30 /kWh. Furthermore, during HDS, the energy cost

is 65c/kWh during the off-peak period, with is more than two times less, compared to the regular cost of energy on the current tariff.

Peak periods last approximately 5 hours a day, which amounts to 1.15kWh of energy needed a day, to supply the CP system selected. With 50% Depth of Discharge (DOD) and considering system losses, the BESS capacity size should be 3 kWh. If the BESS system is configured for 24V, the battery bank should have at least 96Ah capacity. The BESS will have an initial cost of about R5, 300.00 [48], giving a saving of about R 19.85 a day, on TOU tariff, during HDS, which is a R3, 573.00 saving for every HDS. Furthermore, as much as energy is much lower during LDS, the use of BESS may still make a huge saving. This is due to the energy cost being 56c /kWh during off-peak and R1.30 /kWh, in both the current tariff and in a TOU tariff.

3.5.3 Hybrid system

The use of renewable energy resources for CP systems is proposed [8]. CP systems, however, require a constant reliable supply of energy. Hence, combining two or more Renewable Energy Sources (RES), to form a hybrid system, will eventually provide an advantage in supporting the shortcoming of electrical energy and give strength to unpredictable renewable energy resources [49]. To this end, solar and wind power are considered, due to great interest being shown in these two RES in literature [50, 51]. Furthermore, they are the most affordable and highly growing in the market, with governments in many counties, including South Africa, encouraging cleaner and more sustainable energy sources [52, 53].

Based on the evaluations done in the previous section, it is clear that the use of a hybrid system with BESS will be the most economical way of supplying Power to CP systems. This is due to the selected site having adequate solar irradiance and wind resources. However, the system will need to provide power to a peak load of 230W, for 24 hours a day. The peak daily energy required is 4.74 kWh, according to Figures 3.6 and 3.9. Hence the BESS capacity should be 10kWh, considering system losses and 50% DOD. Taking a 24 V system, the BESS capacity should be at least 420Ah. A combination of a few solar panels and a wind turbine may supply power to the CP unit. This may result in the lack of

payments of electricity bills and a CP system running on an environmentally friendly and cost-effective off-grid hybrid system.

3.6 SYSTEM SIZING AND COSTS

The hybrid system consists of a DC load, wind turbine and solar panels with battery storage. The specified choice of the system design is based on the load requirements. ICCP is mainly the application of DC voltage to the pipeline. This gives an impression to peek the system as purely DC, to avoid the losses due to power conversions. Secondly, a hybrid system is used instead of a single source. The reason for this is to ensure continuity of supply in such a way that, during the day, solar will generate power and the wind turbine will generate power anytime when a sufficient amount of wind blows. Furthermore, since the system will not be generating power evenly, a battery storage is included, to store energy when the generation is higher than consumption. The selection of all components is based on meeting the peak demand of 230W, 24 hours, daily. The cost of system components consists of finance, replacement, and service and repair costs.

. Homer software uses US dollars as currency. At the time of this study, one (1) US$ was equivalent to R14.62. The battery storage was included during simulation, due to the reasons mentioned above. The system has been anticipated for a lifespan of 25 years. Further costs, such as labour, installation and structure, are not included in the simulations. Figure 3.15 shows the schematic diagram for the proposed hybrid system of PV and wind turbine, with battery storage system, as used in HOMER software.

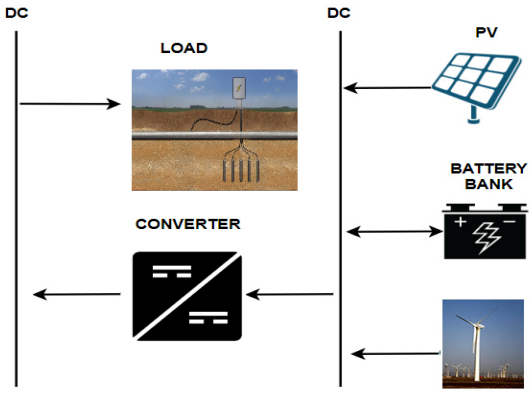

Figure 3.15: Design configuration of a hybrid (WT-PV) system with CPU

The information shown in Table 3.3 is inserted as inputs to HOMER for system sizing. The data from different manufacturers of wind turbines are currently available in HOMER. However, the one proposed is not part of the HOMER database and hence, it was manually entered. In this study, an Aeolos – H 1kW wind turbine, manufactured by Aeolos Wind-Turbine, is used as a system wind turbine. The capital cost of purchasing this turbine, is US$242.43 (R3, 580.90) [54]. The lifespan is estimated to be 20 years, with O&M costs being 10% of the capital cost per year, as given in Table 3.3.

The South African purchase price of a 370W polycrystalline PV panel, is US$138.27 (R2, 042.40). The O&M cost is considered to be 6% of the total cost, with a lifetime of 25 years[55]. The optimum number of solar panels required to meet the load demand was calculated by HOMER, without electricity shortages. This is further explained under the results and discussions. The system further contains an ALLGRAND GEL 200Ah deep cycle battery, for energy storage. Table 3.3 displays the technical parameters of this battery. The retail price for buying this battery in South Africa is US$ 344.12 or R 5, 083.00 and it has a lifetime of 5 years (2500+ cycles), assuming a discharge depth of 50 %. The cost of O&M is estimated to be 2% of the cost of capital per year.

Table 3.3: Cost and technical information for the system components

	Wind turbine	**Solar panels**	**Battery**
Description	Aeolos – H	polycrystalline	ALLGRAND GEL
Size	1KW	370W	200Ah
Voltage	48V	48V	12V
Efficiency	96	19.1%	85%
Cost (US$)	242.43 [15]	138.27	344.12
Life span	20 years	25 years	5 years
O&M/ purchase cost	10%	6%	2%

3.7 HOMER RESULTS AND DISCUSSION

This section discusses the results obtained from HOMER, with the limitations mentioned below:

- Costs of installation; cabling are included in simulations as part of initial costs, since they are reasonably low, compared to the overall system cost [56].
- Replacement costs are considered the same as the capital costs of each component throughout the lifespan of the project.

- The repaid change in renewable energy items are considered as part of O&M. However, yearly inflections are included in the simulations.

The system is specified to have 0% annual capacity shortage for 25 years' lifespan. This is to ensure that the load is adequately supplied at all times during the course of a year.

Figure 3.16, shows the categorized optimal results. These are the economic optimal configurations, in each configuration type. The system contains some or all of the three key components, which are mainly: Battery storage system, Wind turbine and Solar panels. Due to the unreliability of renewable energy, the battery is compulsory for the system. However, the system may still function with either Solar or Wind Turbine omitted. Hence, it is possible to have a hybrid system, Solar PV system with batteries or a wind turbine with batteries. Below is table showing the detailed results for the above-mentioned categories.

	PV (kW)	WT	200AH ...	Initial Capital	Operating Cost ($/yr)	Total NPC	COE ($/kWh)	Ren. Frac.	Batt. Lf. (yr)
	0.74	1	4	$ 1,070	156	$ 4,981	0.115	1.00	5.0
	3.00		6	$ 1,947	231	$ 7,726	0.178	1.00	5.0
		3	8	$ 1,830	311	$ 9,604	0.221	1.00	5.0

Figure 3.16: Categorized optimal configuration

From Figure 3.16 and as further illustrated by Table 3.4, it may be seen that the hybrid system is the optimal selection, based on its generation capacity, low initial capital, low operating costs and the levilized COE, with one-unit costing only US$ 0.115/kWh, R 1.68/kWh. The first solution from Figure 3.16 represents the most feasible and optimal configuration. It consists of two 370W PV panels, four 200AH Deep cycle GEL batteries and a 1kW wind turbine, meeting the load demand at the lowest cost, with 100% renewable energy fraction, at no capacity shortage for 25 years. Each battery has a storage capacity of 2.4 kWh, with solely 1.44kWh, useful due to sustaining the battery.

Table 3.4: Summary of optimal outcomes of simulation for various off-grid networks

Optimal system architecture	Hybrid (PV-WT) with Batteries	Solar with Batteries	Wind Turbine with Batteries
System description	Turbine (1KW) +4 batteries+ 0.74KWPV	5KW PV+ 6 batteries	3 × 1KW turbine + 8 batteries
Total Rated Capacity	1.74 kW	3kW	3kW
Capital cost (US$) (Rand)	1,070 15, 643.4	1, 947 28, 465.14	1, 830 26, 754.6
NPC (US$) (Rand)	4, 981 72, 822.22	7, 726 112, 954.12	9,604 140,410.48
O&M (US$) (Rand)	107 1, 564.34	194.7 2, 846.51	183 2, 675.46
COE (US$/kWh) (Rand/kWh)	0.115 1.68	0.178 2.6	0.221 3.23
Operating cost (US$/year) (Rand/year)	156 2, 280.72	231 3, 377.22	311 4, 546.82

Figure 3.17 below, shows the yearly output production generated by the hybrid system throughout the year. The wind turbine seems to be generating most of the energy, with the system having sufficient power at all times. PV array contributes 1,173kWh/year, which is 33% of the combination. The wind turbine generates 2,358kWh/year, which is 67% of the total system production. Both PV and WT have the lowest production in the month of May and June, highest in October.

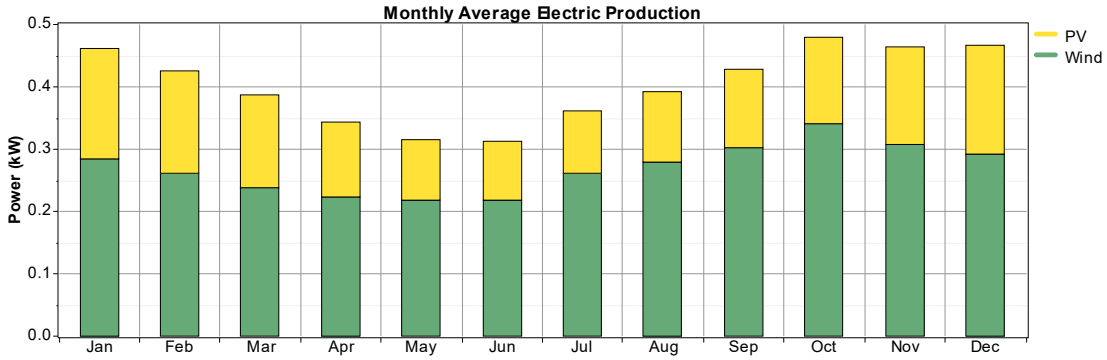

Figure 3.17: Monthly average electricity production

Figure 3.18 below shows an average monthly generation of a wind turbine in annual period. It may be noted that the wind turbine suffers less production during the night and it produces its rated power during the day, for approximately 12 hours a day. The hours of no production are mostly from midnight to 4 am, which is the time when Solar panels are further not producing power. This explains the requirement for the batteries and hence, verifies the behaviour of the batteries as mentioned above.

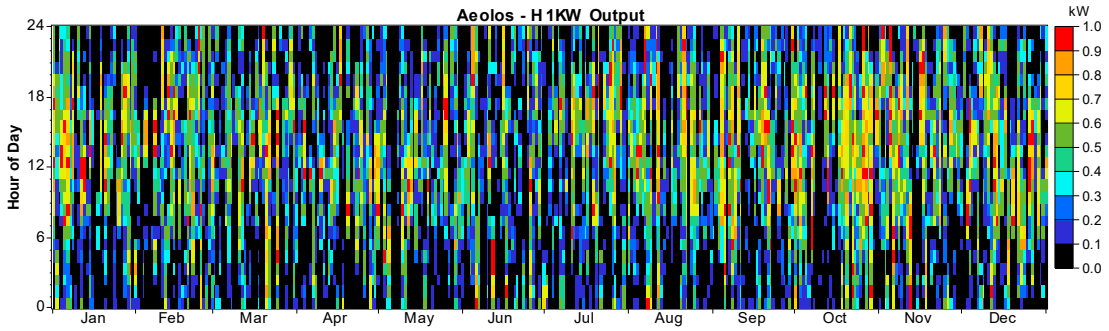

Figure 3.18: Monthly average electricity production of a Wind turbine

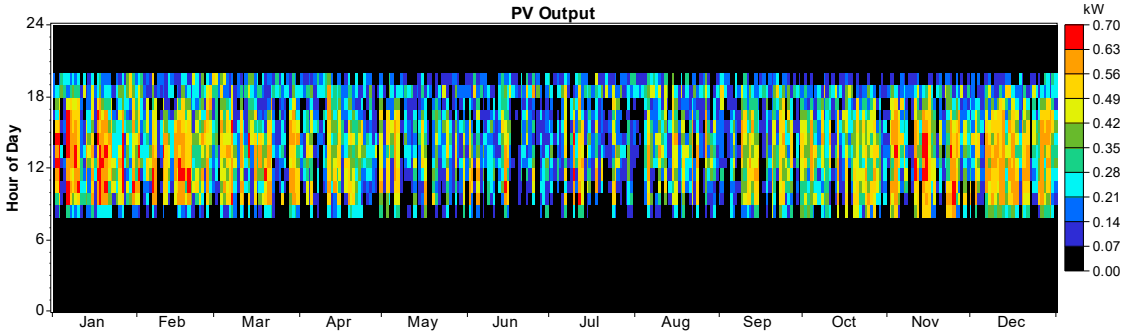

Figure 3.19: Output power generated by a PV system

The wind turbine supplies the major share of the power throughout the year and solely the PV panels supply a few percentages of power. The PV Panel array size is 0.6KW and its production ranges from 60 to 600W, during the day. During the winter period, there is a significant change as the solar resource decreases more, as shown in Figure 3.19. In this period, the production of solar panel drops to half. HOMER software utilizes both wind turbine and the generated PV energy, to meet the load requirement and maintain 0% shortage capacity.

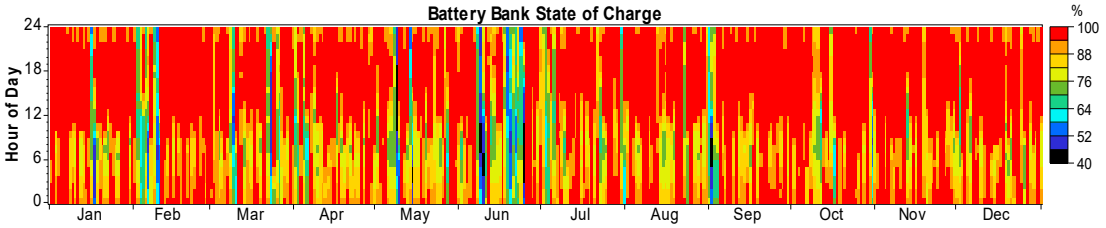

Figure 3.20: Battery state of charge in optimal hybrid system configuration

Figure 3.20, the monthly statistics on the battery charge status for the whole year and the total amount of energy available in the battery, are displayed. This provides a comprehensive hourly battery charging status for each month, during the simulated time. This shows that the battery remains fully charged from 12h00 to 18h00, during most times of the yearly periods (January to December), having a minimal state of charge, more often between 0h00 to 12h00. The batteries only reach their lowest long SOC in winter. During the winter period (June to July), the battery bank reaches a minimum state of 40% around 06h00 in the morning. The battery is mostly used during the hours of night time. Furthermore, Figure 3.20 shows that the battery SOC is above 90% for over 50% of its time. This justifies the fact that the battery utilization is in a manner which enhances it lifespan.

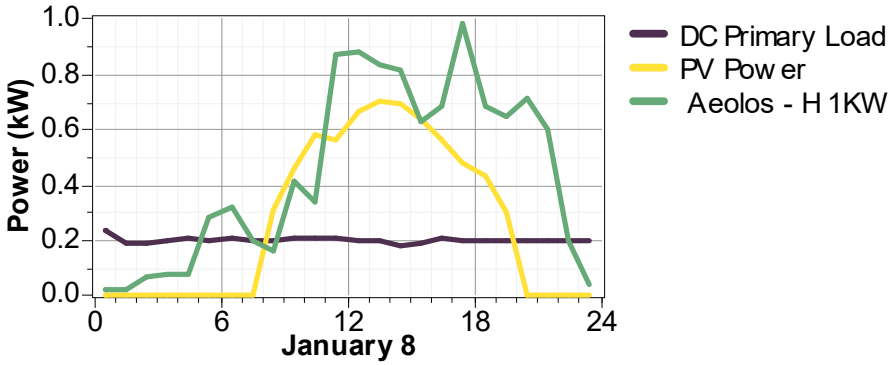

Figure 3.21: System power flow, generation and consumption

Figure 3.21 above, shows the power flow diagram of the designed hybrid system, illustrating the contribution from both power sources. It may be seen that from 00h00 to about 05h00 on the 8th of January, both wind and solar generation are below the load requirement. Hence, the load drains the battery, during this period, the PV system is generating no power at all, due to the unavailability of solar energy. From 05h00 to 07h30,

the WT begins generating sufficient energy to meet the load requirements, while charging the battery. At this point PV is still not generating power.

The same Figure shows that the PV starts generating from 07h30 to 21h10 and solely being able to sufficiently meet the load requirement from 08h00 to 19h30. During this period, the PV generation begins to have excess power and hence charging the batteries. However, from 21h10 to 07h30, the PV system is not generating any power, however, the wind turbine and batteries assist during this period, to supply the load with adequate power. It is further shown that, the wind turbine has power generation running from 01h00 to 23h00 and solely being able to satisfy the load requirements from 07h00 to 23h00. The hybrid charges the batteries with excess power for approximately 14 hours and only draining power from the batteries for about 6 and half hours, which is from 22h30 to 5h00.

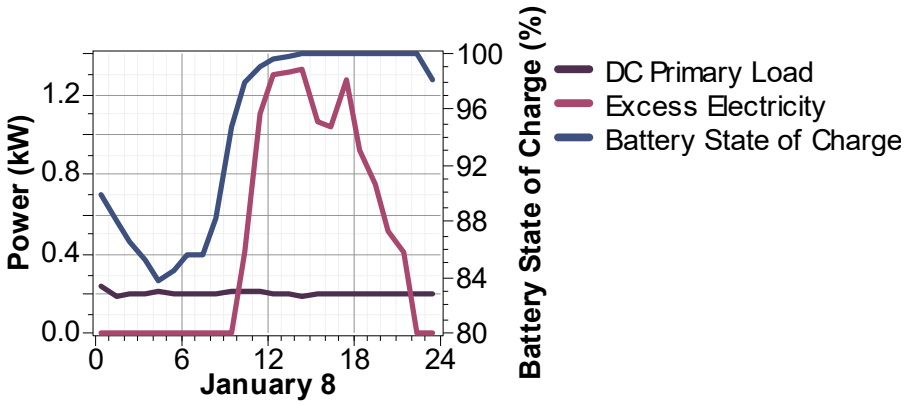

Figure 3.22: System power flow, excess power and battery SOC

Figure 3.22 shows the battery SOC and power excess for 8 January. The diagram shows that, during the period where there is no excess power, the load is draining the battery, until a point where the produced energy starts being sufficient, to reach the load demands as discussed above. The battery however, reaches its lower SOC around 04h00, which is 84% and a DOD of only 16%. From approximately 04h00 to 15h00, the battery bank accumulates the energy, until it is fully charged and only starts discharging after 22h00, when the production starts being inadequate to meet the load requirements.

3.8 CONCLUSION

The main goal of this Chapter, was to conduct sizing and the techno economic analysis of an off-grid PV-WT hybrid system, that may satisfactorily meet the CP load demand, in

the South African context. The objective was to assess the implementation potential of hybrid system to supply CP, rather than to extend the grid and having to pay monthly costs.

The most unfavourable month method was used, to size the proposed system, together with the NPC and the levelized COE. HOMER software was used to size the system with wind speeds, solar irradiance, load demand, components costs and technical specifications, as inputs. The main criteria used to select the optimal system was to levelize COE as the performance index (objective function). The levelized COE currenlty includes net present cost and initial cost.

The results show that the system size for the specific load is 1.74 KW, which comprises of 0.74KW PV and a 1KW wind turbine, with a 200Ah battery. The system has an initial capital of 1,070 US$ and yields to a life expectancy of 25 years at 0.139 US$ /kWh COE at. However, HOMER could not cater for the DC -DC converter required to regulate the energy that suits the load requirement. In order to enhance an optimal decision, this restriction demonstrates a need to further model the system, to enable power flow analysis of each variable.

CHAPTER 4: DYNAMIC SIMULATION AND ANALYSIS OF WIND SOLAR HYBRID SYSTEM POWERING A CPU USING MATLAB/SIMULINK

4.1 INTRODUCTION

In this Chapter, the performance of the proposed off-grid wind solar PV hybrid system, powering the Cathodic protection unit (CPU), is simulated and analysed using MATLAB/SIMULINK. This includes the performance simulation of the battery energy storage system (BESS) with a PV-Wind hybrid energy system solar irradiance and wind speed that constantly varies. The size of the off-grid wind solar PV hybrid system being simulated, is determined in Chapter 3, using HOMER. The 1kW wind turbine used has a Permanent Magnet Synchronous Generator (PMSG) drive, directly from the turbine. The PV system has a total peak power of 740W (two solar modules of 340W each), while the battery bank has four 200Ah 12V batteries, connected in series, to achieve the system voltage of 48V.

4.2 SCHEMATIC LAYOUT OF THE SYSTEM

Figure 4.1 shows the schematic diagram of the proposed wind solar hybrid system powering a CPU. As shown in this Figure, wind turbine and solar panels are both supplying energy to the load. However, due to intolerable potential power failures and the significant need for continuity of power supply to the CP system, the battery bank is incorporated into the system. The arrows in the diagram illustrate the flow of power in the system. The battery bank will store the energy, when there is excessive power and assists in meeting the load demand without shortage.

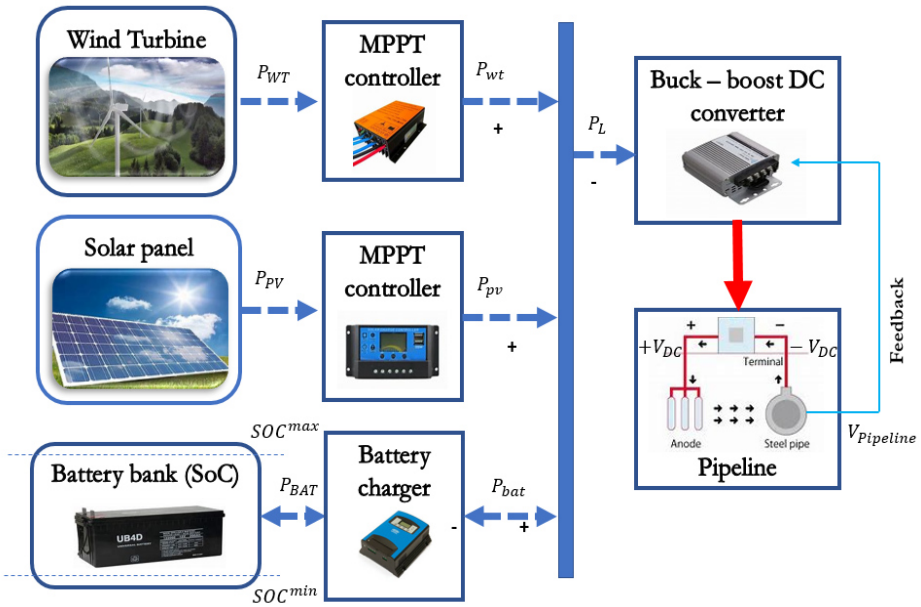

Figure 4.1: Proposed system schematic diagram

In Figure 4.1, P_{PV} is the solar PV generated power supplying electrical energy to the CPU, P_{WT} is the power generated by the turbine generator supplying power to CPU and both generated powers are used to charge the battery bank when there is excess power. The battery power (P_{BAT}) has a bidirectional flow, depending on whether it is charging the battery or supplying the load when needed. P_L is the power supplied to the CP Unit, either from P_{BAT}, P_{PV} or/and P_{WT}. As discussed in Chapter 3, this power is expected to be uniform in consumption, with a peak power demand of about 230W and running 24 hours a day.

4.3 PV SYSTEM MODELLING

4.3.1 Solar photovoltaic module characterises

The PV array used for the hybrid system being modelled in this Chapter, is based on a single diode model. However, the two-diode model is more accurate and precise, compared to the single diode model [57]. The single-diode model is shown in Figure 4.2 below.

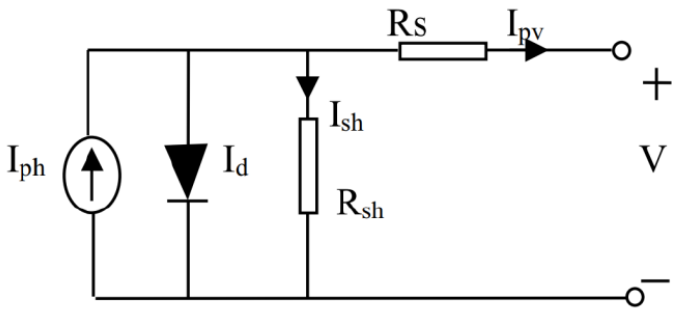

Figure 4.2: PV module single-diode model [1]

A. Mathematical modelling of PV source

The output voltage and current of the module are given by Eq. (4.1) and Eq. (4.2) below, where I, I_{Ph}, I_{sh} are outputs, photo and shunt currents with R_{sh}, R_s and I_d being the shunt resistor, series resistor and diode reverse saturation current respectively:

$$I = I_{Ph} - I_{sh} - I_d; \tag{4.1}$$

$$V = (I_{Ph} - I_d)R_{sh} - I(R_{sh} - R_s). \tag{4.2}$$

The reverse saturation current of the module I_d (Diode current), is represented by the expression given in Eq. (4.3) below. $V_t = kT/q$ and the product of $V_t \times a \times N_s$ is the thermal voltage having N_s cells connected in series. q is the electron charge ($1.6021764 \times 10^{-19} C$), k is the Boltzmann constant given by ($1.3806503 \times 10^{-23}$ J/K) and T is the p-n junction Temperature in K, with a representing the diode ideality constants [58]. The reverse saturation expression is given by Eq. (4.3):

$$I_d = I_o \left[exp\left(\frac{V + IR_s}{a \times V_t \times N_s} \right) - 1 \right]. \tag{4.3}$$

The photocurrent (I_{Ph}) of the Photons performance under standard test conditions (STC) is given below, where the solar irradiance G = 1000W/m² at the temperature of 25℃ is expressed as T=25+273.15 in K. The variable K_I is the coefficient of I_{SC} and is determined by the manufacturer. The photocurrent is specified by the expression given by Eq. (4.4) below:

$$I_{ph} = \frac{G}{1000} \times (T - (25 + 273.15) + I_{sc}), \tag{4.4}$$

Where: I_{sc} is the short circuit current at STC given by the manufacturer. I_{sh} is given by Eq. (4.5) below.

$$I_{sh} = \frac{V + IR_s}{R_{sh}}. \tag{4.5}$$

It is of great importance to consider the effect of R_s and R_{sh} in the performance of a PV module [59].

4.3.2 PV output power control modelling

One of the most significant challenges in solar power generation, is the change in generated power when irradiance and temperatures continuously change. This becomes a concern, due to the low efficiency in solar energy generation, which ranges from 9-20% [60]. However, if the output power of the PV array is maintained at the maximum power point (MPP), the given efficiency may further be maintained.

The I-V curve depends on both irradiance and temperature, where the higher the irradiance, the better the I-V curve and the higher the temperature, the worse the I-V curve and vice versa. To obtain the maximum power (P_{mpp}) delivered to the load by the PV module, it is important to force the PV module to operate at a point corresponding to the MPP. This point corresponds to the peak of the PV curve or the knee of the I-V curve [23]. This is achieved by forcing the voltage of the PV module to equal that of P_{mpp}, or by regulating the current to the correct amount of that at Maximum Power (MP) using convertors. However, weather conditions may change at any given time, therefore the MPP should be tracked at all times.

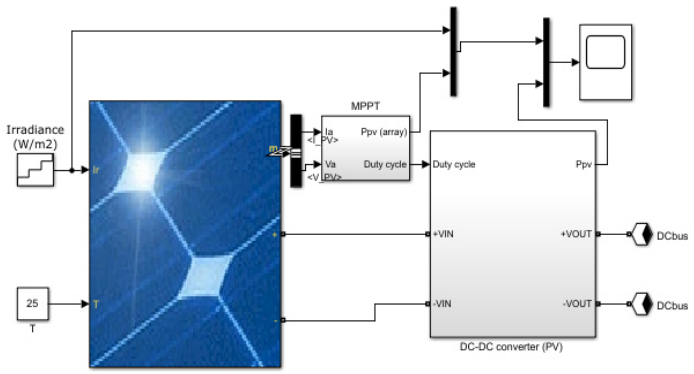

Figure 4.3: PV system with maximum power point tracker (MPPT) analysed

Figure 4.3 shows a PV system with an MPPT. Since the location of the MPP is unknown, it has to be determined through calculations or search algorithms. There are several MPPT techniques identified from practice, as well as in the literature. These are categorised as direct and indirect algorithms, which include the Fixed Voltage method (FV), Fractional Open Circuit Voltage method, Perturb and Observe (P&O) method, Increment Conductance (IC) method, Artificial Neural Network method, the Fuzzy Logic method, etc.[60].

In this study, the P&O MPPT technique is used. The reason being that the P&O is one of the most commonly used MPPT techniques. This is due to the simplicity, convergence speed, effectiveness they both offer, together with lower cost, availability of sensors required and easy hardware implementation, compared to other methods [60, 61]. The P&O algorithm is implemented in this model using MATLAB. Figure 4.4 shows the flow chart of the algorithm for n>0 with its operation explained below, where n is the term at which data is requested.

In P&O, algorithm direct measurements of voltage, current and power are taken to perform the hill-climbing algorithm. To translate an increase or decrease in power, a perturbation is given to a PV module voltage. If an increase in voltage leads to an increase in power, this means that the operating point is to the right of the MPP, so more disturbance in voltage to the left is needed to hit the MPP. Conversely, if an increase in voltage leads to a decrease in power, it means that the left is a current operating point and therefore a disruption is needed to hit the MPP to the right. The essence of the PV curve is rising to the left of the curve and decreasing to the right of the PV curve. The divergence of P&0 from MPP, is shown in Figure 4.5.

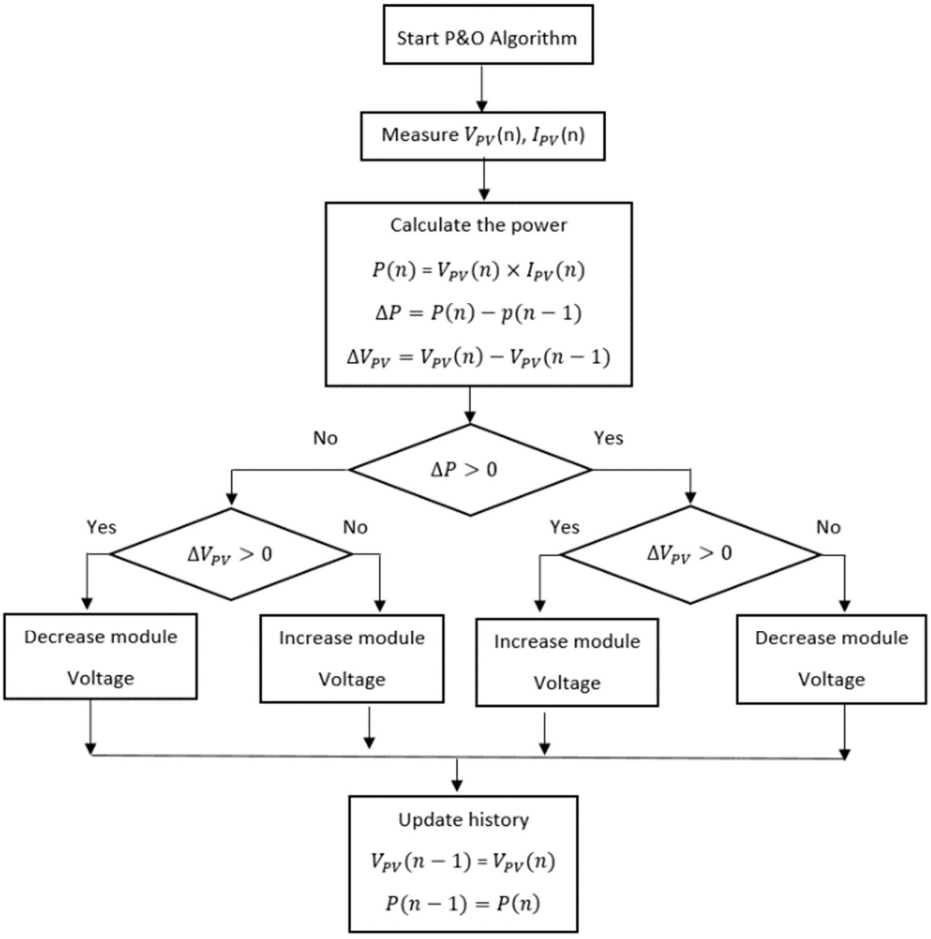

Figure 4.4: P&O algorithm flow chart [62]

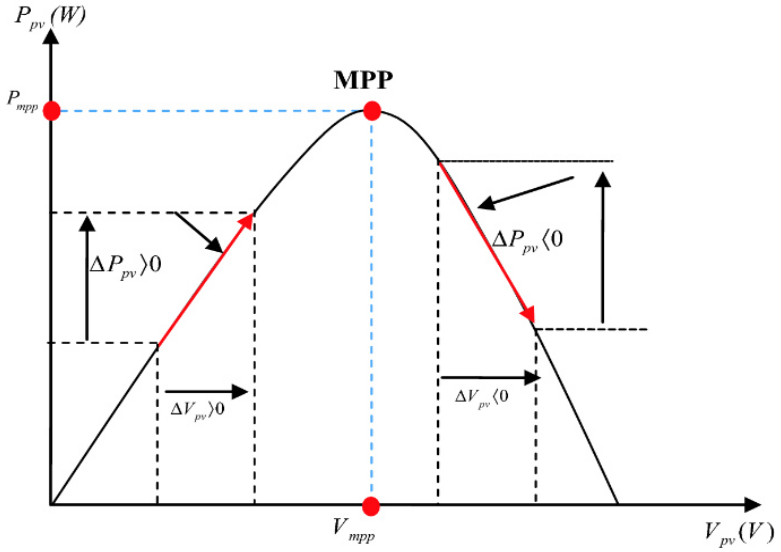

Figure 4.5: Divergence of P&0 from MPP [62]

4.4 WIND TURBINE MODELLING

The amount of electricity that may be produced from wind, depends on the wind resource's velocity. It works, in terms of operation and rotor blade configurations, similarly to a hydropower generation system. The segment addresses the modelling of the overall wind turbine operation.

4.4.1 Modelling of the wind turbines

When using wind turbine blades, the kinetic energy from moving wind velocity is converted to mechanical rotational energy, then to electricity. The mechanical power (Pm) extracted by a wind turbine, using the swept rotor blade area, is lower than the available moving wind power (Pw). Due to the losses involved, wind turbines may solely harness a fraction of the total kinetic power. By the well-known Betz rule [65], the coefficient (C p) is limited to 16/27=0.593. The upper limit is for highly efficient machines, with low mechanical losses. More losses are created by mechanical devices, such as gearboxes, bearings, blade shapes, etc. Therefore, less wind power is converted into available energy. By the use of blades and the rotor coupled to the low-speed shaft, the wind power is converted into mechanical power. The expression below, where β is the angle of blade pitch in degrees, gives the mechanical power [59].

$$P_m = C_p \times P_w = \frac{1}{2} \times C_p(V, \beta) \times \rho \times A \times V^3 \ , \qquad (4.5)$$

Where: ρ = Density of air (kg/m^3) = 1.225 kg/m^3; A = Area swept by the rotor blades (m^2); V = Wind speed (m/s); C_p = Betz law coefficient; β= Angle of blade pitch (^{o}).

Therefore, the mechanical torque (T_m) is given as:

$$T_m = \frac{1}{2} \times C_p(V, \lambda) \times \rho \times A \times \frac{1}{\omega_m}, \qquad (4.6)$$

Where: λ = Rotor blade tip velocity ratio to the wind velocity.

These empirical power coefficients depend on the turbine type and may differ for various turbines [63]. The parameters of a modelled turbine are given in Table 4.1 below:

4.4.2 Modelling of the wind turbine generator

The wind turbine used in this study utilises a permanent magnet synchronous generator (PMSG) for energy conversion. The stator of the PMSG is connected to the three-phase full-bridge rectifier, that converts the AC voltage into DC voltage. In this section, an equivalent PMSG model is developed, to demonstrate how the electrical power is generated from the wind kinetic energy. In this model, both rotor and magnets, damping effects are negligible. The magnetic circuit is assumed to be unsaturated, iron losses are negligible and the distribution of magnetic flux in the rotor is sinusoidal [64].

The electromagnetic torque expression is given below, followed by the electrical power expression:

$$T_e = \frac{3p}{2}(\lambda_m i_{qs} + (L_d - L_q) i_{qs} i_{ds}; \tag{4.9}$$

$$P_{dq} = \frac{3}{2}(v_{ds} i_{ds} + v_{qs} I_{qs}). \tag{4.10}$$

Figure 4.7 shows the complete SIMULINK model of the PMSG-based wind turbine.

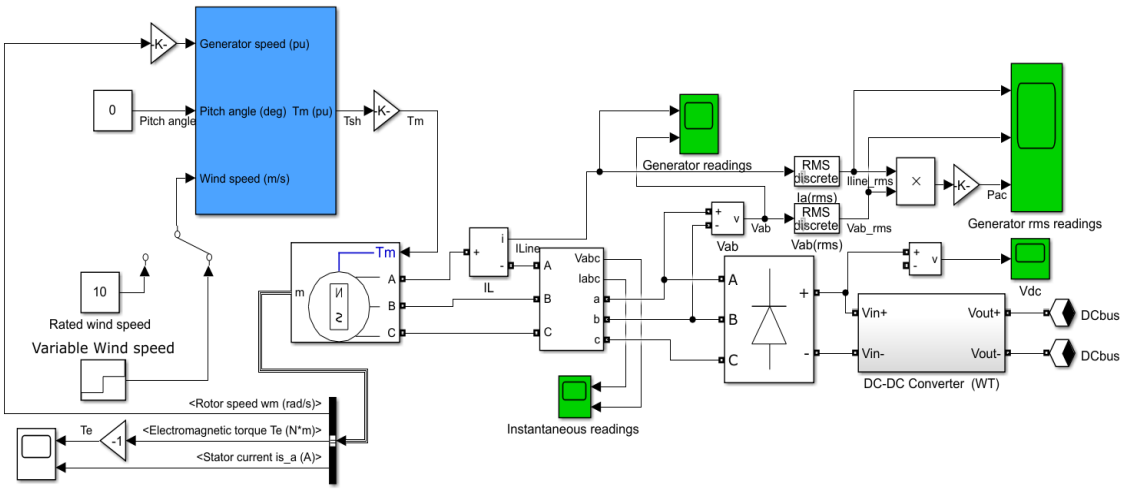

Figure 4.7: Wind turbine model in Simulink with PMSG and Rectifier

To achieve maximum power extraction from a varying speed wind turbine, a turbine should operate at a maximum power point (MPP)[65]. For every wind speed, there is an MPP, as illustrated in Figure 4.8 below. To locate the MPP for a wind turbine, the speed and torque control are essential [66]. In Ref.[67], the author performed the speed and

torque control, by the control of interfacing DC-DC converter. Due to the fluctuating nature of wind, tracking the MPP requires the use of algorithms, such as P&O, optimal torque control (OTC), fuzzy logic or any other applicable algorithm presented in the literature [67]. In this study, the control used is the P&O algorithm with the DC-DC converter, where the rectified output voltage and current are measured and used as inputs to the MPPT, as shown in Figure 4.9. This method is commonly used, due to its simplicity and eliminating the requirement to measure the speed, which brings economic benefits to the selected method [21]. The P&O algorithm is the same as that used in Figure 4.5, except for V_{PV} having to be replaced with V_{DC} and I_{PV} with I_{DC}. The OTC method is presented with details in [68].

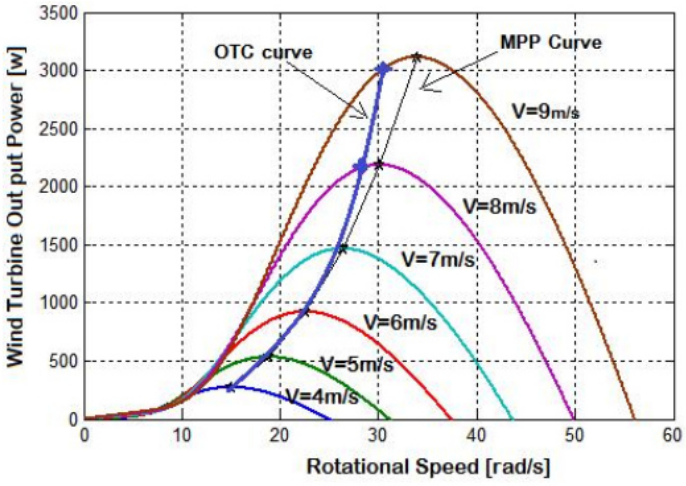

Figure 4.8: Wind turbine (WT) output power and rotor speed for different wind velocity [68]

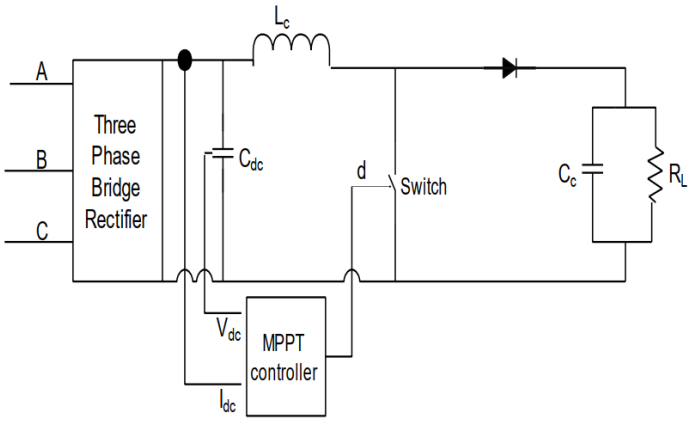

Figure 4.9: Circuit diagram for boost converter with an MPPT controller [67]

4.5 BATTERY BANK MODEL

The excess energy from the PV system and WT may be stored in the battery bank. The stored energy is used for supplementing the unmet load demand, when the net generated power by WT and PV system is insufficient to meet the load demand [23]. For safe operation of the battery bank, the storage limit is restricted, according to the designed specified limits. The battery storage is referred to as a State of Charge (SOC). The system consists of four 200Ah 12V GEL batteries, which are connected in series, to match the system voltage of 48V. The total battery bank capacity is 9.6 kWh, with only 5.76 kWh being useful, due to the 40% selected DOD. To prevent both overcharging and deep draining, the constraints are imposed, such that the battery bank stops charging when it is at 100% SOC and not being discharged when it reaches 40% SOC. The reason for this, is to enhance the battery performance, maintaining its efficiency, as well as ensuring its life span. Furthermore, the charging or discharging current (I_{batref}), is compared to the maximum charging (I_{ch-max}) current and maximum discharging current ($I_{dis-max}$).

The flow chart and Simulink model of the battery control algorithm, are presented in Figure 4.10 and 4.11. The algorithm monitors the net power and the power required, such that when the net power is positive, it will charge the battery and when power required is positive, it will discharge the battery. The constraints mentioned above, are further taken into consideration. The generated power (P_g), is given by Eq. (4.11). The expressions used to determine the net power (P_{net}) and (P_r), are given in Eq. (4.12) and Eq. (4.13), as follows[69]:

$$P_g = P_{WT} + P_{PV}; \tag{4.11}$$

$$P_{net} = P_g - P_L\ ; \tag{4.12}$$

$$P_r = P_L - P_g\ . \tag{4.13}$$

Where: P_g is the total power generated from renewable energy, P_L is the power demand and $P_r$is the power required to supplement the load supply power.

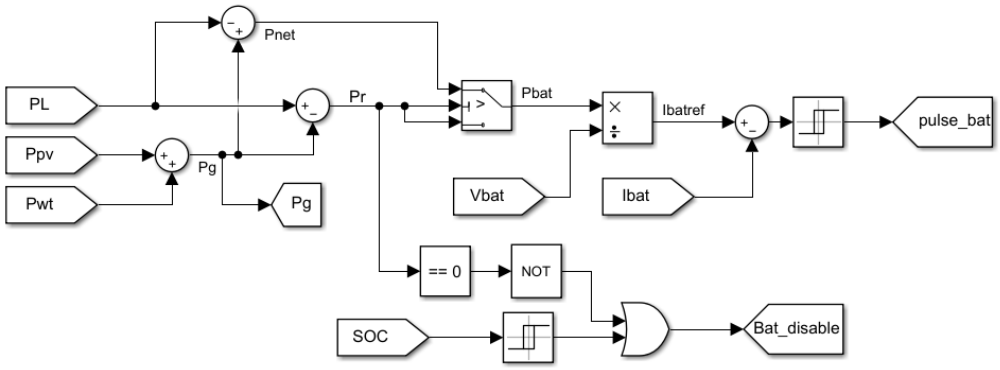

Figure 4.10: This is a Simulink model of the battery control algorithm [69]

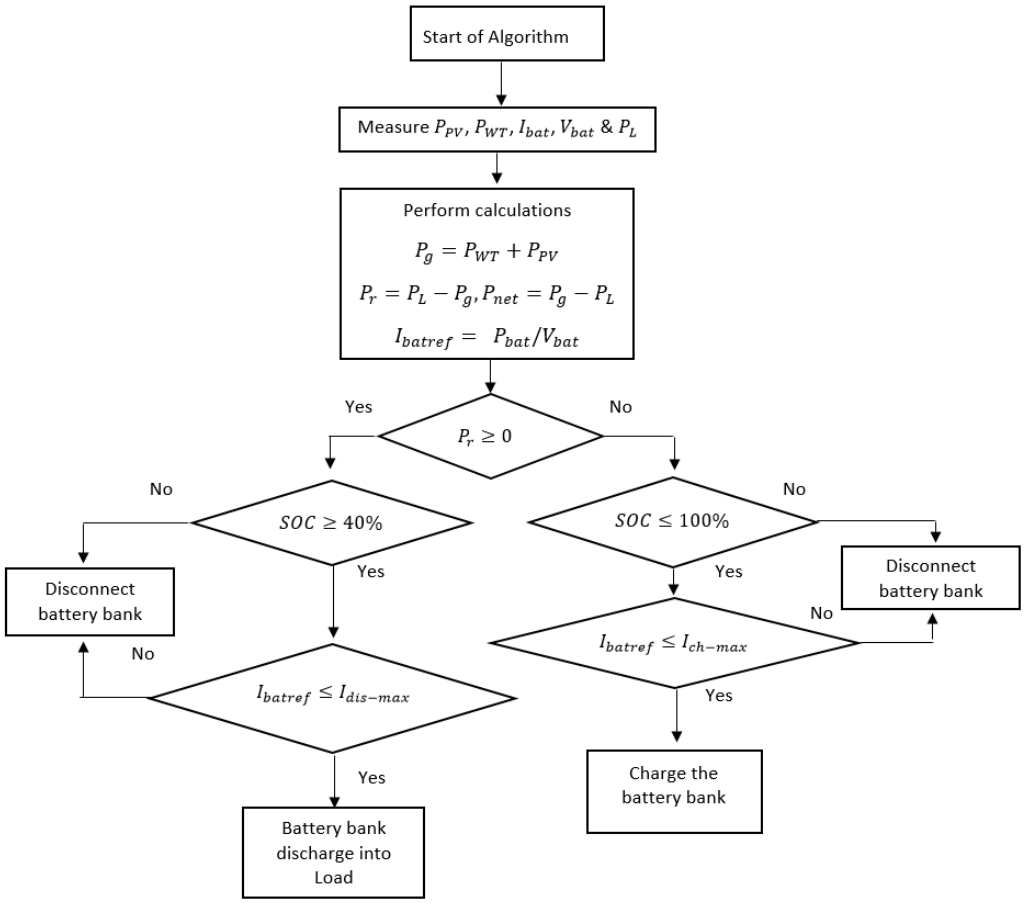

Figure 4.11: Flow chart of the battery control algorithm

Figures 4.10 and 4.11 above, show the battery control algorithm and flow chart, respectively. As discussed above, when both the WT and/ PV array generate power, more than required and depending on the weather conditions, the excess power is used to charge

the battery. Where the generated power fails to meet the demand load, the battery bank is used to supplement the load supply.

4.6 SIMULINK MODEL OF AN OFF-GRID WT-PV HYBRID SYSTEM

The Simulink model of an off-grid WT-PV hybrid system supplying a CP unit model is built, by connecting different blocks from MATLAB/Simulink. The PMSG-based wind turbine, PV system, MPPT's and CPU unit models are all built separately and then converted to subsystem blocks, for simplicity of the overall diagram. The overall system model is shown in the Figure 4.12 below. The output power of the system, from both PV and WT, as well as a battery bank, depending on the weather conditions, is used to power the CP system. The input of the overall system is the wind speed, solar irradiance, ambient temperate and turbine pitch angle.

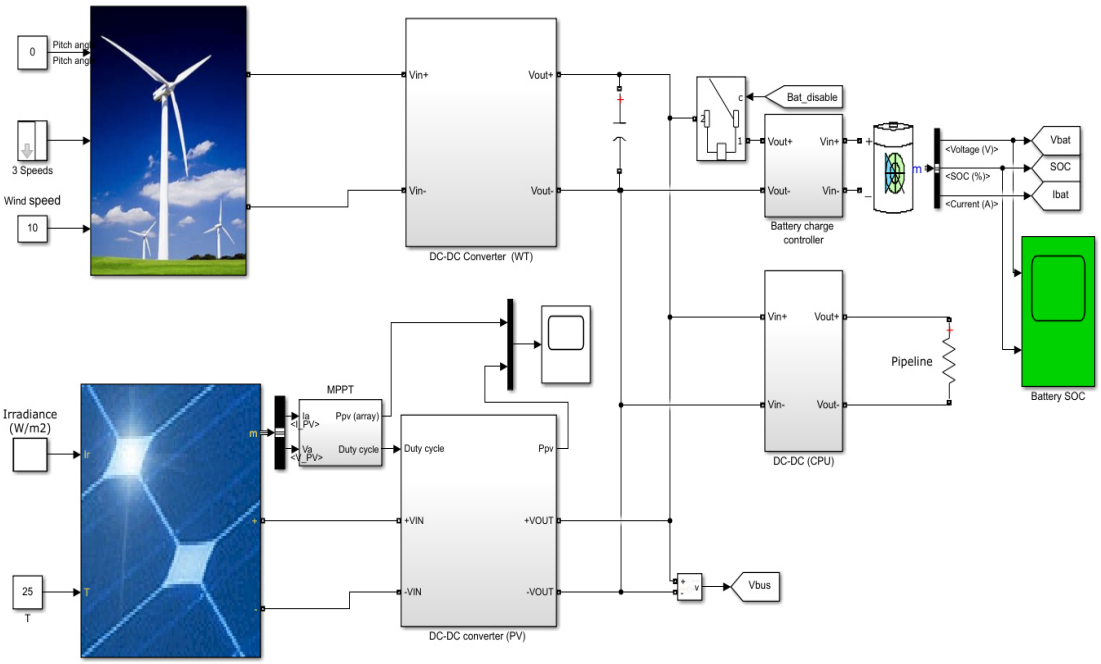

Figure 4.12: Simulink model of an off-grid WT-PV hybrid system

4.7 SIMULATION RESULTS AND DISCUSSION

This section presents the results of the simulations. The inputs are the wind speed, solar irradiance, temperature and technical specification of the selected equipment. Figure 4.13

shows the performance of the PV array at different irradiances, under a constant temperature of 25℃. The specification of the selected panels used to form the simulated array is given in Table 4.1. Specification of the selected horizontal wind turbine and Battery parameters are shown in Table 4.3 and 4.3, respectively, further given below.

Table 4.1: Used PV panel specification at STC [70]

Parameters	**Value with SI units**
Open circuit voltage (V_{OC})	48.2 V
Short circuit current (I_{SC})	9.8 A
Maximum power (W_p)	370 W
Maximum Power current (I_{mp})	9.35 A
Maximum Power Voltage (V_{mp})	39.6 V
Temp coefficient of I_{SC}	0.050%/°C
Temp coefficient of V_{OC}	-0.30%/°C
Operational Temp	-40 to +85°C
Module efficiency	19.1 (%)

Table 4.2: Specifications of the selected horizontal wind turbine [71]

Parameters	**Value with SI units**
Rotor radius (R)	1.6 m
Number of blades	3
The swept area by the rotor blade (A)	7.55 m^2
Maximum Power coefficient	0.45
Cut-in Wind speed	3 m/s
Working wind speed	3-25 m/s
Survival wind speed	45 m/s
Gearbox	None (Direct drive)
Rated power	1kW at 10m/s
Rotor speed	350rpm
Frequency	50Hz or 60Hz
Voltage	110V-240V
Generator efficiency	>85%
Stator resistance	2.9 mA
Armature inductance	0.308 mH
Flux linkage	0.0714394 Wb
Q-axis Inductance	0.971 mH
D-axis Inductance	3.21 mH

The battery bank contains four 12V batteries, which provide the voltage of 48V and 800Ah Capacity. The battery bank SOC is set to the initial value of 100%.

Table 4.3: Battery parameters [72, 73]

Parameters	Value with SI units
Model	6-CNF-200
Nominal voltage (V)	12 V
Capacity (Ah)	200Ah
Rated Depth of Discharge (DOD)	30% for 1000 cycles
Operating temperature	-25 °C to 45 °C
Internal resistance	5 mΩ
Approximation weight	58.5 Kg ± 3%
Self-discharge	≤ 2% per month (25%)

The performance of the array is further evaluated by simulating the output power for five different irradiance levels (200, 400,600,800 and 1000W/m^2), at a constant temperature of 25℃. The output is recorded for both the MPPT and the array power output. It may be seen that, as the irradiance increases, so does the power. However, the power increases with the irradiance, while the temperature remains constant. Furthermore, the PV array output is seen to be higher than the MPPT output at all times, however, the MPPT output lacks harmonics, caused by a change in irradiation.

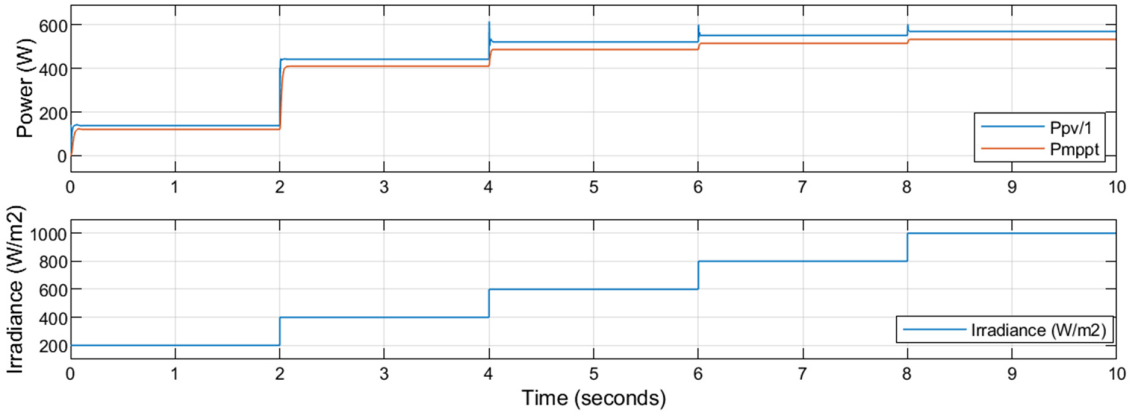

Figure 4.13: PV array and MPPT output power.

In Figures 4.13 and 4.14, it can be seen that when the irradiance is 200W/m^2, the PV array output is around 150W, slightly above 400W for 400W/m^2, 500W for 600W/m^2 and for the irradiance at standard test conditions, (STC), which is 1000W/m^2, provides the output of about 590W. The DC-DC converter output, driven by the MPPT gives an output, which is a few watts lower than that of the PV array output.

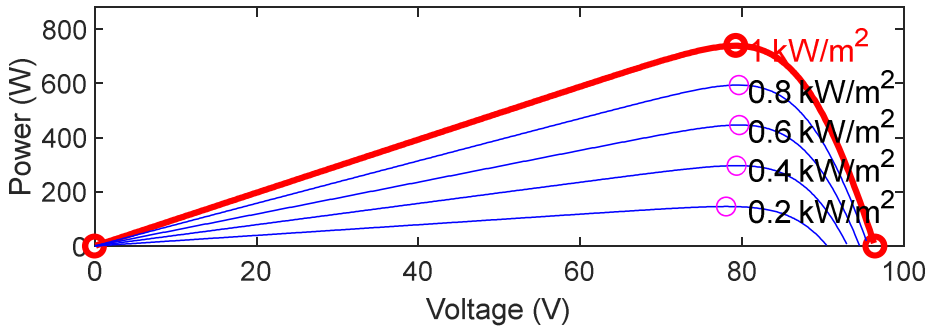

Figure 4.14: Array P-V characteristic curve for different irradiance levels.

Figure 4.2 presents data for the PMSG-based wind turbine. To study the dynamic response of the wind turbine system, the model is first simulated, with the rated wind speed of 10m/s at the rated power of 1kW. The system is then simulated at 4 different wind speeds of 8, 10, 15 and 20m/s, respectively, at a time interval of 0.2 seconds. The rated wind speed, which is 10m/s, is further included.

The wind turbine is simulated with a 1kW-3 phase balanced load, connected directly to the output of the PMSG. This condition represents the full load capacity of the wind turbine. The line voltages (V_{ab}, V_{bc}, V_{ca}), phase voltages (V_a, V_b, V_c) and currents (I_a, I_b, I_c) are given in Figure 4.16. With reference to Figure 4.15, it is clearly seen that the load is purely resistive and distributed evenly to the wind turbine, as a balanced Load. The line voltages have a peak voltage of approximately 110V in steady state. The phase voltages have peak values of approximately 80V, while the currents drawn, are in phase with the voltages, confirming the fact that the load is purely resistive. Furthermore, the output voltage and current drawn increase gradually, as the wind turbine generator picks up speed. The load current has a peak value of about 8 A, which provides an RMS value of about 6 A.

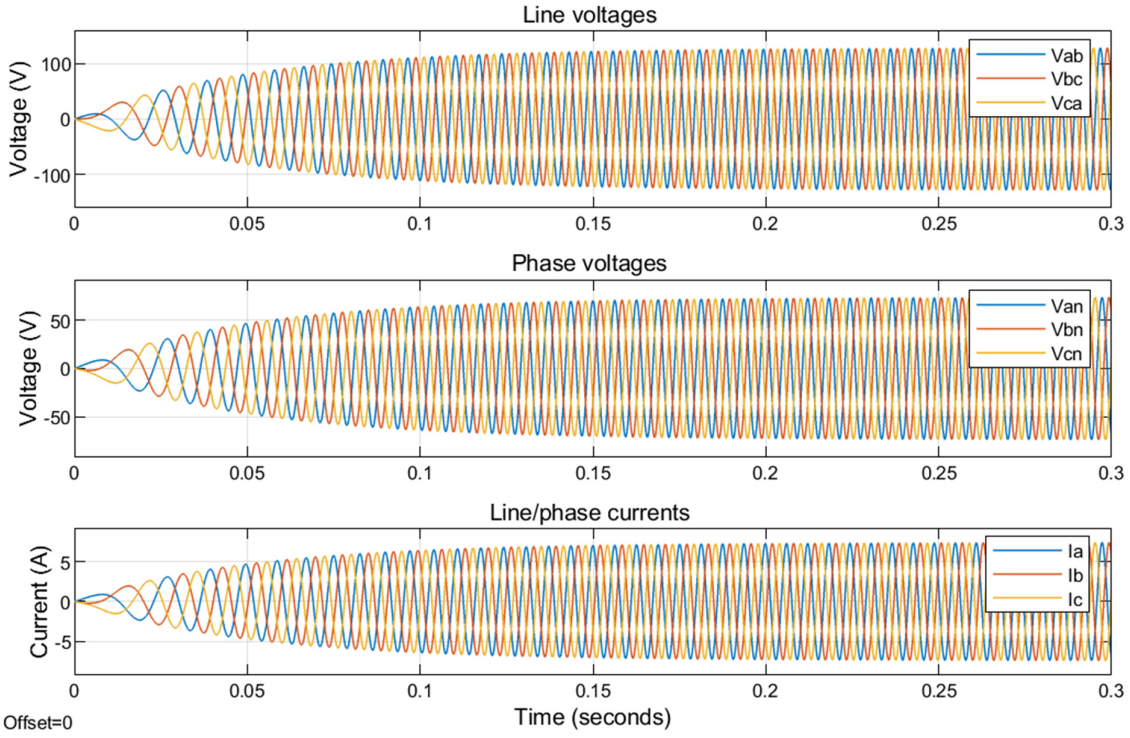

Figure 4.15: Line and phase voltages, and currents at the rated wind speed.

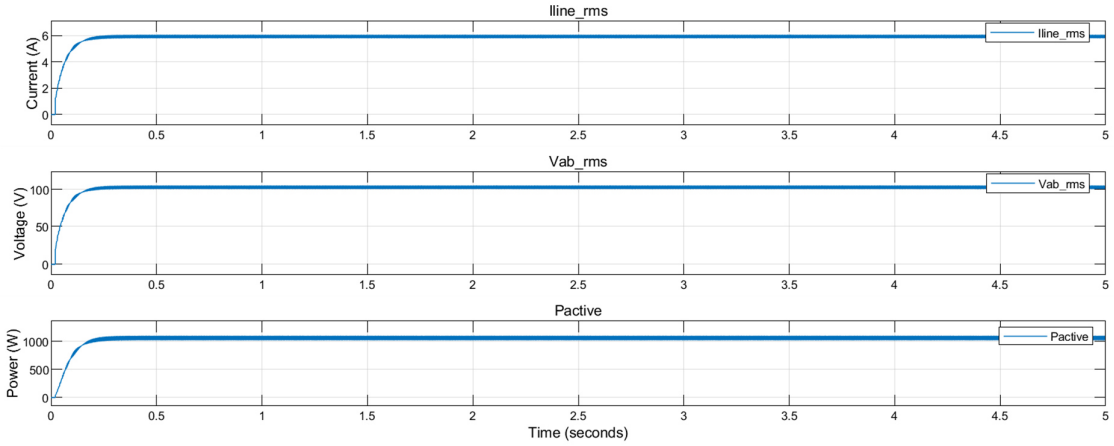

Figure 4.16: RMS voltage, current and active power (P_{active}) at the rated wind speed of 10m/s.

Figure 4.16 below, gives the active power (P_{active}), RMS line voltage and load current. The results show that the wind turbine generator takes approximately 0.2s, to reach the steady state values of line voltages (100V), currents (6A) and power (1kW), respectively. The steady-state RMS line voltage is approximately 100V, with RMS line current of 6A and hence, the power of 1kW. Furthermore, the generator produces nothing for the first 20μs

and this may result in the load draining from the battery bank, if the PV array should further produce insufficient power, to meet the load demand.

The electromagnetic torque and stator current are both shown in Figure 4.17. Results show that the electromagnetic torque starts from zero and it rises, gradually, until it reaches the steady-state value of 3 N.m. The stator current behaves similarly to the electromagnetic torque, besides the fact that the current has a steady-state value of approximately 8A peak. The electromagnetic torque is 1.5, 3.7, 5 and 8Nm at wind speeds of 8, 10, 15 and 20m/s, respectively, as shown in Figure 4.17.

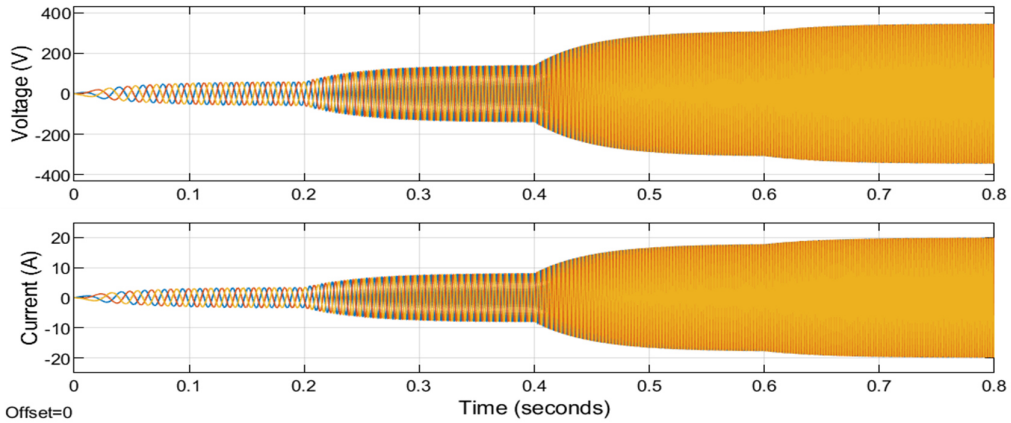

Figure 4.17: Electromagnetic torque and Stator current for different wind speeds.

From Figures 4.17 and 4.18, it seems that the produced voltage, current and electromagnetic torque are gradually rising as the wind speed increases. In addition, as the torque grows, the current rises higher. The output voltage at 8m/s is around a peak value of 50V, 100V for 10m/s, which is the rated wind speed and it maintains an increase to a value of 350V at 20m/s. These voltages in RMS are 35V, 71V and 247V, respectively.

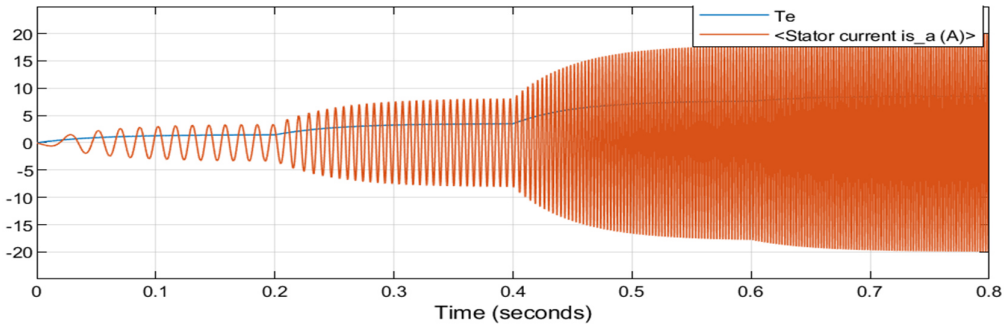

Figure 4.18: Generated voltage and load current for different wind speeds.

The output voltages of both wind turbine and PV array are connected to the DC bus through DC-DC converters. These converters are used to track the maximum power, while regulating the output voltages to match the desired value at the DC bus, for Battery bank charging and for supplying the load. The DC bus reference voltage (V_{busref}), is 48V DC. Figure 4.19 shows the actual bus voltage, with its desired (reference) value. It may be seen that, within the first 10ms, the actual bus voltage shoots up to a value of approximately 90V, which is due to the system start-up, however, it rapidly drops to the expected voltage output of 48V.

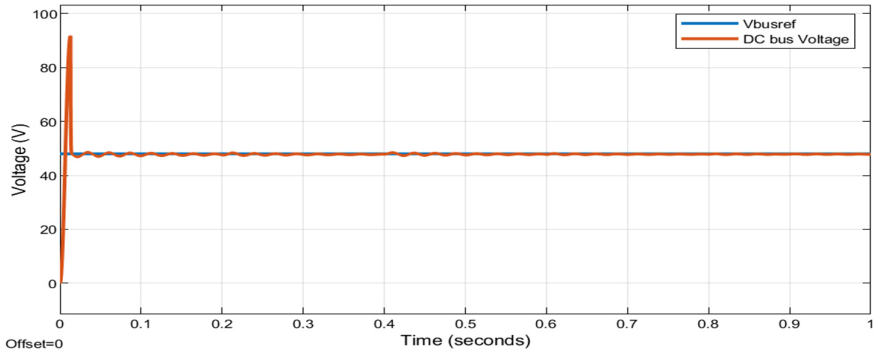

Figure 4.19: DC bus voltages.

The powerflow results are presented in Figure 4.20, under different scenarios, in order to show the dynamic of the system. Different scenarios are achieved by using different irradiance and wind speeds, to acquire less or no power generation, at desired times of the simulations. The inputs are changed every 2 seconds of the simulation, at the beginning of the first interval (0 to 2 seconds). The irradiance is set to 200W/m², with the wind speed of 0 m/s. During this period, the load power demand (PL), remains constant at 230W and for the rest of the simulation, while there is no wind power (Pwt) production, due to the fact the wind turbine is expected to be stationary. Furthermore, the PV generated power (Ppv) is insufficient in meeting the load, hence the battery bank is discharged to supplement the power demand. During this period, the excess power is zero.

A second scenario is presented in an interval between 2 to 4 seconds, where the PV irradiance is increased to 800W/m², with the wind speed of 8m/s. At the beginning of this period, the wind turbine does not produce power. However, after a few milliseconds, the generator picks up and produces approximately 600W, while the PV is generating 500W

immediately with the irradiance increase. Results further show that, when the power demand is less than the generated power, the excess power is approximately 870W. This energy is therefore used to fully charge the battery bank to its capacity.

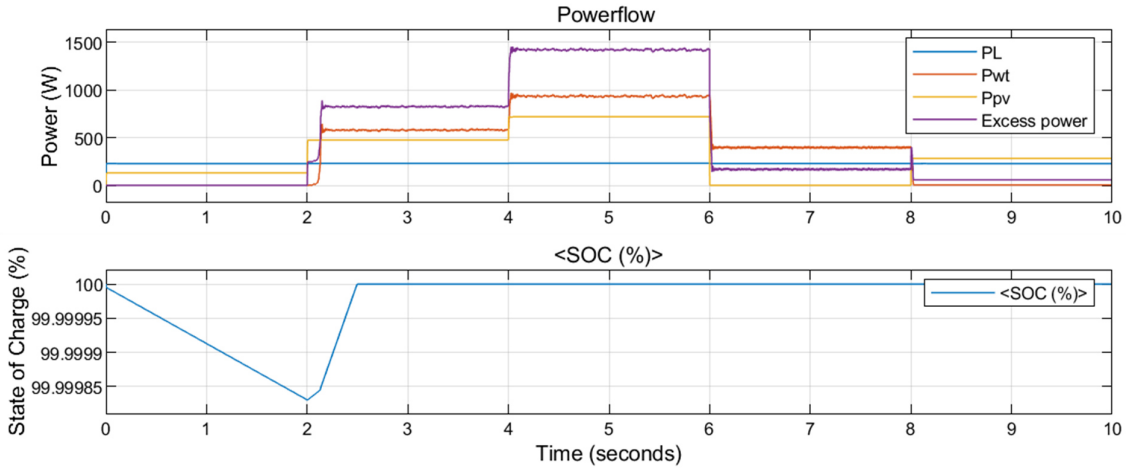

Figure 4.20: Powerflow and Battery State of Charge (SOC)

The third scenario is similar to previous one, except that the irradiance is increased to 1000W/m², with the wind speed being 10m/s. The objective is to evaluate the performance of hybrid energy system at rated inputs. This scenario is analysed between the time interval of 4 to 6 seconds as seen in Figure 4.20. The results show that both the wind turbine and PV system are currently operating at their rated power outputs of 1kW and 740W, respectively. During this period, the excess power is approximately 1500W. The fourth scenario is analysed within the time interval of 6 to 8 seconds, where the irradiance is set to 0W/m² and the wind speed up to 7m/s. The results show that, during this period, the PV system does not generate any power, while the wind turbine generates about 400W. The excess power is about 170W, however, this will be dumped, since the battery is currently fully charged. The last scenario is the time interval between 8 and 10 seconds, where the wind speed is set to 2m/s and the irradiance to 600W/m². The results indicate that the PV system produces an amount of power of 250W, which is sufficient to meet the demand. During this period, the wind turbine power output is zero, while the excess power is 20W.

4.8 CONCLUSIONS

This Chapter models and simulates a hybrid energy system, consisting of a wind turbine, a solar PV system and battery bank, using MATLAB/SIMULINK. Simulation results have revealed that with a change in wind speed, the output power of the wind turbine further changes with the wind speed. Similarly, when the solar irradiance changes, the PV power output changes, accordingly.

Furthermore, it is observed that when the PV and wind generated power fails to meet the power demand, the system discharges the battery bank to supply the load. When there is excess power, the wind turbine generator charges the battery bank. With this in mind, simulation results, therefore, demonstrate the effectiveness of the proposed model.

CHAPTER 5: PROTOTYPE IMPLEMENTATION AND ANALYSIS

5.1 INTRODUCTION

This Chapter presents the prototype of the CPU powered by the hybrid energy system. The aim is to verify the technical feasibility of the proposed system. The CPU supplies a maximum voltage of 24V DC, at a current of 10A, supplied by a wind/PV/battery hybrid energy system. The prototype is of a smaller size compared to the actual proposed system. However, the architecture is maintained.

The CPU is controlled by a microcontroller, which regulates the voltage output of the hybrid system, using PWM technique. Furthermore, the system uses a fixed potential concept, to manage the controller. Furthermore, the remote monitoring is being experimented, where the unit monitors the voltage, current and upload the readings on the Cloud, for remote accessibility.

5.2 BLOCK DIAGRAM AND DESCRIPTION

This section outlines the block diagrams of the CPU powered by the wind/PV/battery energy system. In these block diagrams, all components of the proposed system are clearly shown. These are: the hybrid energy system, control unit, CPU monitor and the test-post unit, which monitors a dedicated point on a pipe.

5.2.1 Control circuit

Figure 5.1 shows the block diagram of the CPU control circuit, with the hybrid system. Furthermore, the system has the DC-DC buck-boost convertor, which regulates the 12DC voltage from the hybrid system to a value required to protect the pipeline. This voltage is regarded as having a maximum point of 24V DC and a minimum of 0V DC. The voltage is controlled by a microcontroller ATmega328. The microcontroller is used to increase and decrease the duty cycle, hence achieving the pulse width modulation (PWM). This is carried out with reference to two input signals, namely, the setpoint and the feedback.

The setpoint is obtained from CP standard document, named SANS 155891:2009. The standard requires that the pipeline potential should be more negative than - 850mV and not less than − 1200mV, with reference to the copper-copper sulfate reference electrode (CSE), to avoid the detrimental effects of hydrogen production and a high pH level at the metal surface[18]. Therefore, for this project, the aim is to maintain the voltage setpoint to 1200mV, throughout the design life of the pipeline. The second input is the feedback voltage, measured from the pipeline, with reference to the CSE. To maintain the voltage to 1200mV, the control system pushes more power from the hybrid energy system, when the feedback voltage is less than the set value. When the feedback voltage is higher than the set value, the control system decreases the power output from the hybrid energy system.

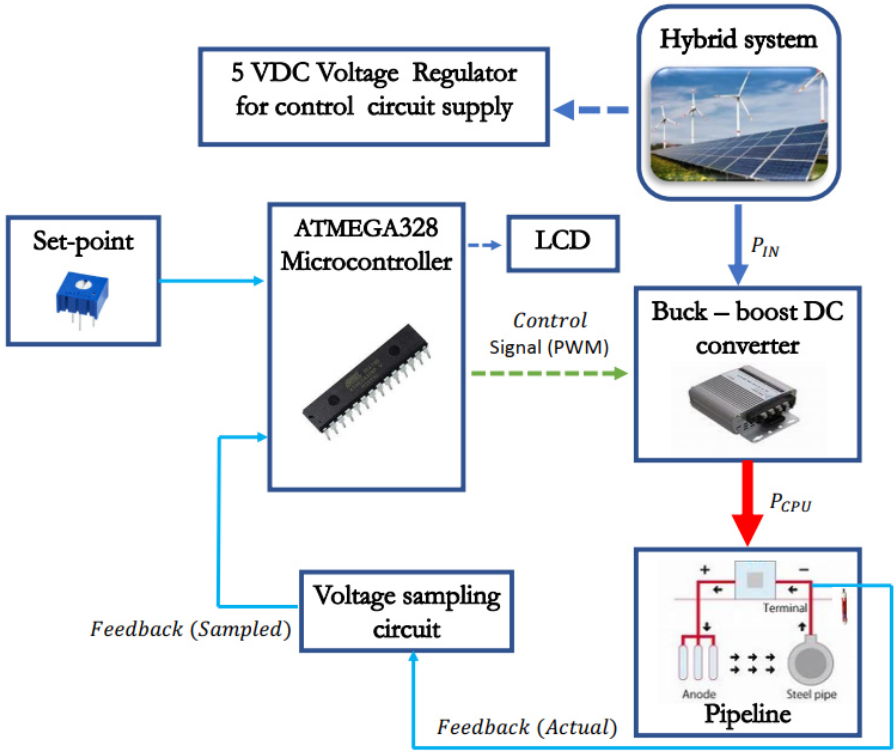

Figure 5.1: Block diagram of the CPU control circuit with the hybrid system and load.

The potential measurements are obtained through the use of the voltage sampling circuit, which will be discussed later. The sampling circuit is mainly for safety purposes, in case the pipeline potential rises beyond the maximum specified voltage input of the microcontroller. The Liquid crystal display (LCD), shows the status of operation, by displaying the duty-cycle in percentage, the specified voltage setpoint, as well as the

feedback voltage, at the point where the CPU is installed. The power supply for the control circuit is achieved using a 5VDC voltage regulator, rated at 3A. This voltage is obtained from the hybrid output terminals, which have a nominal voltage of 12VDC. The power drawn by the whole CPU circuit is referred to as P_{IN}, while P_{CPU} is the power impressed to the pipeline for its protection.

5.2.2 CPU monitoring circuit

Due to the fact that the networking takes a few seconds for signal reception, and further, the fact that the DC-DC convertor runs at a high frequency, the CPU monitoring circuit had to run on a separate microcontroller. Figure 5.2 shows the block diagram of the CPU monitoring circuit, where the setpoint and feedback are obtained, as previously mentioned. This circuit is connected in parallel with the circuit in Figure 5.1. Furthermore, the voltage sampling circuit functions the same as the one used in the control circuit, where two resisters 7.5kΩ and 30 kΩ are connected in series, to implement the voltage divider circuit.

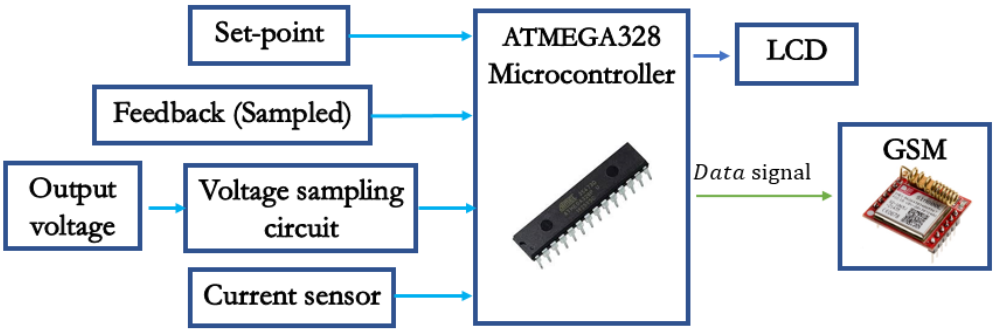

Figure 5.2: CPU remote monitoring circuit

The reason for this, is to lower the voltage to levels suitable for those of the microcontroller operation. The sampled voltage ratio used, is 1:5. The output voltage is the voltage measured from the terminals of the DC-DC converter, with the positive terminal connected to the anode and negative terminal to the pipeline. The LCD displays the output voltage, current, power, voltage feedback and the setpoint. The current is measured using the current sensor ACS712, rated at 20A. The current sensor samples the current and provides a DC voltage signal, corresponding to the input current. All the measured

parameters are transmitted to the server thingspeak, using the Global system of mobile communication (GSM) module SIM800L. The system is programmed to send short message texts (SMS), when the pipeline penitential rises above - 850mV, or significantly below – 1200mV. However, the measuring cables polarities have been reversed for circuit simplicity.

5.2.3 Test post (TP) monitoring

The pipeline with cathodic protection, has to be monitored at different intervals. This is carried out, mainly, after every 500m interval, at both ends of the pipeline and/or each end of the possible isolation point, such as river crossings, road or rail crossings, ensuring that the pipeline is protected. Figure 5.3 shows the block diagram of the monitoring circuit used to monitor all the test posts. The circuit reads the pipeline voltage at the specified point. The microcontroller reads the input signal from the sampling circuit and calculates the actual voltage, while displaying this on the LCD. The measured value is transmitted to the thingspeak, so that when the value falls outside of the range, a warning SMS is sent to the maintenance supervisor.

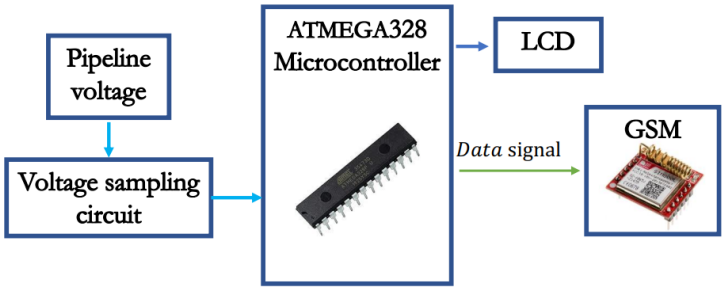

Figure 5.3: TP remote monitoring circuit

5.3 HARDWARE DESCRIPTION

Shown in Figure 5.4, is the soldered control circuit, CPU monitoring circuit and TP on hard PCB, respectively. The circuits contain all components required to perform the function of the proposed system, namely, the CPU control and remote monitoring. The PCB circuits were cased and installed in a CPU unit, with charge controllers and protection

fuses, to form a complete the CPU panel, for cathodic protection. All termination and connection tests were conducted.

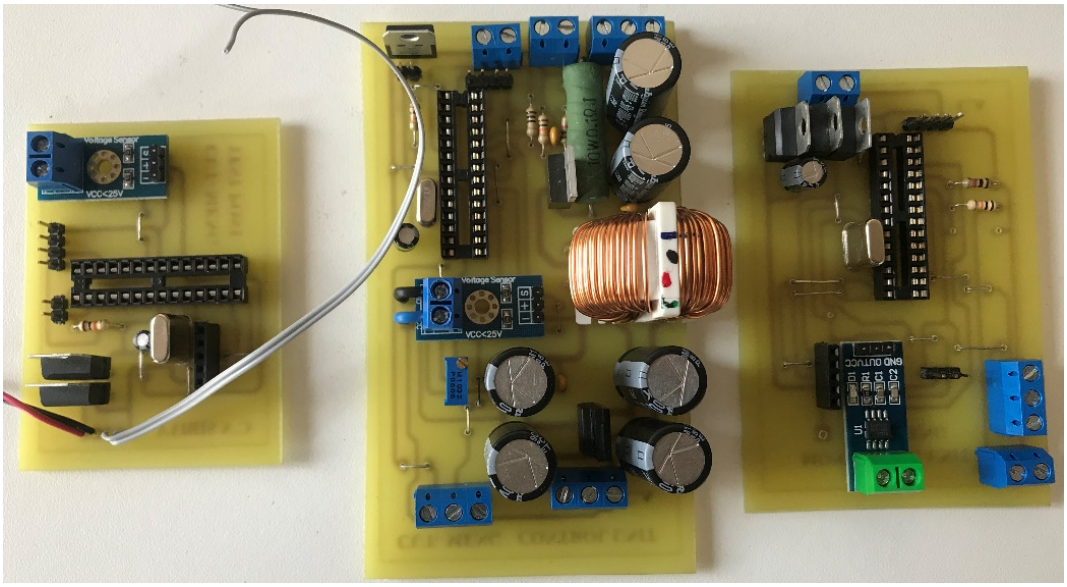

Figure 5.4: Soldered PCB circuits

These soldered PCB circuits were cased and installed in a CPU unit, with charge controllers and protection fuses, to form a complete CPU panel for cathodic protection. All the termination and connection tests were conducted and the results are presented in the sections below.

Figure 5.5 (a) and (b), show the installation of the metal bar and an anode underground. The two were installed half a meter apart, in parallel, to enhance better conductivity. The metal bar representing a pipeline of 2 m long, with the anode being 1m long. Both of them were covered underground at a depth of 0.2 m, with cables exposed for further connections. The anode was connected to the positive side of the voltage source and the metal bar (pipeline), to the negative side.

Figure 5.5: (a) left, ground installations, (b) right, Anode and metal bar installed.

Figure 5.6 shows the complete project setup with solar panel, DC generator 12 V battery, laptop and internet connection router, GSM module antennas and testing devices, such as an oscilloscope and multi-meter. The inverter is installed to power the oscilloscope for testing purposes, as well as for changing the laptop during on-site testing. The DC generator, acting in place of a wind turbine, is coupled to a DC motor, to drive the generator as a prime mover.

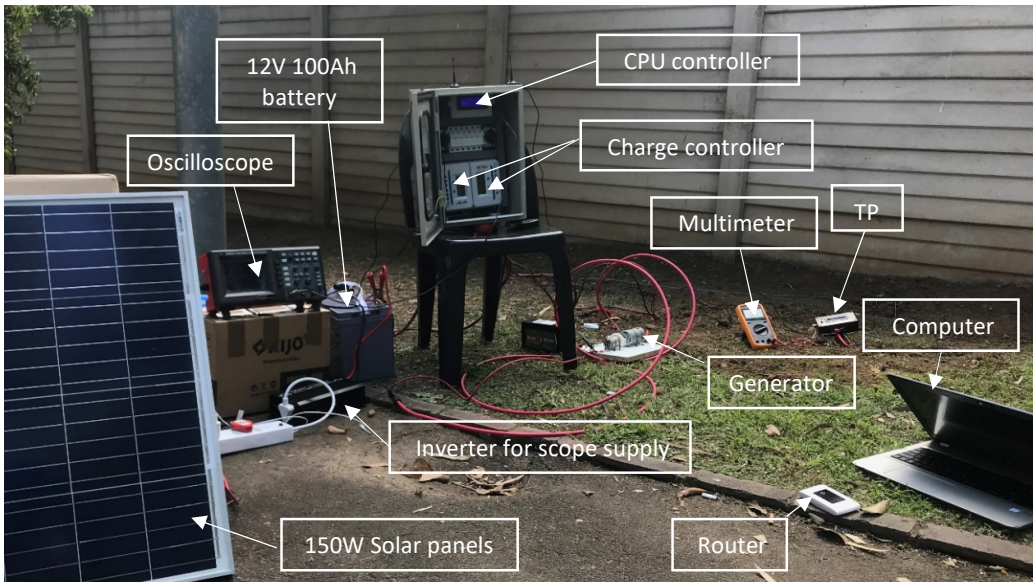

Figure 5.6: Final project setup

5.4 TESTING, ANALYSIS AND DISCUSSION

In this section, the test results and analysis of the CPU are discussed. Figure 5.7 and 5.8, show the measurement setup to monitor the ground potential of the selected test site. The ground potential was first measured to monitor whether the ground is corrosive and the reading was -0.785 V DC, which is more than the required minimum of -0.85V DC. This was further tested using the designed TP unit, to monitor its measurement accuracy. It was discovered that the TP unit has an error of approximately 0.07V. This is due to various factors, such as the resistor tolerance, as well as the voltage drop on the testing leads, caused by test lead resistance.

Figure 5.7: Ground test with reference to CSE

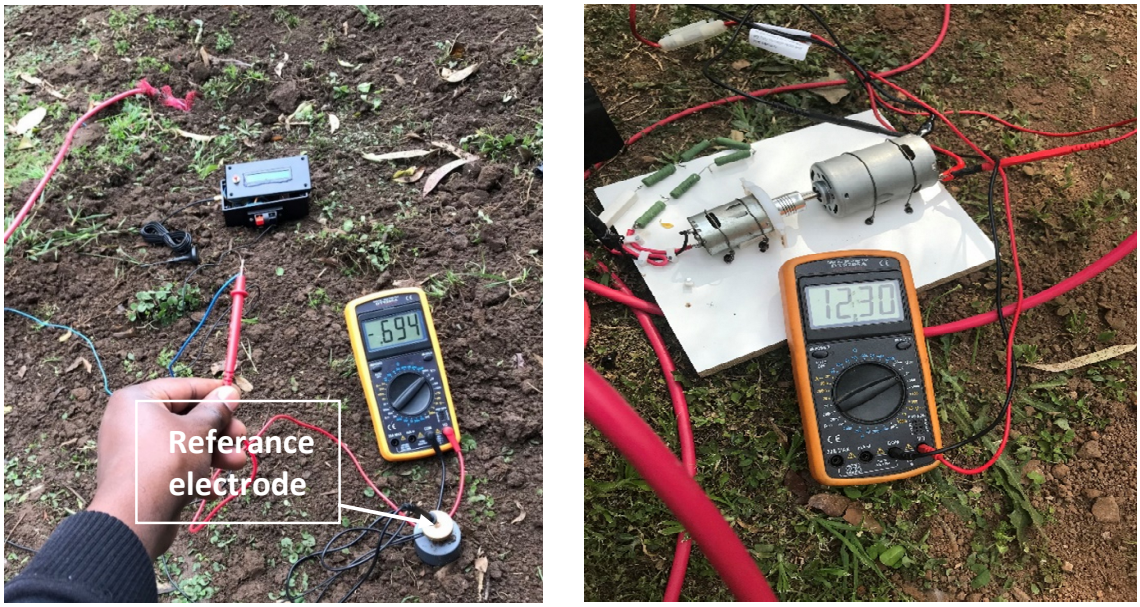

Figure 5.8: (a) left, Ground test setup, (b) right, DC generator output voltage (V).

Figure 5.8 (b), shows the DC generator output feed to the CPU via a Charge controller. The CPU is supplied from the solar panel and wind turbine, of which the total power is fed to the battery bank, through the charge controller. The power is later used to impress current to the ground, via the CPU. Initially, the feed was not detected by the CPU, due to the polarity of the connection. When this occurred, the unit increases the duty of the PWM, in order to increase the voltage output and raise the pipeline voltage to the required value. Hence, Figure 5.9 shows that the duty cycle is 38% and this constantly rises, so long as the power generated by the wind turbine and PV system is less than required. During this time, the CPU reaches the feedback voltage of -1.22V, while drawing a current of 0.15A. A voltage of 0.95V is therefore supplied to the pipeline via the anode, which translates into a power consumption of 0.14W. At this point, the battery voltage is 12.7V, as shown in Figure 5.10.

Figure 5.9: CPU site testing with 38% duty cycle

Figure 5.10: Tested with a feedback of -1.22V

The pipe to ground voltage was further tested at one end of the metal bar, to test whether the anode is showering the whole bar. This is shown in Figure 5.11. May be seen that the unit measured the voltage of -1.22V, which is verified by the multimeter to be corrected, owing to the fact that it measured 1.2V later, while the TP monitoring unit measured -1.22V, with the lead reversed.

Figure 5.11: Pipeline test using TP

The waveforms obtained using the oscilloscope during testing, are displayed in Figures 5.12 and 5.13. Figure 5.12 shows the PWM signal, when the CPU is switched off, while Figure 5.13 shows the signal for a duty cycle of 7%, which corresponds to the operation point, where the feedback voltage meets the desired value. For demonstration purposes, the anode supply was taken off, to get the feedback to a lower value than the setpoint. At this point, the CPU increased the output voltage, to push more current, to pick up the feedback to the desired value, as shown in Figures 5.13 (a) and 5.13 (b).

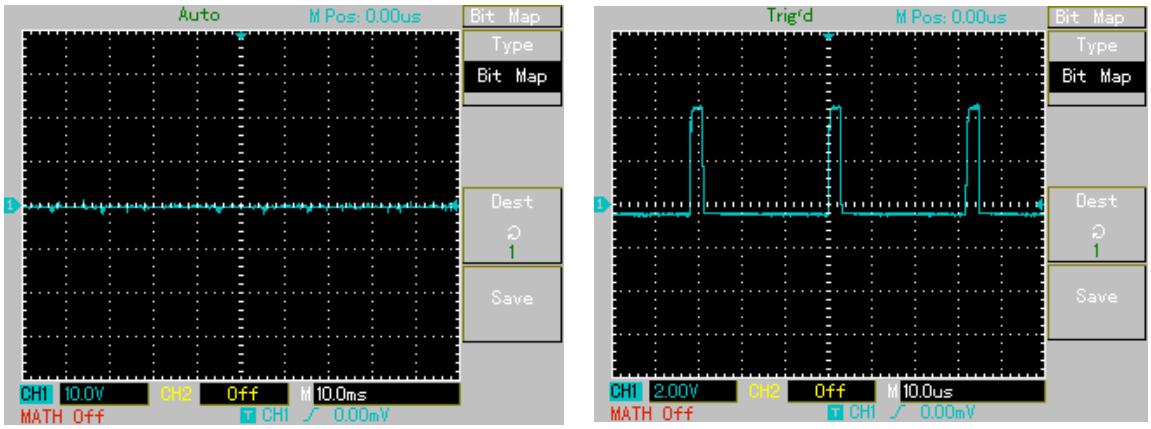

Figure 5.12: (a) left, PWM waveform at no output, (b) right, PWM waveform at duty cycle of 7%.

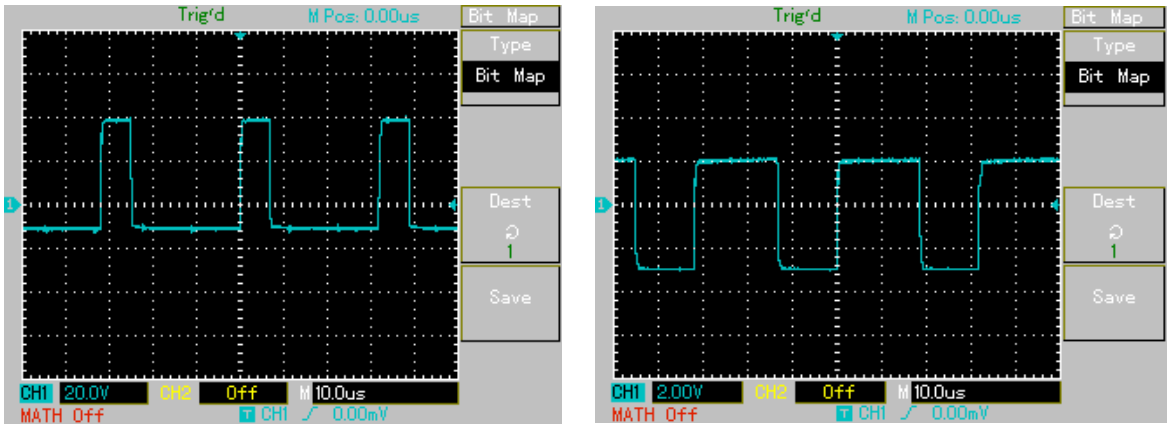

Figure 5.13: (a) left, PWM waveform at duty cycle of 23%, (b) right, PWM waveform at duty cycle of 63%.

Shown by Figures 5.14 to 5.19, are the results for current, voltage and power, obtained during testing. These results were recorded using hardware and software components. The telemetry, part of the prototype as previously described, was utilised, to remotely measure the current, system voltage, power output, setpoint voltage and pipe potential and vail these to the server (thingspeak). The information is sent via a GSM network to the Cloud. The voltage for the pipe to the ground has been inverted, to simplify reading and analysing.

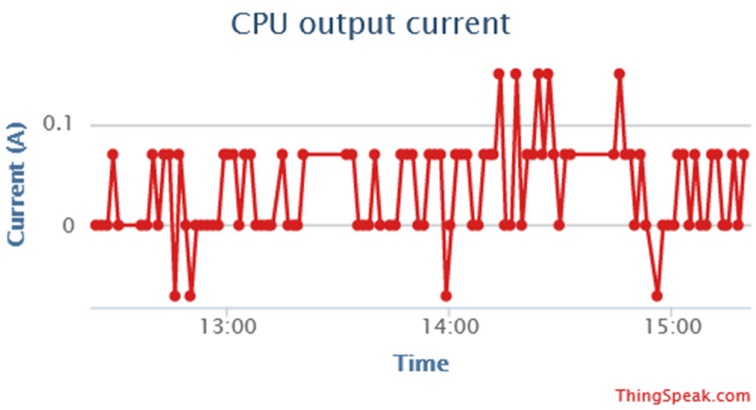

Figure 5.14: CPU output current

Shown in Figure 5.14, is the CPU output current being delivered to the steel plate installed underground, via an anode. As seen from the graph above, the highest current value on record for the given setpoint of 1.2V is 0.15A, with the lowest value of -0.07A, occurs when where the CPU control unit is switched off. Furthermore, the current stays at 0.07A during operation and fluctuates between 0 and 0.07A. The results displayed were recorded from 12:30 to 15:30, on the day of tests.

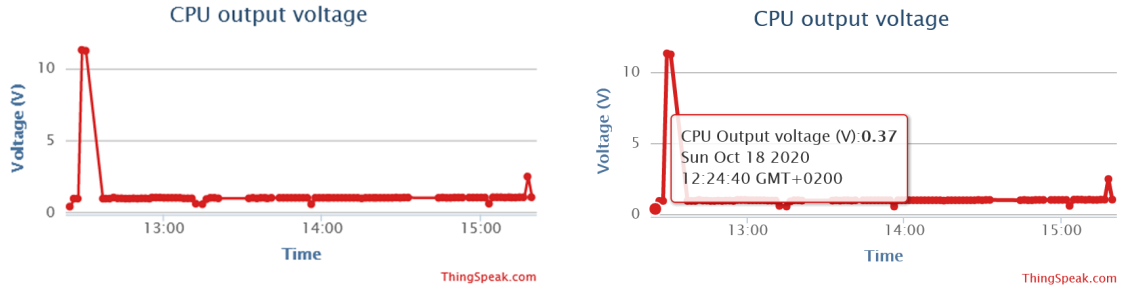

Figure 5.15: CPU output voltage

As seen from Fig. 5.15, the first point is recorded at 12:24:40 with a voltage of 0.37V. The controller starts with the lowest voltage and constantly increases, until the feedback voltage is obtained from the CPU measuring unit. The voltage increased to the value of approximately 11.28V DC, since the feedback was not yet connected. After the connection of the feedback cable, the voltage dropped to a value of 0.93V DC, measured between the steel bar and the ground, through the reference electrode. The voltage is then maintained around the value of 0.93V DC, while the feedback is maintained on the set-point value.

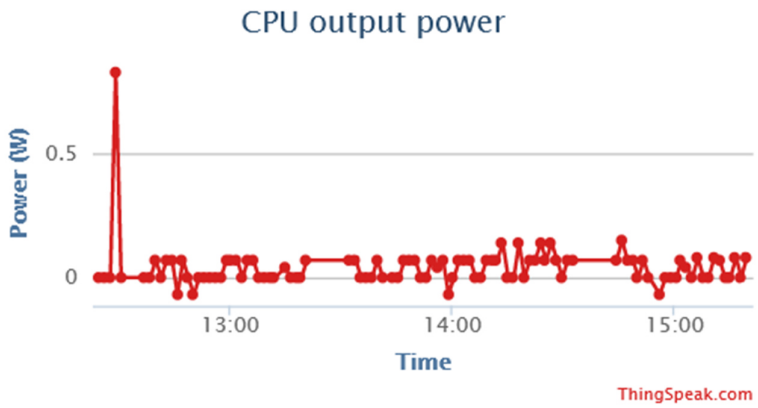

Figure 5.16: The output power of the CPU protecting a 2 m

Figure 5.16, shows the output power for the CPU to protect the steel piece against corrosion. The power starts from zero and increases as the CPU feeds more power to the anode to shower the steel piece with electrons. The power becomes negative when the CPU is suddenly switched off, while the anode provides feedback power to the CPU unit. This may be prevented by connecting a diode on the anode feeder cable. The set-point is set to -1.2V, which is 1.2V in Figure 5.17, due to ground values, inverted for simplicity of measurement. The inversion was carried out by swapping the positive and negative terminals on the measuring unit. Results show that the setpoint fluctuates between 1.18V to 1.21V DC, which is due to the sampling changes in the measuring unit.

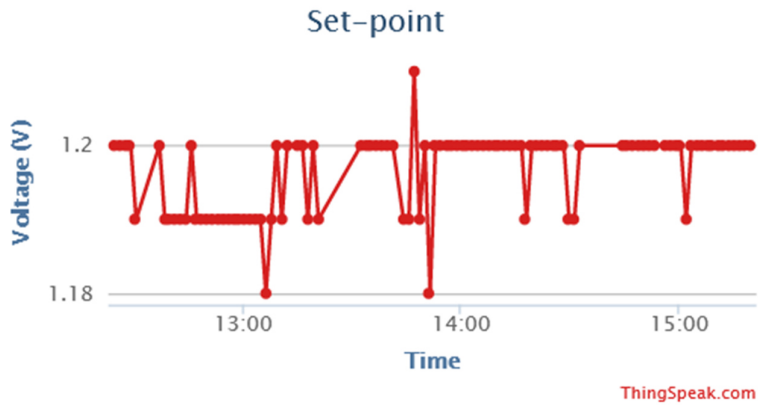

Figure 5.17: CPU set-point voltage

The set-point is used as a reference to the feedback voltages obtained from the CPU point pipe (metal 2m bar) to the ground, as well as the end of the metal piece. Figure 5.18 shows the metal piece to ground measured voltages, where the lowest point is 0.5V, -0.5V

dc when not inverted. The voltage picks up with time and maintained at the set-point voltage of 1.2V, -1.2V DC, when not inverted.

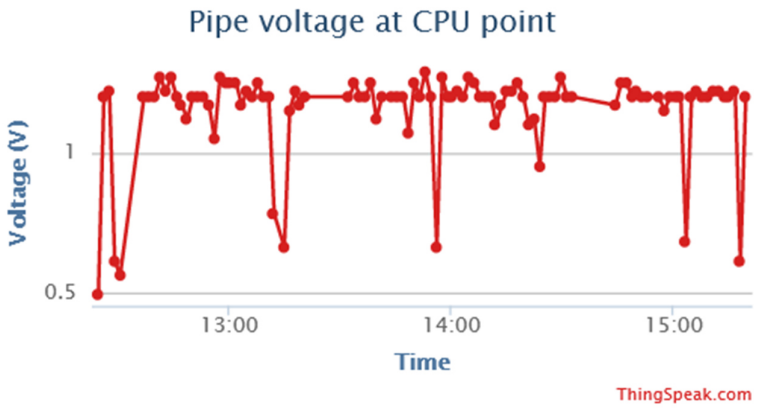

Figure 5.18: Pipe voltage at the CPU location

In practice, the pipeline is sufficiently protected when the pipe to ground potentials are within the allowable range. Hence, it is important to test as many points as possible on the pipeline. The results are shown in Figure 5.19, outlining the readings obtained from a test point (TP). The lowest value on record is 0.56 V, with 1.2V being observed at most times during the test. The highest value on record is 6.67 V, which is the value recorded when the feedback was discounted and the CPU was pushing more voltage to, increase the pipe potential. The metal to ground voltages reaches 0.66V, 0.66V, 0.68V and 0.61V at 13h14, 13h56, 15h03 and 15h17, respectively.

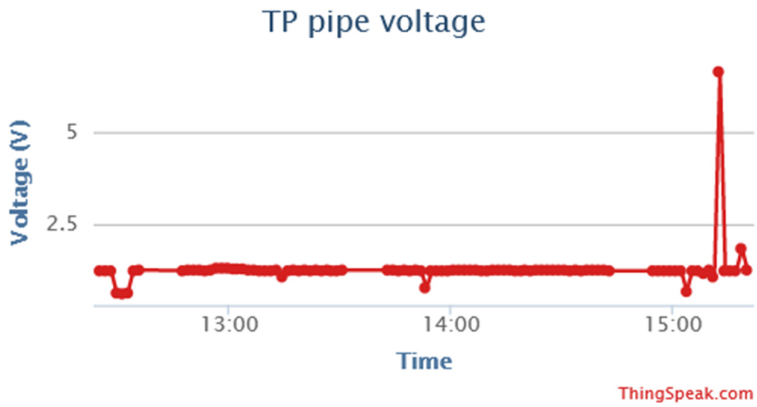

Figure 5.19: Test post (TP) pipe voltage

The metal to ground voltages was, again, measured from the end of the bar, to ensure that the entire bar is protected against corrosion. This point is referred to as a test post one

(TP1). A pipeline may have as many TPs as possible, depending on the owner affordability. However, the TPs have to be placed every 500m to 1km, depending on the length of the pipeline. Figure 5.19 shows the voltages on record for the end of the bar. As seen in this Figure, between 14h00 and 15h00, the voltage is maintained at 1.2V DC, which is -1.2V when not inverted. When the feedback was disconnected, the voltage raised to a value of 6.67V, after 15h00 and later decreased to a normal value of 1.2V, when the connection was re-established.

5.5 CONCLUSION

This Chapter focused on the prototype of the proposed system, where the CPU was constructed. The built CPU was supplied by the PV panel together, with a 12V DC generator, coupled to 12V DC motor, used as a prime mover of the wind turbine generator. The CPU further contained as a separate module, which is a monitor and records voltage, current, power, pipe to ground voltages, as well as the set-point voltage. All monitored measurement values were uploaded to the Cloud, for recording purposes.

The experimental results have demonstrated the technical feasibility of the proposed hybrid energy system, powering a CPU. Moreover, the online monitoring system was effective and provided a true reflection. The power consumed by the CPU is significant, thus making the supply sufficient for the system. The experimental results, therefore, confirm that the combination of solar and wind resources with battery storage, may be employed for the operation of CPUs.

CHAPTER 6: ECONOMIC ANALYSIS

6.1 INTRODUCTION

To evaluate and analyse the cost-effectiveness of the proposed ICCP system, which is fully dependent on renewable energy, numerous economic performance indicators may be utilised. In this study, the Life Cycle Cost (LCC) method will be used, to analyse the cost-effectiveness of the proposed system. This is due to the LCC method considering inflation, the life expectancy of the project and, hence, it discounts all future worth cash flows to a Present Worth (PW) [74]. Apart from LCC, there are other cost performance indicators, such as benefits to Cost Ratio (BCR), Simple Payback Period (SPP) and Initial Rate of Return (IRR). However, SPP is the simplest economic analyses method, however, it does not consider inflation and the costs associated with the lifespan of the project. Furthermore, BCR and IRR methods do consider inflation and project lifetime, however, for this study, LCC and Breakeven Point (BEP), evaluation and analysis are performed, together with the "True PBP", to determine whether the investment will pay off. The life expectancy of the project, is 25 years.

6.2 BASELINE

To evaluate the effectiveness of the developed hybrid PW-WT system model, the energy cost savings achieved by the hybrid system will be compared to the energy cost accumulated by the TRU unit, when running from the grid and operating on a landrate tariff. As discussed in Chapter 3, the average total daily consumption is 4.74 kWh, for the selected TRU and the load has a uniform behaviour. According to the landrate tariff Non-local authority rates, the energy charge is 130.67 c/kWh, giving a total of R185.81 per month. However, there are other charges associated with the assigned tariff and these are: the network demand charges, Ancillary service charges, Network capacity charge and service charges, which in cost are 32.65c/ kWh, 0.51c/kWh, R34.9/day and R28.98/day respectively [75]. Hence, the total monthly electricity is R2, 149.36, inclusive of 15% VAT, giving a total of R25, 792.32 for the current financial year 2019/2020.

6.3 INITIAL INVESTMENT COSTS OF THE HYBRID SYSTEM WITH CPU

The proposed hybrid renewable energy system with a CPU, will be designed, using several components. The system consists of two 370W solar panels, one 1kW wind turbine, four 200Ah GEL barriers, two MPPT controllers, a battery charger, a CPU and cabling. The average prices obtained for each component are outlined in Table 5.1, below.

Table 6.1: Bill of quantities of a 1.74kW standalone hybrid system with CPU

Component description	Life span	Number of replacements	Qty.	Net price	
				(R)	USD
1kW wind turbine 3 blades	20	1	1	3, 580.90	244.93
370W mono-crystalline panels	25	0	2	4, 084.8	279.4
200AH 12V GEL battery	5	4	4	20, 332.00	1, 390.7
MPPT 48V	15	1	2	2, 557.48	174.93
CPU	25	0	1	1, 850.00	126.54
Battery charger	15	1	1	1, 325.22	90.64
Structures and Installations costs	25	0	1	18, 804.37	1, 286.21
Total initial investment cost				52, 534.77	3, 593.35

6.4 LIFE CYCLE COST ANALYSIS

The project lifetime of 25 years is determined for the proposed system. This is based on the 25 years giving a guarantee for the PV panels and the life expectancy of the pipeline. However, other components, such as batteries and MPPTs, should be replaced after 5 and 15 years, respectively. 20% of the initial cost of investment will be taken as the salvage cost for the hybrid WT-PV system with CPU. Due to the change of components pricing, which is mainly affected by inflation, the future replacement cost should be calculated. This will be carried out by assuming that the average inflation rate will be equal to the interest rate [74]. The replacement cost of components may be calculated, using an expression shown in Eq. (5.1) below:

$$C_{rep} = \sum_{k=1}^{N_{rep}} C_{cap} \times (1+r)^{n*k}\,, \tag{5.1}$$

Where: C_{rep} = Initial capital cost for each component;

N_{rep}= Number of component replacements of the 30-year lifetime;

n = lifespan for a specific component (years);

r= Average inflation rate shown as 4.5% in Figure 5.1.

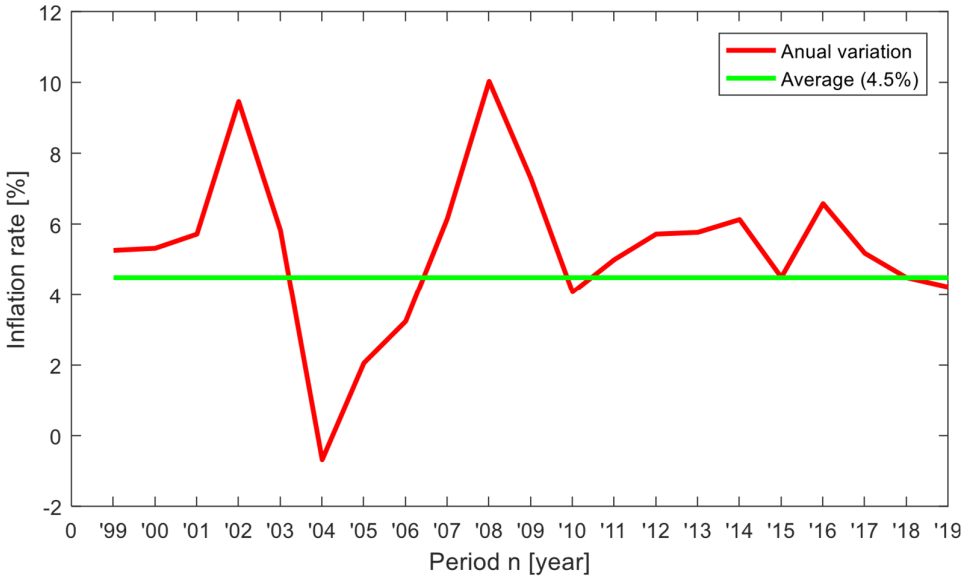

Figure 6.1: Inflation rate of South Africa from 1999 to 2019 [76].

6.4.1 Baseline life cycle cost analysis

The current TRU is supplied by the grid system as explained in section 5.2 and the utility company handles the salvage cost, as well as the replacement cost since it is their due restriction. However, the accumulated cost of energy for the duration of the project will be considered, with an interest rate of 10%, annually. The total cumulated electricity cost C_{EC} may be obtained by Eq. (5.2), given below:

$$C_{EC} = \sum_{K=1}^{25} C_{initial-EC} \times (1+a)^k \tag{5.2}$$

Where: $C_{initial-EC}$ = Cumulative cost of energy at the end of year one (ZAR);

k = The year at which the cumulative cost should be calculated (years);

a = Annual increase of 10%.

The initial cost $C_{initial}$, is the amount that is an application for a new connection in remote areas, however, for this study, the cost will be assumed to be zero, due to the system that currently exists. The operation and maintenance costs at the end of each year are calculated, using Eq. (5.4). However, in this case, it is assumed to be zero, since the grid does not require maintenance by the end-user. The total life cycle cost for the baseline is obtained by using Eq.5.3 below:

$$LCC_{Grid} = C_{initial} + C_{rep} + C_{EC} + C_{OM} - C_{salvage}\,. \quad (5.3)$$

However, taking into consideration that $C_{initial}, C_{rep}, C_{OM}\ and\ C_{salvage}$ costs are the responsibility of the utility company, the life cycle cost, due to Umgeni water, may be revised, given by Eq. (5.4). For the grid-supplied energy, the total life cycle costs are shown in Table 5.2 below, for 25 years and the total amount is approximately R2, 790, 258.71, that should be spent if the company is to use the grid instead of the hybrid system.

$$LCC_{Grid} = C_{EC}. \quad (5.4)$$

Table 6.2: Total life cycle cost of the grid

Cumulative Cost	Value (R)	Value (USD)
$C_{initial}$	0	0
C_{rep}	0	0
C_{OM}	0	0
C_{EC}	2, 790, 258.71	190, 852.17
$C_{salvage}$	0	0
LCC_{Grid}	2, 790, 258.71	190, 852.17

6.4.2 Standalone Hybrid renewable WT-PV system life cycle cost analysis

In the case of the proposed system, there are further considerations that should be made. These are mainly the components that should be replaced during the project lifetime, as well as the salvage cost, operation and maintenance costs and the initial cost of the project. The cumulative energy cost for the standalone hybrid system, will be zero, since there will not be any sales or purchases from the grid. The calculations associated with obtaining the above-mentioned variables are outlined in the following sections below.

A. *Cumulative replacement cost*

The total cumulative replacement costs of the proposed system components, at the end of the project lifespan is calculated, by anticipating the future cost of the components, using inflation and the current price of the components. C_{EC} may be obtained by utilizing Eq. (5.1). The total replacement cost for the proposed system, is given in Table 5.2. Therefore, the total replacement cost of components for the project lifetime C_{rep-TC}, can be obtained, by using Eq. (5.5) below:

$$C_{rep-TC} = C_{rep-BAT} + C_{rep-MPPT} + C_{rep-WT} + C_{rep-BC} + C_{rep-PV}\,. \qquad (5.5)$$

Wher: $C_{rep-BAT}$; $C_{rep-MPPT}$; C_{rep-PV}; C_{rep-BC} and C_{rep-WT}, are the replacement cost for the battery bank, MPPTs, PV panels, Battery charger and Wind turbine, respectively.

Table 6.3: Total replacement cost for the proposed system

Components description	Number of replacement (s)	Component lifespan	Cost (R)	Cost (USD)
Batteries 200Ah GEL	4	5 years	145, 295.48	9,938.13
Wind Turbine 1kW	1	20 years	8, 636.11	590.71
MPPTs	1	15 years	4, 949.45	338.54
Battery Charger	1	15 years	4, 295.83	239.83
Solar panels	0	25 years	0	0
	Total replacement cost		163, 176.87	11, 161.21

B. *Operation and maintenance costs*

The operation and maintenance costs ($C_{initial-OM}$), at the end of the first year, may be taken as 6% of the initial investment cost($C_{initial}$) of the system. The total operation and maintenance cost (C_{OM}), for the lifetime of the system, may be calculated using Eq. (5.6) [77].

$$C_{OM} = \sum_{K=1}^{N} C_{initial-OM} \times (1+r)^{k} . \quad (5.6)$$

Where: $C_{initial-OM}$ = Operation and maintenance cost for the first year;

k = Represent each year in the project lifetime;

r = 10% annual energy price increase;

N = Number of years in the project lifetime.

C. Salvage costs

At the end of the project lifetime, the system will be refurbished, salvaged and sold, to allow for upgrades. At this point, the system components would have lost value and most will be out of their anticipated lifespan. Therefore, the salvage cost ($C_{salvage}$), may be taken as 20% of the initial investment cost($C_{initial}$) of the hybrid system, with a CPU unit. The salvage cost may be obtained, using Eq. (5.7).

$$C_{salvage} = 20\% \times C_{initial} . \quad (5.7)$$

D. The life cycle cost

The total life cycle cost of the system, may be obtained, by summing the costs affecting the project costs through the project life cycle, the subtraction of the salvage cost ($C_{salvage}$).The total life cycle cost may be obtained, using Eq. (5.8) below:

$$LCC = C_{initial} + C_{rep-TC} + C_{OM} + C_{EC} - C_{Salvage}. \quad (5.8)$$

The total life cycle cost value (ZAR), is calculated, using the above equation. Table 5.3, shows the total replacement cost for the proposed system. For the project lifetime and the total life cycle cost, approximately R351, 999.37, will be spent during the life cycle of this project.

Table 6.4: Total life cycle cost for the proposed system

Cumulative Cost	Value (R)	Value (USD)
$C_{initial}$	52, 534.77	3, 593.35
C_{rep-TC}	163, 176.86	11, 161.21
C_{OM}	146, 794.67	10, 040.68
C_{EC}	0	0
$C_{Salvage}$	10, 506.95	718.67
LCC	351, 999.37	24, 076.56

6.5 Break-even point (BEP)

The break-even point, is when the total initial investment, maintenance and operating costs or the proposed system equal or crosses any point of the baseline energy costs and operating costs, incurred throughout the projects lifetime. In this study, the proposed system is compared to the baseline, which is the grid supply, in terms of the total cumulative annual energy cost in the project lifetime of 25 years. The cumulative cost curves, including the initial investment cost and the total annual costs incurred over this period, are plotted. The baseline and proposed system are plotted on the same axis, to enhance a clear comparison. The point where these two curves intersect shows the point in time (years), where the break-even point occurs.

The initial total investment cost of the proposed system and the grid-connected is R52, 534.77 and R0, respectively. The values are, therefore, considered as the starting points of the two curves, as shown in Figure 5.2. The accumulated energy costs increase at a 10% rate, from the end of the first year, as the grid supply is applied and 4.5% is applied to the O&M accumulated costs for the proposed system. The replacement costs are further added, when certain system components run over their estimated lifespan. The O&M costs are taken as 6% of the initial investment cost; this is the average from the 10% maintenance requirement for a wind turbine, 6% for PV panels and 2% for the battery bank, as discussed in Chapter 3. From Figure 5.4, it may be seen that the break-even point occurs within 2 years, at R59, 270, after the project has begun. The project accumulated life cycle costs and break-even point, are shown below:

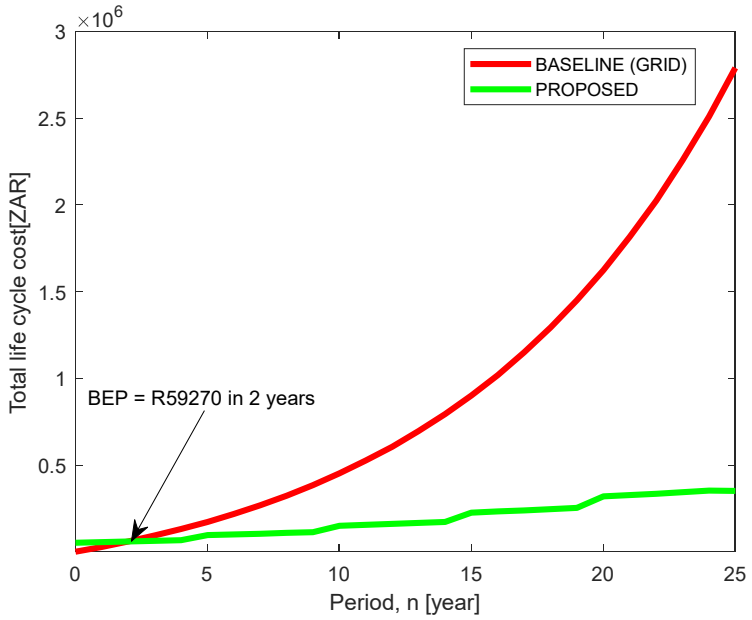

Figure 6.2: Breakeven point

6.6 PAYBACK PERIOD ESTIMATION FOR THE PROPOSED SYSTEM

In this section, a true PBP analysis will be performed. In the previous section 5.4, the LCC analysis is performed, to evaluate the total cost of the project throughout its life cycle. From there, the overall saving was determined to be 55.6%. PBP is used to determine the estimate payback period. SPP is the ratio between the annual benefit (AB) and initial investment cost, however, does not provide an accurate payback period, due to the neglect of the inflation rate. On the other hand, "true" PBP, takes into account the inflation rate and PBP is determined by the ratio between the Present worth (PW) of the total costs (PW_{TC}) and the annual average of the PW of the total benefits (PW_{TB}) [74]. The resulting "True" PBP is shown in Table 5.5 and the expression used is shown below:

$$\text{"True"}PBP = \frac{PW_{TC}}{PW_{TB-av}}. \tag{5.9}$$

Where: PBP = Payback period in years; $\mathrm{PW_{TC}}$ = Algebraic sum of the discounted concerning initial investment cost, salvage and replacement costs; $\mathrm{PW_{TB-av}}$ = Annual average of $\mathrm{PW_{TB}}$.

6.6.1 Present worth of total benefits

As explained above, PW_{TC} is the present worth of the total costs. This covers the initial investment cost, the salvage costs and replacement costs. The total initial investment costs ($C_{initial}$) are taken from Table 5.1. The $C_{initial}$ is the same for the two methods, since this is the amount spent to establish the proposed system. The salvage cost ($C_{salvage}$), is 20% of the ($C_{initial}$) and it will be taken from Table 5.6, as previously worked out. In PBP economic analysis, since the inflation rate is assumed to equal the real interest rate, the PW of replacement cost (C_{rep}) of the components that should to be replaced during the lifetime of the project, will be contained as follows (adapted from [78]):

$$C_{rep} = C_{cap} N_{rep}. \tag{5.10}$$

Where: C_{rep} = replacement cost;

C_{cap} = Capital cost;

N_{rep} = Number of replacements during the period lifetime.

The total replacement cost, therefore, will be calculated, using Eq. (5.5), in the previous sections above. Hence, by calculating the algebraic sum of costs explained above, PW_{TC} may be obtained, as shown by Eq. (5.11) below:

$$PW_{TC} = C_{rep-TC} + C_{initial} - C_{salvage}. \tag{5.11}$$

The obtained PW_{TC} is R130, 819.42, which is the result of the algebraic sum of a Salvage value of R10, 506.95, being subtracted from the sum of the total replacement cost of R88, 791.6, and the initial investment amount of R52, 534.77. Refer to Table 5.5 for the tabulated results.

6.6.2 Present worth of total benefits

As described in Ref. [74], PW_{TB} is the PW of total benefits, which are the annual cost savings, less any annual costs discounted to a PW and incurred by the user during operation. Since the proposed system is the standalone hybrid system with battery storage, the annual

costs are the O&M, which are estimated to be 6% if the initial costs. The PW_{TB} may be calculated as follows (adapted from Ref. [79]):

$$PW_{TB} = AB\left[\frac{(1+r)^n - 1}{r(1+r)^n}\right]. \quad (5.12)$$

Where: AB= Annual benefits;

r = Discount or interest rate taken as an inflation rate of 4.5% from Figure 5.1;

n = Project lifetime.

The annual benefits (AB), are the annual savings obtained as the annual difference of the energy costs from the baseline and the O&M annual costs, to run the proposed system. The monthly energy cost (C_{EC}) is R2, 149.36 monthly, obtained from an Eskom bill (landrate tariff) and it provides R25, 792.32 per year. O&M costs are obtained, as shown in Eq. (5.13) below:

$$C_{OM} = 0.06 \times C_{initial}. \quad (5.13)$$

Where: C_{OM} = Maintenance and operation costs;

$C_{initial}$ = Initial investment costs.

Therefore, The AB may be obtained, as shown in Eq. (5.14) below:

$$AB = C_{EC(A)} - C_{OM}. \quad (5.14)$$

Where: AB = Annual benefits;

$C_{EC(A)}$ = Annual energy cost for the first year;

C_{OM} = Operation and maintenance cost for the first year.

As shown in Table 5.8, the AB was found to be R22, 642.39, from the difference between the annual energy cost of R25, 792.32 and the O&M annual cost of R3, 179.93. After calculating AB the present value of total benefits (PW_{TB}) was also calculated for 25 years estimated project lifetime and an inflation rate of 4.5%, PW_{TB} is found to be R33, 5746.09.

6.6.3 Annual average Present worth of total benefits

The Annual average Present worth of total benefits (PW_{TB-av}), is expressed as the ratio of the PW_{TB} to the estimated project lifetime, which is taken as 25 years in this study. The obtained PW_{TB-av} for the proposed system is R13, 429.84 and the expression used to obtain PW_{TB-av}, given below:

$$PW_{TB-av} = \frac{PW_{TB}}{n}. \tag{5.15}$$

Where: PW_{TB} = Present worth of total benefits; n = Estimated project lifetime.

Table 6.5: Payback period for the proposed system

Parameters	Unit	Value (R)	Value (USD)
Total initial investment	Amount	52, 534.77	3, 593.35
Project lifetime, n	Years	25	25
PV life span	Years	25	25
N_{rep-PV}	Sum	0	0
C_{rep-PV}	Amount	0	0
Wind turbine life span	Years	20	20
N_{rep-WT}	Sum	1	1
C_{rep-WT}	Amount	3, 580.9	244.93
MPPT lifespan	Years	15	15
$N_{rep-MPPT}$	Sum	1	1
$C_{rep-MPPT}$	Amount	2, 557.48	174.93
Battery charger lifespan	Years	15	15
N_{rep-BC}	Sum	1	1
C_{rep-BC}	Amount	1, 325.22	90.64
Battery bank lifespan	Years	5	5
$N_{rep-BAT}$	Sum	4	4
$C_{rep-BAT}$	Amount	81, 328.00	5, 562.79
CPU lifespan	Years	25	25
$N_{rep-CPU}$	Sum	0	0
$C_{rep-CPU}$	Amount	0	0
AB	Amount	22, 642.39	1, 548.73
PW_{TC}	Amount	130, 790.62	8, 946.01
PW_{TB}		335, 746.09	22, 964.85
PW_{TB-av}		13, 429.84	918.59
"True" PBP	Years	9.74	9.74

6.7 LIFE CYCLE COST COMPARISON

The life cycle costs for the grid operated system and the proposed off-grid wind-solar PV hybrid system, are compared in Table 5.6, below. The break-even point analysis, shows the period, in which it will take both systems to reach a point of cost equalization. The difference in LCC is calculated, in order to note the savings in cost, at the end of the project lifespan. From Table 5.6 below, it may be concluded that a saving of approximately R2, 438, 259.34, may be obtained at the end of the project lifespan, if the proposed off-grid Hybrid wind-solar PV system with CPU, is implemented. This translates into a saving of 87.38%. This is due to solely R185.81, being the cost of electricity and the rest of the bill amounting to R1, 963.56, being the sum of the Network demand charge, Network capacity charge, ancillary service and service charges. The payback period on the proposed system, is below 10 years, 9 years, 8 months and 26 days, to be precise.

Table 6.6: Life cycle cost comparison

LCC	Value (R)	Value (USD)
LCC_{Grid}	2790258.71	190852.17
$LCC_{Proposed}$	351999.37	24076.56
Total savings over 25 years	2438259.34	166775.60

6.8 CONCLUSION

The purpose of this Chapter was to assess and evaluate the effectiveness of the proposed system, in terms of investments. The evaluation was successful, through the evaluation of "True" PBP, LCC and BEP analysis. This analysis reveals that, after 2 years, the cumulative costs of operating the CP system from the baseline (Grid), become higher than those of the proposed system. Furthermore, after the break-even point, the savings begin to accumulate drastically. The LCC of the proposed system, as compared to the baseline, reveals 87.38% savings, for the project lifetime. Therefore, the LCC analysis substantiates the hypothesis in Chapter 1, that the proposed ICCP system running on an off-grid wind-solar PV system, should return the investment within 10 years, from the date of installation.

CHAPTER 7: GENERAL CONCLUSION

7.1 SUMMARY

In this work, solar PV/wind/battery off-grid hybrid system is proposed, to power the CPU. This research work is significant, as it aims to improve the lifespan of the water pipeline in South Africa, where the grid extension is not possible. The work is further relevant for locations with grid availability, however which, regrettably, unfortunately, experience multiple load sheddings, or power failure. The use of renewable energy, as a means to decrease Carbone emission, is another factor. The research study demonstrates the technical and economic feasibility of the proposed CPU, powered by an off-grid hybrid energy system.

In Chapter 2, research gaps have been established, allowing adequate technology selection and raising awareness, based on the potential use of CP's renewable energy resources. A global analysis of the current state of solar and wind energy, with a focus on various technologies, producers and recent developments, was presented. The fact that there is a large amount of solar and wind power in South Africa, is further revealed in this Chapter.

In Chapter 3, the optimal size of the proposed off-grid Hybrid wind-solar PV system, with battery storage, was determined using HOMER software, as the main optimization tool. The optimal configuration results revealed that, the load demand was adequately met, without power shortages and incurred the levelized cost of energy of R 1.68/kWh. The techno-economic analysis of the proposed off-grid Hybrid wind-solar PV system, was further performed, to demonstrate the potential benefits when using wind and solar resources. The results further revealed that, the proposed system has an initial capital of R 15, 643.40 and a total NPC of R 45, 014.98, with the system configuration made up of 0.74 kW of PV array, 1kW Wind turbine and four 200Ah batteries.

In Chapter 4, a model was proposed for the off-grid PV hybrid wind-solar system. This model aims to research the system's behaviour, using a permanent magnet synchronous generator and a PV array, with a wind turbine under variable water velocity and solar irradiance, respectively. In addition, it aims to enable designers, based on a power flow

analysis, to make informed decisions during the project planning stage. The dynamic behaviour of an off-grid hybrid wind-solar PV system, under variable water velocity and solar irradiance, was simulated, using the software package MATLAB/Simulink and the model provided. The simulation results obtained, show that the off-grid hybrid wind-solar PV system is the optimal small-scale choice to consider for remote ICCP system electrification in areas with both sufficient wind speed and solar resources in South Africa. In addition, the built model was used to evaluate, under different scenarios, the effects of the variance of wind and solar resources on the desired voltage output, as well as the power flow.

Chapter 5, covered the practical experimenting of the proposed system, where a small scale system was designed and tested, proving the proposed concept. The experimental results have shown that it is possible to use a PV/wind/battery, to power a CPU.

In Chapter 6, the economic analysis was carried out for a period of 25 years. The initial investment cost of the proposed off-grid hybrid energy system was R52, 534.77. Simulation results have shown that the total grid energy cost incurred, will be R2, 790,258.71, over the project lifetime, whereas the proposed off-grid hybrid energy system would lead to a life cycle cost of R351, 999.37. This translates into an energy cost saving of 87.4%. Furthermore, a break-even point of R59, 270.00 in 2 years is possible. This means that once the 2 years have elapsed after the start of the project, merely the savings may be noticed, for the entire life cycle of the project, with a true payback period of 10 years. Therefore, from the analysis and evaluation above, it may be noticed that the system is economically feasible and technically viable, in the South African context.

With the above in mind, results have revealed that cathodic protection may be supplied, using renewable energy, without power shortage, with a remote monitoring system, to enhance the cost effectiveness of the proposed system. The use of renewable energy for the ICCP system will increase the utilization of cathodic protection, to prevent corrosion, due to the reduction in implementation and running costs.

7.2 FUTURE WORK

Implementation is the next stage after prototype development. However, this will depend on the availability of funds and permission by Umgeni water. Hence, the work proposed in this work may be continued as follows:

- Since this research focused on a case study in KwaZulu-Natal, the study could be adapted to fit various geographical locations with different input parameters, which could change the configuration of the off-grid Hybrid wind-solar PV system, in turn.
- Further work should be carried out in developing a grid-tied system, where feasibility of the off-grid hybrid system is limited.
- Furthermore, it would be of interest to investigate how the model would perform, when applied to the other small-scale loads, such as network towers, traffic lights and national roads monitoring camera systems.

REFERENCES

[1] "Design Criteria of Cathodic Protection Systems," *Engineering Encyclopedia of Saudi Aramco Standards,* pp. 1 - 64, 2008.

[2] A. W. PEABODY, "Control of Pipeline Corrosion," *National Association of corrosion Engineers,* pp. 1-347, 1967.

[3] B. Jim, "Impressed current retrofits on offshore platforms: The good, the bad and the Ugly," *Corrosion 2001,* 2001.

[4] Y. Song, "Electrochemical corrosion behaviour of carbon steel with bulk coating holidays," *Journal of University of science and Technology Beijing,* vol. 13, 2006.

[5] J. A.-K. Luay, "Natural Gas in the Republic of Iraq," *James A.Baker III Institute for Public Policy Rice University,* 18 November 2013.

[6] T. Hill. (2016, April 11th, 2016). *Corrosion management is a critical part of maintaining pipeline integrity*. Available: https://blog.applus.com/corrosion-management-crucial-to-pipeline-integrity/

[7] V. Ashworth, "Principles of Cathodic Protection," *Shrier's Corrosion,* vol. Elsevier. V2, 2010.

[8] C. A. Sibiya, K. Kusakana, and B. P. Numbi, "Smart System for Impressed Current Cathodic Protection Running on Hybrid Renewable Energy," 2018.

[9] D. L. Basham, J. W. Wright, K. I. Ferguson, and G. W. Moy, ""Operation and Maintenance of Cathodic Protection Systems", Unified Facilities Criteria (UFC), Department of Defense USA, 2003, pp.1-220."

[10] W. Muhammad, N. M. Mubarak, S. Shahrukh, and I. Inamuddin, "Factors influencing corrosion of metal pipes in soils".

[11] G. A. Jacobson, "Summer Bridge on Issues at the Technology/Policy Interface, July 1, 2016 Volume 46 Issue 2. NACE International's IMPACT Study Breaks New Ground in Corrosion Management Research and Practice. ."

[12] A. Groysman, " Corrosion problems and solutions in oil,gas, refining and petrochemical industry. 2017. ."

[13] G. Kakuba, ""Master Thesis of the Impressed Current Cathodic Protection Systems", Technische Universiteit Eindhoven Department of Mathematics and Computer Science, 2005, pp.1-95."

[14] M. Karami, "Review of Corrosion Role in Gas Pipeline and Some Methods for Preventing It," *Journal of Pressure Vessel Technology* vol. 134, no. 5, September 6, 2012 2012.

[15] "C. Christodoulou, G. Webb, S.Austin, C. Goodier. Assessing the long term benefits of Impressed Current Cathodic Protection. ."

[16] E. Aksu, "Thermosets for pipeline corrosion protection, in Thermosets (Second Edition), 2018.."

[17] "Mitigation of External Corrosion on Buried Carbon Steel Pipeline Systems, July/2018.."

[18] "International organization for standardization. South African National Standard (SANS) 15589-1:2009, Edition 1" Petroleum and natural gas industries-CP of pipelines transportation systems, Part 1: On-land pipelines". ."

[19] "D. Talbot and J. Toalbot. ‘ corrosion science and technology’, CRC Press L.L.C, New York, the USA,1998.."
[20] "W.Von Baeckmann, W. Schwenk and W Prinz, ‘Handbook of cathodic corrosion protection’, Third Edition, Elsevier Science, 1997. ."
[21] "Engineering Encyclopedia of Saudi Aramco Standards, “Design Criteria of Cathodic Protection Systems”,2008, pp.1-64. ."
[22] otds. *Impressed Current Cathodic Protection (ICCP).* Available: http://www.otds.co.uk/products/42/impressed-current-cp
[23] M. I. AI-Hazzaa and M. O. AI-Abdullatif, "Effect of soil conductivity on the Design of Cathodic Protection Systems used in the Prevention of Pipeline corrosion. J.King Saud Univ., Vol.22, Eng. Sci.(2),pp. 111-117, (2010/1431H.) ".
[24] "ISO 15589-1:2003."
[25] Available: http://www.corrosiontechnologies.ca/what-is-cathodic-protection/
[26] A. W. PEABODY, "Peabody’s Control of Pipeline Corrosion Second Edition," 2001.
[27] "Standard for the Selection and Design of Cathodic Protection (CP) Systems. DESIGN STANDARD DS 91.October 2017.."
[28] U. K. Mudali, H. S. Khatak, and B. Raj, "Anodic and Cathodic Protection," *Encyclopedia of Electrochemistry: Online,* 05 September 2014 2014.
[29] A. Mukasa, E. Mutambatsere, Y. Arvanitis, and T. Triki, "Development of wind energy in Africa. In: Kayizzi-Mugerwa S, Shimeles A, Lusigi A, Moummi A, editors. Incl. growth Africa policies, pract. lessons learn. New York: Routledge; 2017.."
[30] M. R. Davidson, F. Kahrl, and V. J. Karplus, "Towards a political economy framework for wind power. Does China break the mould? In: Arent D, Arndt C, Miller M, Tarp F,Zinaman O, editors. Polit. Econ ".
[31] A. Castellano, A. Kendall, M. Nikomarov, and T. Swemmer, "Brighter Africa. The growth potential of the sub-Saharan electricity sector. Electr Power Nat Gas Bright; 2015.."
[32] "GWEC. Global wind report 2017. Brussels: Global Wind Energy Council; 2018.."
[33] J. A. Duffie and W. A. Beckman, "Solar engineering of thermal processes. New Yoke: John Wiley & sons; 2013. ."
[34] B. Laoun, K. Niboucha, and L. Serir, "Cathodic protection of a buried pipeline by solar energy. 2008.."
[35] A. W. PEABODY, " Control of Pipeline and Corrosion " *National Association of corrosion Engineers,* pp. 1-347, 1967.
[36] "Remote Monitoring of Pipeline Cathodic Protection Systems by Neil Summers April – June 2009."
[37] "Ashraf I. EL-Alem, Ahmed M. Azmy and A. Hosam-Eldin “Design of A Cathodic Protection System to prevent corrosion of metallic structures using hybrid renewable energy. April 2013. ."
[38] "Prolonging the lives of buried crude-oil and natural-gas pipelines by cathodic protection. M.T. Lilly, S.C. Ihekwoaba , S.O.T. Ogaji ,*, S.D. Probert. 2007 Elsevier Ltd. ."
[39] EBAA Iron, "CORROSION AND CATHODIC PROTECTION IN UNDERGROUND PIPING SYSTEMS " 1994.
[40] "D. Bailey, “Practical SCADA for Industry – 1st edition”, UK, 2003. ."

[41] W. Keir, J. Mohammed, and N. Vitalis, "The selection and use of cathodic protection systems for the repair of reinforced concrete structures," *Construction and Building Materials 39* pp. 19-25, 2013.
[42] B. P. Numbi and S. J. Malinga, "Optimal energy cost and economic analysis of a residential grid-interactive solar PV system- case of eThekwini Municipality in South Africa," *Appl. Energy,* vol. 186, pp. 28-45, 2017.
[43] "Eskom tariffs and charges 2019/2020, Ruraflex non-local authority.."
[44] K. Kusakana, "Economic performance of a grid-interactive system with storage under a dynamic electricity pricing environment," February 2019 2019.
[45] R. C. Oudalov and A. Beguin, "Sizing and Optimal Operation of Battery Energy Storage System for Peak Shaving Application," *in Proc. 2007 IEEE Powertech Conf.,* pp. 1-5.
[46] S. Lichtner, R. Brindle, L. Kishter, and L. Pack, "Advanced Materials and Devices for Stationary Electrical Energy Storage Applications," *Nexight Group, Tech. Rep,* December 2010.
[47] H. Ibrahim, A. Ilinca, and J. Perron, "Energy storage systems. Characteristics and comparisons," *Renew. and Sustain. Energy Rev,* vol. 12, pp. 1221-1250, June 2008.
[48] "https://artsolar.net/solar-batteries/ ".
[49] J. R. González, Riba, and A. Rius, "Optimal sizing of a hybrid grid-connected photovoltaic wind-biomass power system," *Sustainable Energy Technologies and Assessments,* vol. 7, no. 9, pp. 47-67, 2017.
[50] M. Abdel-Salam, K. Sayed, A. Ahmed, M. Amery, and M. Swify, "Design, implementation and operation of a stand-alone residential photovoltaic system," *International Journal of Power and Energy Conversion,* vol. 8, pp. 47-67, 2017.
[51] S. Bilgen, "Structure and environmental impact of global energy consumption," *Renewable and Sustainable Energy Reviews,* vol. 38, pp. 890-902, 2014.
[52] "Intergovernmental Panel on Climate Change and Intergovernmental Panel on Climate Change 2015 Drivers, Trends and Mitigation Climate Change 2014 Mitigation of Climate Change. ."
[53] "Intergovernmental Panel on Climate Change 2014 Climate Change 2014 Synthesis Report - IPCC ".
[54] "Alaskan, A. B. S. "Excel 7.5 kW high voltage DC turbine." Accessed February 13 (2020).".
[55] T. H. Larsen and E. H. Ulrich, "Sustainable industrialization in Africa: the localization of wind-turbine component production in South Africa," *Innovation and Development (2020),* pp. 1-20.
[56] K. Kusakana and H. J. Vermaak, "Hydrokinetic power generation for rural electricity supply: Case of South Africa," *Renewable energy 55 (2013),* pp. 467-473.
[57] L. Obaidullah, k. Nitin, V. Satyanand, and M. Gazia, "Modeling and Simulation of Wind Solar Hybrid System using Matlab/Simulink," *International Journal of Innovative Technology and Exploring Engineering (IJITEE),* vol. Volume-8, no. Issue-9S, pp. 218-224, July 2019 2019.
[58] H. S. Naggar, A. E.-S. Ahmed, E.-A. Abd, and M. Mansour, "A novel control strategy for grid connected hybrid renewable energy systems using improved particle swarm optimization," *Ain Shams Engineering Journal,* 2017.

[59] A. D. Dhass, E. Natarajan, and P. Lakshmi, "Influence of shunt resistance on the performance of solar photovoltaic cell," *Emerging Trends in Electrical Engineering and Energy Management (ICETEEEM), 2012 International Conference on,* 2012.
[60] R. Faranda and S. Leva, "Energy comparison of MPPT techniques for PV Systems," *WSEAS TRANSACTIONS on POWER SYSTEMS,* vol. 3, no. 6, pp. 446 - 455, June 2008 2008.
[61] E. Osisioma, F. Zhongwen, and L. Zhijun, "Energy Performance and Cost Comparison of MPPT Techniques for Photovoltaics and other Applications," *Energy Procedia 107:297-303,* February 2017.
[62] L. Badreddine, Z. Smail, M. Bourhaleb, and L. E. Mohamed, "Real time study of P&O MPPT control for small wind PMSG turbine systems using Arduino microcontroller," *8th International Conference on Sustainability in Energy and Buildings, SEB-16, 11-13 September,* pp. 1000-1009, 2017 2016.
[63] E. Sandra, B. Hans, and L. Mats, "Evaluation of different turbine conceps for wind power," *Renewable and Sustainable Energy Reviews 12(5):1419-1434,* June 2008.
[64] M. G. Molina, A. G. Sanchez, and L. A. M. Rizzato, "Dynamic Modeling of Wind Farms with Variable-Speed Direct-Driven PMSG Wind Turbines," *IEEE, Transmission and Distribution Conference and Exposition,* pp. 816-823, November 2010 2010.
[65] M. Kesraoui, K. Noureddine, and A. Belkadi, "Maximum power point tracker of wind energy conversion system," *Renewable Energy 36(10):2655-2662,* October 2011.
[66] Y. Minghui, L. Weijie, C. Chi Yung, and Z. Lianjun, "An Optimal Torque Control Based on Effective Tracking Range for Maximum Power Point Tracking of Wind Turbines under Varying Wind Conditions," *IET Renewable Power Generation* November 2016.
[67] T. Debabrata, "DESIGN, CONTROL AND SIMULATION OF PMSG BASED STAND-ALONE WIND ENERGY CONVERSION SYSTEM," Thesis
[68] H. J. N. Mohammd and A. Mahdi, "Optimal Torque Control of PMSG-based Stand-Alone Wind Turbine with Energy Storage System," *JOURNAL OF ELECTRIC POWER AND ENERGY CONVERSION SYSTEMS (JEPECS),* vol. 1, pp. 52 - 59, May 2016 2016.
[69] G. Raviteja, "SOLAR PV WIND HYBRID ENERGY SYSTEM(https://www.mathworks.com/matlabcentral/fileexchange/72764-solar-pv-wind-hybrid-energy-system), MATLAB Central File Exchange. Retrieved April 9, 2020.."
[70] https://artsolar.net/product/370-watt-solar-panel-mono-perc/.
[71] AEOLOS WIND TURBINE LLC, "AEOLOS HORIZONAL AXIS WIND TURBINE - 1kW."
[72] https://artsolar.net/solar-batteries/.
[73] https://www.solarpanelenergy.co.za///pg194873/agm-deep-cycle-batteries.
[74] B. P. Numbi and S. J. Malinga, "Optimal energy cost and economic analysis of a residential grid-interactive solar PV system- case of eThekwini municipality in South Africa," *Applied Energy,* vol. 186, pp. 28-45, 2017.
[75] Eskom, "Tariffs and Charges 2019/2020."
[76] Inflation.eu, " Historic inflation South Africa - CPI inflation," 3/18/2020.

[77] P. A. Hohne, K. Kusakana, and B. P. Numbi, "Optimal energy management and economic analysis of a grid-connected hybrid solar water heating system: A case of Bloemfontein, South Africa," *Sustainable Energy Technologies and Assessments,* vol. 31, pp. 273-291, 2019.

[78] A. S. O. Ogunjuyigbe, T. R. Ayodele, and O. A. Akinola, "Optimal allocation and sizing of PV/wind/split-diesel/battery hybrid energy system for minimizing life cycle cost,carbon emission and dump energy of remote residential building.," *Applied Energy,* 2016;171:153–71.

[79] B. L. Capehart, W. J. Kennedy, and W. C. Turner, "Guide to energy management. 5th ed. Indian Trail, United States: The Fairmont Press, Inc. 2008.."

APPENDICES

APPENDIX A: PROTOTYPE DESIGN DIAGRAMS

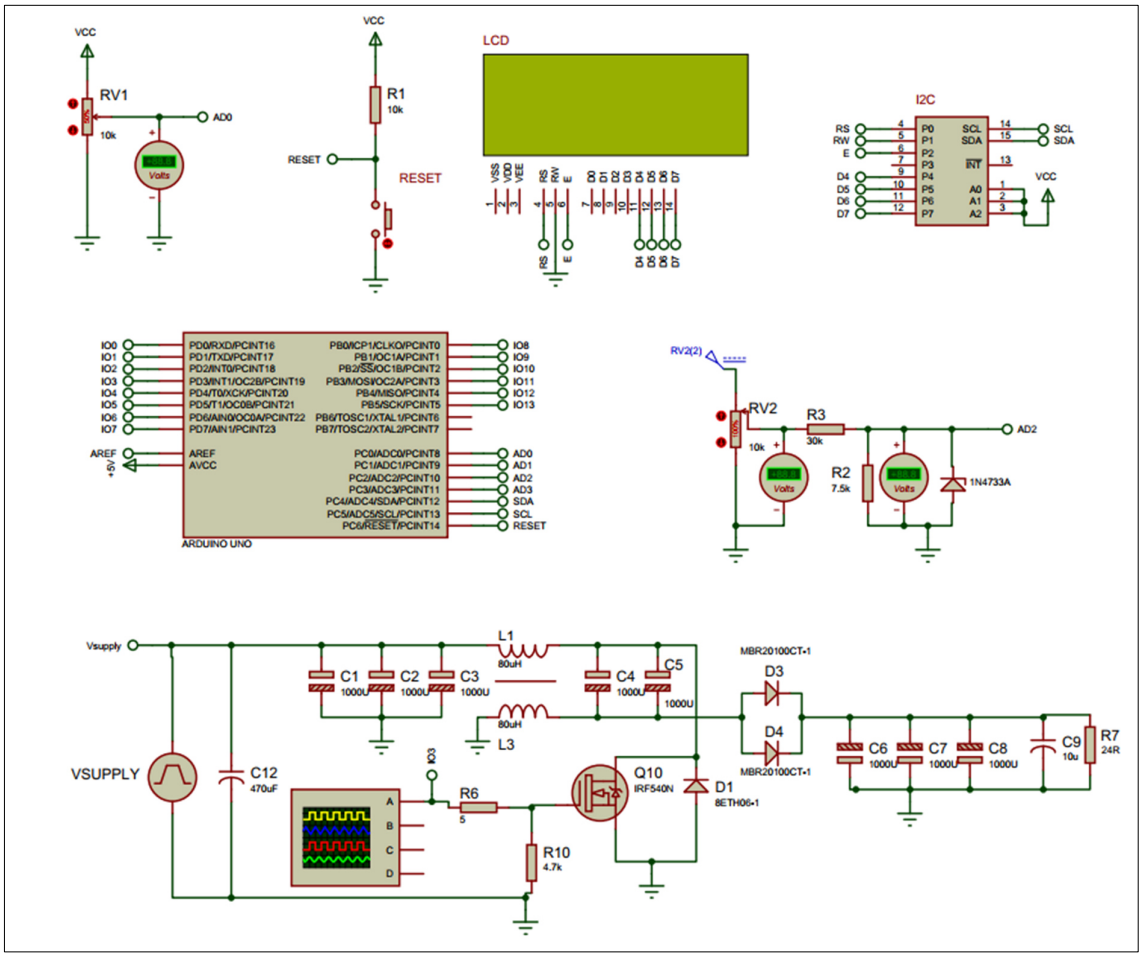

Figure A1: Schematic of the CPU control circuit

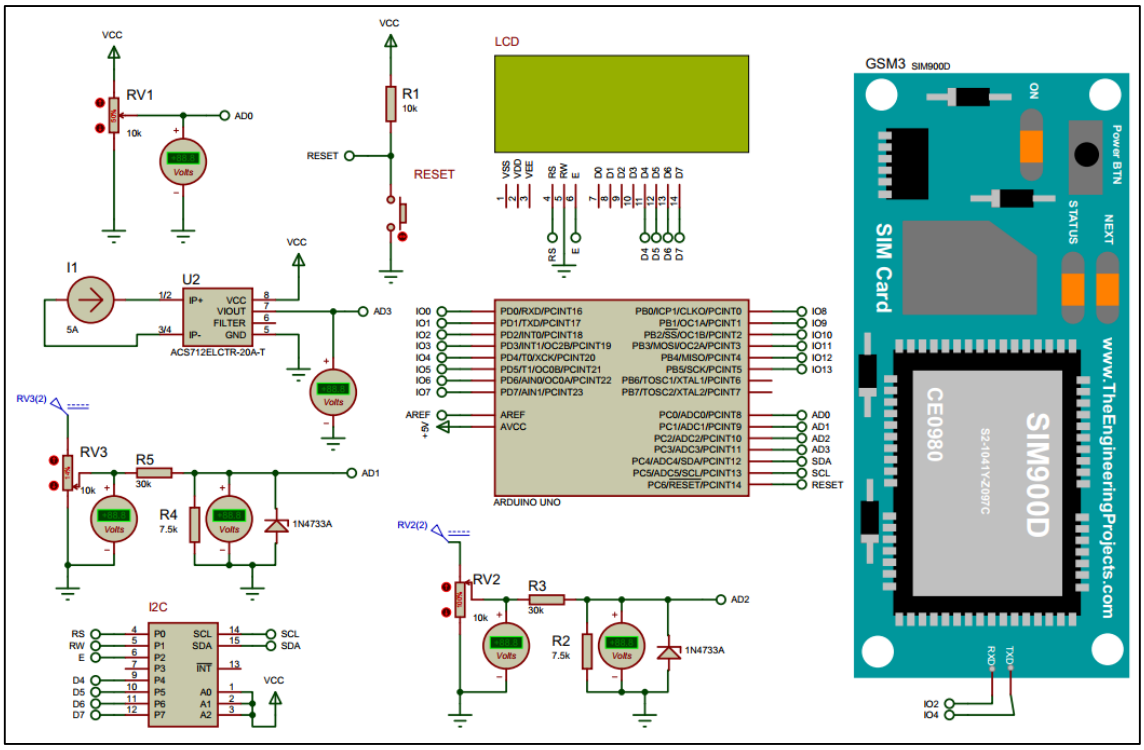

Figure A2: Schematic of CPU remote monitoring circuit

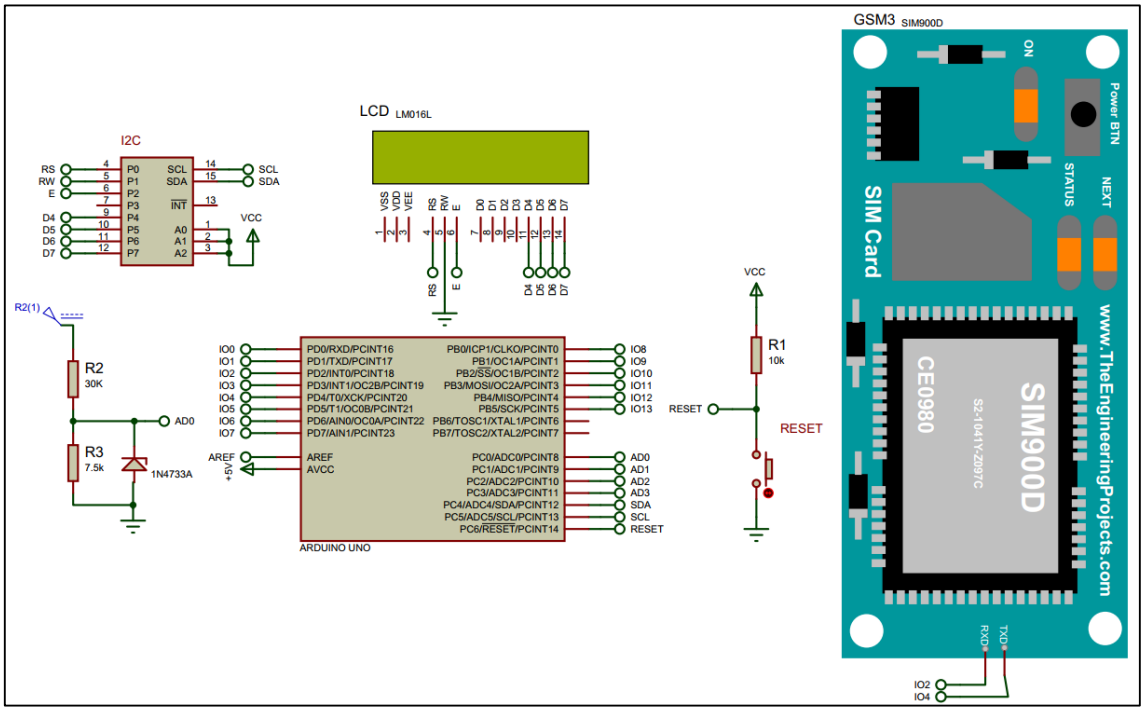

Figure A3: Schematic diagram of TP remote monitoring circuit

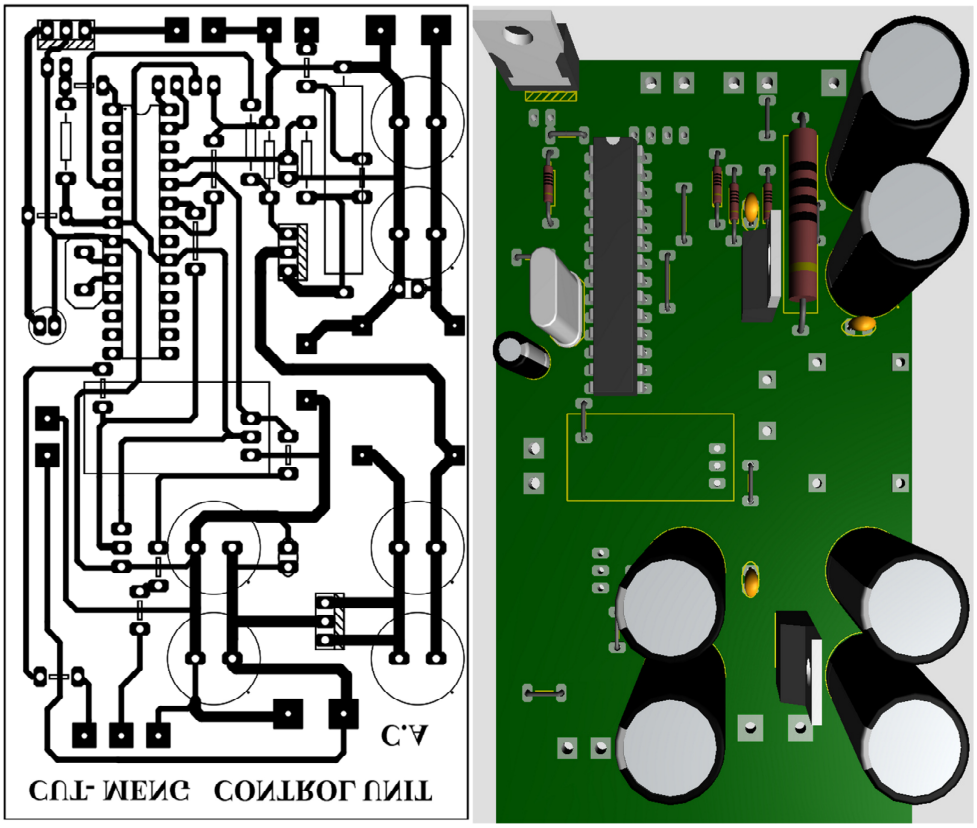

Figure A4: PCB layout of the CPU control circuit

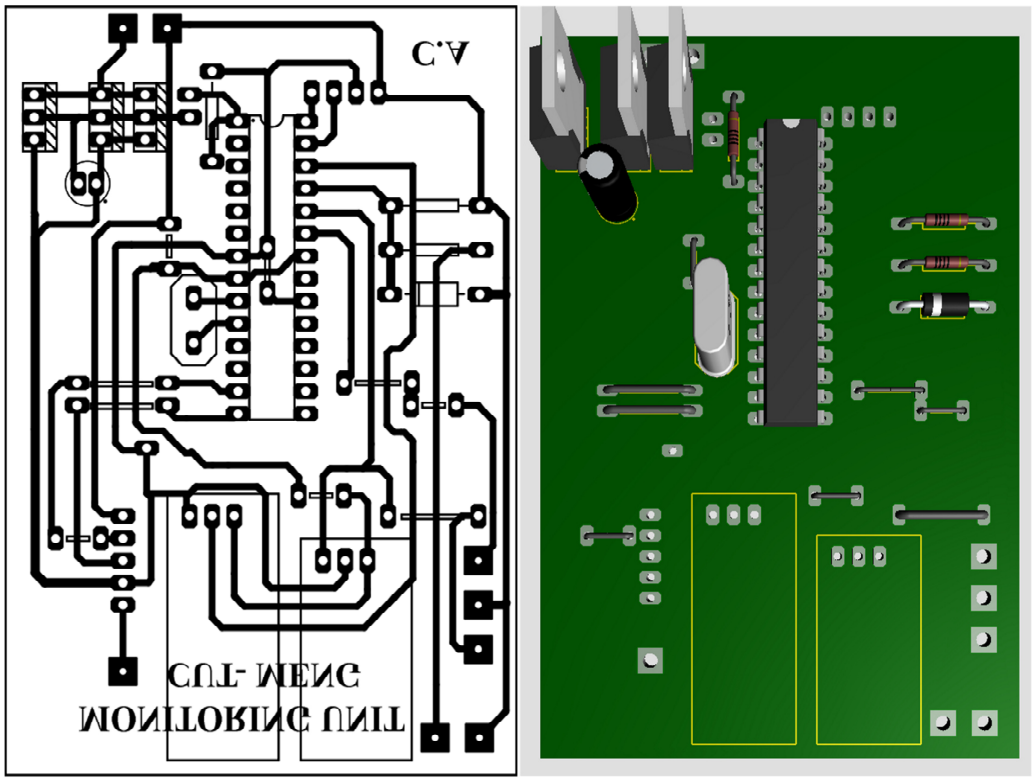

Figure A5: PCB layout of CPU remote monitoring circuit

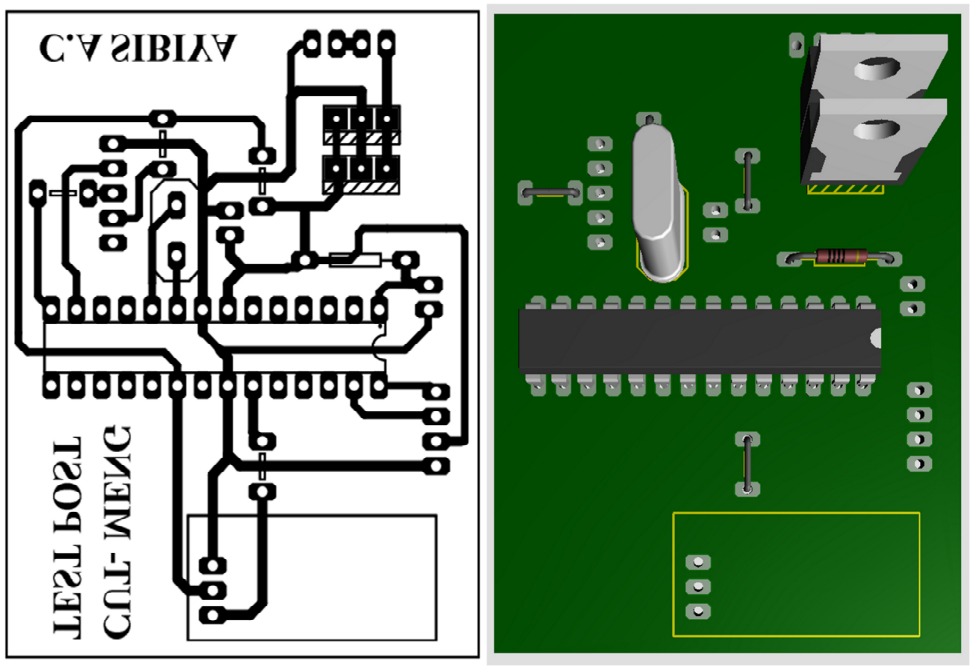

Figure A6: PCB layout of TP remote monitoring circuit